การสังเคราะห์อนุภาคระดับนาโนเมตรของพอลิสไตรีน/ซิลิกาและพอลิไอโซพรีน/ซิลิกา
ผ่านพอลิเมอไรเซชันแบบกราฟต์อิมัลชัน

นางสาวดุษฎี ตำนานทอง

บทคัดย่อและแฟ้มข้อมูลฉบับเต็มของวิทยานิพนธ์ตั้งแต่ปีการศึกษา 2554 ที่ให้บริการในคลังปัญญาจุฬาฯ (CUIR)
เป็นแฟ้มข้อมูลของนิสิตเจ้าของวิทยานิพนธ์ ที่ส่งผ่านทางบัณฑิตวิทยาลัย
The abstract and full text of theses from the academic year 2011 in Chulalongkorn University Intellectual Repository (CUIR)
are the thesis authors' files submitted through the University Graduate School.

วิทยานิพนธ์นี้เป็นส่วนหนึ่งของการศึกษาตามหลักสูตรปริญญาวิทยาศาสตรดุษฎีบัณฑิต
สาขาวิชาเคมีเทคนิค ภาควิชาเคมีเทคนิค
คณะวิทยาศาสตร์ จุฬาลงกรณ์มหาวิทยาลัย
ปีการศึกษา 2559
ลิขสิทธิ์ของจุฬาลงกรณ์มหาวิทยาลัย

SYNTHESIS OF POLYSTYRENE/SiO$_2$ AND POLYISOPRENE/SiO$_2$

NANOPARTICLES VIA RAFT EMULSION POLYMERIZATION

Miss Dusadee Tumnantong

จุฬาลงกรณ์มหาวิทยาลัย
CHULALONGKORN UNIVERSITY

A Dissertation Submitted in Partial Fulfillment of the Requirements
for the Degree of Doctor of Philosophy Program in Chemical Technology
Department of Chemical Technology
Faculty of Science
Chulalongkorn University
Academic Year 2016
Copyright of Chulalongkorn University

Thesis Title	SYNTHESIS OF POLYSTYRENE/SiO$_2$ AND POLYISOPRENE/SiO$_2$ NANOPARTICLES VIA RAFT EMULSION POLYMERIZATION
By	Miss Dusadee Tumnantong
Field of Study	Chemical Technology
Thesis Advisor	Professor Pattarapan Prasassarakich, Ph.D.
Thesis Co-Advisor	Professor Garry L. Rempel, Ph.D.

Accepted by the Faculty of Science, Chulalongkorn University in Partial Fulfillment of the Requirements for the Doctoral Degree

....Dean of the Faculty of Science
(Associate Professor Polkit Sangvanich, Ph.D.)

THESIS COMMITTEE

....Chairman
(Associate Professor Prasert Reubroycharoen, Ph.D.)

....Thesis Advisor
(Professor Pattarapan Prasassarakich, Ph.D.)

....Thesis Co-Advisor
(Professor Garry L. Rempel, Ph.D.)

....Examiner
(Associate Professor Napida Hinchiranan, Ph.D.)

....Examiner
(Associate Professor Sirilux Poompradub, Ph.D.)

....External Examiner
(Associate Professor Kitikorn Charmondusit, Ph.D.)

ดุษฎี ตำนานทอง : การสังเคราะห์อนุภาคระดับนาโนเมตรของพอลิสไตรีน/ซิลิกาและพอลิไอโซพรีน/ซิลิกา ผ่านพอลิเมอไรเซชันแบบราฟต์อิมัลชัน (SYNTHESIS OF POLYSTYRENE/SiO$_2$ AND POLYISOPRENE/SiO$_2$ NANOPARTICLES VIA RAFT EMULSION POLYMERIZATION) อ.ที่ปรึกษาวิทยานิพนธ์หลัก: ศ. ดร. ภัทรพรรณ ประศาสน์สารกิจ, อ.ที่ปรึกษาวิทยานิพนธ์ร่วม: ศ. ดร. Garry L. Rempel, 113 หน้า.

อนุภาคระดับนาโนเมตรพอลิสไตรีน-ซิลิกาและพอลิไอโซพรีน-ซิลิกาถูกสังเคราะห์ผ่านราฟท์อิมัลชันพอลิเมอไรเซชัน โดยไม่ใช้สารลดแรงตึงผิว โครงสร้างแกน-เปลือกของพอลิเมอร์-ซิลิกามีส่วนในการลดการเกาะกลุ่มกันของอนุภาคซิลิกา งานวิจัยนี้ศึกษาผลของอัตราส่วนระหว่างความเข้มข้นของมาโคร-ราฟท์เอเจนต์และตัวริเริ่มปฏิกิริยา ต่อร้อยละการเปลี่ยนของมอนอเมอร์ ขนาดอนุภาค การกระจายตัวของอนุภาค ประสิทธิภาพการกราฟต์ และประสิทธิภาพการเอนแคปซูเลชันของซิลิกา พบว่าเมื่ออัตราส่วนระหว่างความเข้มข้นของมาโคร-ราฟท์เอเจนต์และตัวริเริ่มปฏิกิริยาเพิ่มขึ้น ทำให้ขนาดของอนุภาคนาโนพอลิสไตรีน-ซิลิกาและพอลิไอโซพรีน-ซิลิกามีขนาดลดลง และการกระจายตัวของอนุภาคค่อนข้างแคบในกระบวนพอลิเมอไรเซชันทั้งหมด สำหรับการเตรียมอนุภาคนาโนพอลิไอโซพรีน-ซิลิกามีการศึกสารผลของชนิดตัวริเริ่มปฏิกิริยาที่ละลายน้ำ พบว่าขนาดอนุภาคของอิมัลชันที่เตรียมด้วยตัวริเริ่มปฏิกิริยา ACP มีขนาดเล็กกว่าอิมัลชันที่เตรียมด้วยตัวริเริ่มปฏิกิริยา V50 เนื่องจากความแตกต่างของโครงสร้างตัวริเริ่มปฏิกิริยา นอกจากนี้ อนุภาคระดับนาโนเมตรพอลิเมทิลเมทาคริเลต-ซิลิกาและพอลิ(สไตรีน-โค-เมทิลเมทาคริเลต)-ซิลิกาถูกสังเคราะห์ผ่านดิฟเฟอเรนเชียลไมโครอิมัลชันพอลิเมอไรเซชัน งานวิจัยนี้ศึกษาผลของปริมาณซิลิกาและความเข้มข้นของสารลดแรงตึงผิว พบว่าอนุภาคนาโนพอลิเมทิลเมทาคริเลต-ซิลิกามีขนาดอยู่ในช่วง 30-50 นาโนเมตรและร้อยละการเปลี่ยนของมอนอเมอร์สูงถึงร้อยละ 99.9 โดยใช้ปริมาณสารลดแรงตึงผิวค่อนข้างต่ำเพียงแค่ 5.34 เปอร์เซนต์โดยน้ำหนักของปริมาณมอนอเมอร์ สำหรับการสังเคราะห์ของอนุภาคนาโนพอลิ(สไตรีน-โค-เมทิลเมทาคริเลต)-ซิลิกาแสดงร้อยละการเปลี่ยนของมอนอเมอร์สูงและอนุภาคที่มีขนาดเล็กเพียง 20-40 นาโนเมตร ภายใต้ภาวะที่เหมาะสมโดยใช้ปริมาณสารลดแรงตึงผิวค่อนข้างต่ำเพียงแค่ 3 เปอร์เซนต์โดยน้ำหนักของปริมาณมอนอเมอร์ นาโนคอมพอสิตดังกล่าว สามารถใช้เป็นสารตัวเติมในน้ำยางธรรมชาติ และยังพบว่ายางธรรมชาติที่ถูกเติมด้วยพอลิเมอร์-ซิลิกาเหล่านี้มีการปรับปรุงสมบัติทางความร้อนและสมบัติเชิงกล

ภาควิชา	เคมีเทคนิค	ลายมือชื่อนิสิต	_____
สาขาวิชา	เคมีเทคนิค	ลายมือชื่อ อ.ที่ปรึกษาหลัก	_____
ปีการศึกษา	2559	ลายมือชื่อ อ.ที่ปรึกษาร่วม	_____

5472892023 : MAJOR CHEMICAL TECHNOLOGY

KEYWORDS: NANOCOMPOSITES / RAFT POLYMERIZATION / EMULSIFIER-FREE EMULSION / DIFFERENTIAL MICROEMULSION POLYMERIZATION / SILICA

DUSADEE TUMNANTONG: SYNTHESIS OF POLYSTYRENE/SiO$_2$ AND POLYISOPRENE/SiO$_2$ NANOPARTICLES VIA RAFT EMULSION POLYMERIZATION. ADVISOR: PROF. PATTARAPAN PRASASSARAKICH, Ph.D., CO-ADVISOR: PROF. GARRY L. REMPEL, Ph.D., 113 pp.

Polystyrene-silica (PS-co-RAFT-SiO$_2$) and polyisoprene-silica (PIP-co-RAFT-SiO$_2$) nanoparticles were synthesized via reversible addition-fragmentation chain-transfer (RAFT) emulsifier-free emulsion polymerization. The core-shell morphology of polymer-silica nanoparticles have attributed to reduce the agglomeration of silica. The effects of macro-RAFT agent to initiator ratio on monomer conversion, particle size, particle size distribution, grafting efficiency and silica encapsulation efficiency were investigated. The particle size of PS-co-RAFT-SiO$_2$ and PIP-co-RAFT-SiO$_2$ nanoparticles decreased with increasing macro-RAFT agent to initiator ratio ([R]:[I]) and showed a narrow size distribution for all polymerizations. For PIP-co-RAFT-SiO$_2$ preparation, the type of water-soluble initiator were also studied. The particle size of emulsion prepared using ACP initiator was smaller than that using V50 initiator due to the different structure of the initiators. Furthermore, Poly(methyl methacrylate)-silica (PMMA-SiO$_2$) and poly(styrene-co-methyl methacrylate))-silica (poly(ST-co-MMA)-SiO$_2$) nanoparticles were prepared via differential microemulsion polymerization. The effects of silica loading and surfactant concentration on monomer conversion, particle size, particle size distribution and silica encapsulation efficiency were investigated. PMMA-SiO$_2$ nanoparticles with a size range of 30–50 nm and high monomer conversion of 99.9% were obtained at a low surfactant concentration of 5.34 wt% based on monomer. For poly(ST-co-MMA)-SiO$_2$ nanoparticles, a high monomer conversion and small particle size (20–40 nm) were obtained under optimum reaction conditions with a low surfactant concentration (3 wt% based on monomer). The nanocomposites have been used as nano-filler in natural rubber latex. Accordingly, NR/polymer-SiO$_2$ blends had improved thermal and mechanical properties.

Department:	Chemical Technology	Student's Signature	....
Field of Study:	Chemical Technology	Advisor's Signature	....
Academic Year:	2016	Co-Advisor's Signature	....

ACKNOWLEDGEMENTS

CONTENTS

LIST OF TABLES

LIST OF FIGURES

LIST OF ABBREVIATIONS

ACP	:	4,4'-azobis(4-cyanopentanoic acid)
APS	:	ammonium persulfate
ASTM	:	American Society for Testing and Materials
CRP	:	controlled /living radical polymerization
CTA	:	chain transfer agent
DLS	:	dynamic light scattering
DMA	:	dynamic mechanical thermal analyzer
DMP	:	Differential microemulsion polymerization
D_n	:	number-average diameter
DRC	:	dry rubber content
DSC	:	Differential scanning calorimetry
FTIR	:	Fourier Transform Infrared Spectroscopy
GE	:	Grafting Efficiency
GPC	:	Gel Permeation Chromatography
IP	:	Isoprene
ISO	:	International Standardization for organization
MMA	:	methyl methacrylate
N	:	number of polymer chains per particle
NaSS	:	sodium styrene sulfonate
NMR	:	Nuclear Magnetic Resonance
N_p	:	The total number of latex particle in the system
NR	:	natural rubber
OsO_4	:	Osmium Tretraoxide
PIP	:	polyisoprene
PMMA	:	poly(methyl methacrylate)
PS	:	polystyrene
PSD	:	particle size distribution

RAFT	:	reversible addition-fragmentation chain-transfer polymerization
SDS	:	sodium dodecyl sulfate
SEM	:	Scanning electron microscopy
ST	:	Styrene
TEM	:	Transmission Electron Microscope
TGA	:	Thermogravimetric analysis
T_g	:	Glass Transition Temperature
T_{id}	:	initial decomposition temperature
T_{max}	:	maximum decomposition temperature
V50	:	2,2'-Azobis(2-methylpropionamidine) dihydrochloride
VTS	:	Vinyl trimethoxysilane
ZDEC	:	zincdiethyl dithiocarbamate
ZnO	:	zinc oxide

จุฬาลงกรณ์มหาวิทยาลัย
CHULALONGKORN UNIVERSITY

CHAPTER I

INTRODUCTION

1.1 Motivation

Nanocomposite material are composed of the properties of the inorganic particles and an organic polymer; their combined effects have more potential for many applications. Silica is an important inorganic nano-fillers in composite preparation and widely used as effective reinforcement component in improving mechanical properties of polymers and rubbers. Therefore, polymer/silica nanocomposites have grown to being the focus of substantial academic and industrial research. Nevertheless, the silica particle is incompatible with the polymer because of high polarity of the silica surface and low polarity of polymer matrix, resulting in the agglomeration of silica particles. Thus, the silica surface should be modified with silane coupling agents to improve adhesion between the silica filler and the polymer. Grafting of polymer chains onto silica nanoparticles is one of the effective methods to increase the hydrophobicity of the particles and to improve interfacial interactions in nanocomposites resulting in better compatibility and dispersion of silica particles in the polymer matrix.

Recently, reversible addition-fragmentation chain-transfer polymerization (RAFT) is one of controlled /living radical polymerization (CRP) which synthesizes polymers with well-defined structure, high molecular weight and narrow polydispersity of molecular weight. However, the RAFT mechanism lacks the ability for propagating chains under RAFT control such as slow polymerization rate, poor control of molecular weight, low colloidal stability due to the interaction between the RAFT agent and emulsifier. Hence, the RAFT agent is developed with a water-soluble polymer and can be successfully employed in emulsifier-free emulsion polymerization. Moreover, the emulsion polymerization method is an industrial process because it provides environmental-friendly process, the heat of reaction is easily released during the polymerization and the viscosity of medium remained close to that of water during the polymerization. Therefore, RAFT emulsifier-free emulsion polymerization has been applied to synthesize the nanocomposite material.

1.2 RAFT Polymerization

Controlled /living radical polymerization (CRP) has been one of the most effective methods to synthesize polymers with well-defined structure, high molecular weight and narrow polydispersity of molecular weight [1-3]. Based on this technique, three main types of CRP have been investigated: nitroxide-mediated polymerization (NMP), atom-transfer radical polymerization (ATRP) and reversible addition-fragmentation chain-transfer polymerization (RAFT). Among the CRP techniques, RAFT polymerization is advantageous and efficient since it can be readily applicable to a wide range of monomers and reaction conditions [4-7]. The key of the RAFT polymerization process is the RAFT agent as a small organic molecule (thioester) which is responsible for controlling chain growth. This RAFT agent is composed of weak C-S bonds, reactive C-S double bonds, free radical leaving groups R• (which must be able to reinitiate polymerization) and a Z-group which controls the reactivity of the C-S double bond (influences the rate of radical addition and fragmentation) [8, 9]. The mechanism of RAFT polymerization is shown in Figure 1.1. The control in a RAFT polymerization is achieved by a degenerative transfer mechanism due to the presence
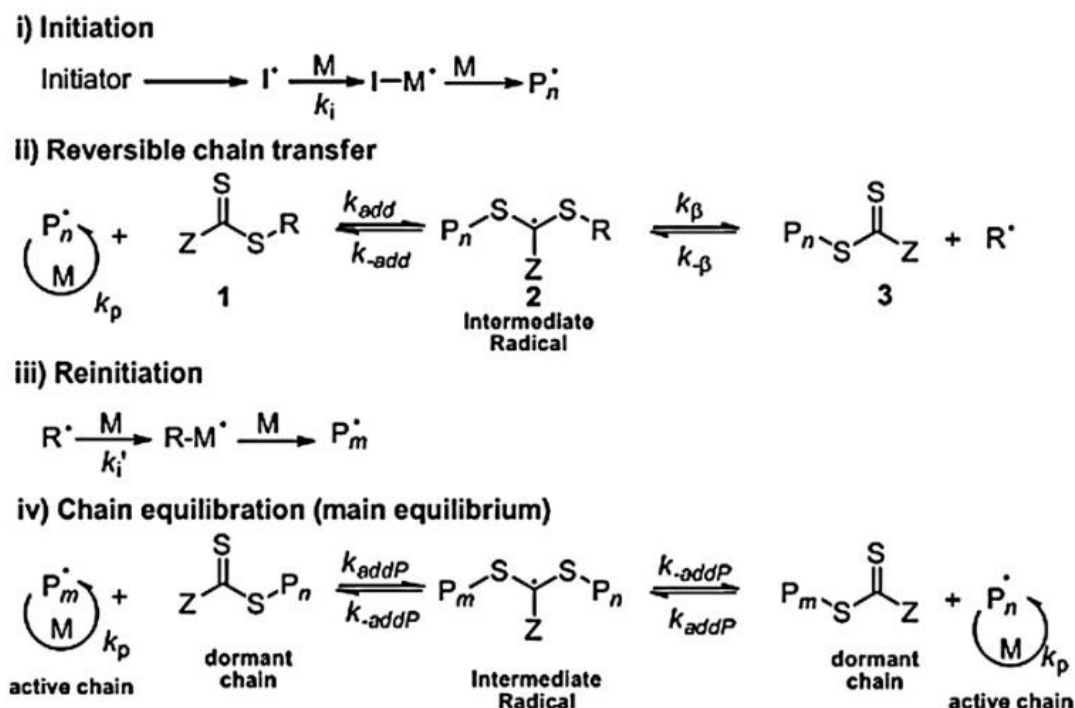
Figure 1.1 Mechanism of RAFT polymerization [10].

of a chain transfer agent (CTA) with the general structure RSC(=S)Z (1). As in conventional free radical polymerization, initiation is accomplished using traditional thermal, photochemical or redox. Then, the primary radicals formed will rapidly react with the CTA, yielding an intermediate radical (2) that fragments, producing a new thiocarbonylthio compound (3) and the radical R•. This radical reinitiates the polymerization by reaction with a monomer, creating a propagating chain. The rapid equilibrium between propagating (P_n and P_m) and dormant chains leads to the same probability for all chains to grow, providing well defined polymers [10]. It can be noted that the original RAFT functionality is retained at the end of chain when diblock structures are formed using RAFT controlled polymerization. Interestingly, water-soluble polymers are used for cooperating with the RAFT agent and this chemical structure is called the macro-RAFT agent which was achieved in the emulsion polymerization [11, 12].

Ferguson et al. [13] investigated that the synthesis of $(AA)_x$-$(BA)_y$-RAFT molecule via ab initio RAFT emulsion polymerization.

Acrylic acid (AA) as a water-soluble monomer was used to prepare macro-RAFT agent and then butyl acrylate (BA) was added under controlled feed to form polymer. The emulsion showed the small particle size (60.3 nm) with a narrow polydispersity (1.11) at the completed polymerization. Furthermore, this polymerization also had good colloidal stability and thus containing no free stabilizer.

Chaduc et al. [14] studied the preparation of poly(acrylic acid)(PAA)-stabilized polystyrene particles via RAFT emulsion polymerization. The AA monomer was prepared with RAFT agent to produce macro-RAFT agent and further used in water for the polymerization of styrene at different pHs. It was shown that the acidic condition (pH = 2.5) led to stable particles composed of well-defined copolymers with small particle size (<50 nm).

Rieger at el. [15, 16] reported that poly(ethylene oxide) macro-RAFT agent was successfully used in the emulsion polymerization of styrene and n-butyl acrylate (*n*BA). This approach presented the easy formation of copolymer latex with high solid content (24 wt%). Moreover, the copolymerization of *n*BA and MMA (methyl methacrylate) using PEO macro-RAFT agent via RAFT emulsion polymerization was also studied. The formation of copolymer provided that the molar percentage of MMA did not

exceed approximately 75% due to the aggregation of block copolymer micelles, however, the stable particles in all experiments were achieved.

Fréal-Saison et al. [5] investigated the emulsion polymerization of styrene in the presence of sodium acrylate with RAFT agent. The stable latex with narrow particle size distribution was observed. In addition, M_n of the product reached the expected value and the final polymer chains can be extended, when the latex was used for the next step of polymerization.

Mitsukami et al. [17] studied that the synthesis of a block copolymer with sodium 4-vinylbenzoate using a dithioester-capped sodium styrene sulfonate homopolymer as a macro-RAFT agent. These experiment was prepared directly in aqueous solution and the particle diameters of polymer matrix in the range 18-38 nm were achieved.

However, the RAFT mechanism lacks the ability for propagating chains under RAFT control (slow polymerization rate, poor control of molecular weight, low colloidal stability, etc.) due to the interaction between the RAFT agent and emulsifier [12]. In the absence of emulsifier, it was also an environmentally desirable choice for preparation of polymer particles at low impurity content [18, 19]. Therefore, RAFT emulsifier-free emulsion polymerization was investigated to find other stabilizers instead of emulsifiers. Previously, RAFT emulsifier-free emulsion polymerization of styrene was investigated in the presence of sodium acrylate (comonomer) and dibenzyltrithiocarbornate which resulted in a stable emulsion with a narrow particle size distribution [5]. The preparation of n-butyl acrylate using poly(ethylene oxide) based trithiocarbonate as a chain transfer agent presented the well-controlled polymer chains and a high conversion [16].

Ji et al. [12] studied the surfactant-free synthesis of amphiphilic diblock copolymer in aqueous phase by a self-stability process. Amphiphilic polymeric particles with hydrophobic cores and hydrophilic shells were prepared via living radical emulsion polymerization of styrene using a water-soluble poly(acrylamide)-based macro-RAFT agent in aqueous solution in the absence of any surfactants. The stable polymeric nanoparticles with small diameter and narrow particle size distribution, analogous to block copolymer ''crew-cut'' micelles without using an organic cosolvent

were prepared. The formation mechanism of the amphiphilic copolymer in situ was also investigated, and a self-stability process was suggested.

Yeole et al. [11, 20] studied surfactant free emulsion polymerization of styrene in the presence of macro-RAFT agent. A macro-RAFT agent was prepared by homopolymerization of sodium styrene sulfonate (NaSS) in aqueous phase by using dithioester as chain transfer agent. This synthesized polystyrene sulfonate–sodium based macro-RAFT agent, which was essentially water soluble macromolecular chain transfer agent used for the surfactant-free batch emulsion polymerization of styrene. Besides, the different concentration and molecular weight of poly(styrene sulfonate) based macro-RAFT agents had an influence on self-assembly, colloidal stability and particle size distribution.

Chen et al. [3] studied the synthesis and self-assembly of amphiphilic gradient copolymer via RAFT emulsifier-free emulsion polymerization. Amphiphilic gradient copolymers of 2,2,2-trifluoroethyl methacrylate (TFEMA) and acrylic acid (AA) was synthesized by using amphiphilic RAFT agent via emulsifier-free emulsion polymerization with a starved feed method of adding TFEMA. Different co-solvents were added into polymerization system to inhibit homopolymerization of AA in aqueous phase. It was found that adding 5wt% acetone into dispersion medium effectively inhibited the homopolymerization of AA and the copolymerization reaction shows first-order kinetics, demonstrating that the copolymerization proceeds in a controlled manner.

The macro-RAFT agent, which was combined with the RAFT agent and a water-soluble polymer, can be effectively provided in emulsifier-free emulsion polymerization. The emulsion polymerization method was more attractive due to water as the media in process, so this preparation was an environmentally friendly, non-toxic and inexpensive. Therefore, RAFT emulsifier-free emulsion polymerization had been applied to prepare the nanocomposite material.

1.3 Micromulsion Polymerization

Microemulsion polymerization is alternative technique for preparing polymer nanocomposites with small particle size, narrow particle size distribution and stable emulsion. Stoffer et al. [21] firstly reported the concept of microemulsion polymerization. Based on microemulsion method, the surfactant and monomer amount had an effect on this process and the very small particles in a range 10-100 nm of this system were produced. Microemulsions are thermodynamically stable, isotropic with optically transparent dispersion of immiscible liquids (oil and water) and obtained in a surfactant system. An oil-in-water or water-in-oil, microemulsion consists of small droplets surrounded by a surfactant monolayer. The small droplets is commonly used as a criterion for the synthesis of the microemulsions. The very low interfacial tension of the small droplets affect the thermodynamic stability of microemulsions resulting in the formation of the microemulsion is a spontaneous system. Nevertheless, a large surfactant amount (about 10–15% based on monomer weight) is required for achieving thermodynamic stability of the microemulsions [22]. Moreover, microemulsions have been successfully used in many polymeric materials and chemical reactions because of effective qualities of thermodynamic stability, optical transparency, solubilization of substrates, very large interfacial area and very low interfacial tension.

The mechanism of microemulsion polymerization is similar to emulsion polymerization with a large surfactant amount. For mechanism of oil-in-water microemulsions, the polymerization is initiated by radicals generated within the oil droplets (oil-soluble initiator) or by the entry of radicals into the droplets (water soluble initiator). Next, nucleated particles grow by diffusion of monomer from inactive droplets through the continuous phase resulting in the polymer particles are larger than the starting droplets and are accompanied by empty small surfactant micelles at the end of the polymerization [23].

Previously, Gan et al. [24] studied the synthesis of polystyrene via microemulsion polymerization. Potassium persulfate (KPS) as water-soluble initiator, cetyltrimethyl ammonium bromide (CTAB) as surfactant and a glycol type as cosurfactant were used in these process. It was found that a small particle of diameter (20-40 nm) and a high molecular weight ($5\text{-}10\times10^6$) were produced.

Larpent et al. [25] investigated the preparation of styrene-in-water microemulsion using sodium dodecyl sulfate (SDS) as surfactant and hydroxyalkyl acrylates or methacrylates as cosurfactants. The monomer conversion increased to 100% at room temperature and the well-defined highly functionalized nanoparticles (15–25 nm) were achieved. However, the monomer amount was extremely low and lower than the surfactant amount used.

However, the high surfactant amount was used in a microemulsion polymerization process, sometimes even higher than the monomer concentration. For industrial applications, low surfactant amount and high polymer content are required because of the high cost of surfactant and post-treatment for removing the surfactant after polymerization. This problem limits the microemulsion polymerization from being scaled up to an industrial level. Besides, the surfactant also has significantly negative impact on the physical properties of polymers. Thus, the challenges of microemulsions are decreasing surfactant amount, increasing monomer content and improving the purity of the products. Differential microemulsion polymerization (DMP) is a new approach to solve this problem. DMP method is water as solvent, a surfactant, insoluble monomer and a water-soluble initiator and a certain temperature to initiate the polymerization and suitable agitation to form an emulsion are required. The very small droplets of monomer was added continuously and slowly until the polymerization was completed. The DMP process can produce the similar particles as in traditional microemulsion polymerization and use a small surfactant concentration.

He at el. [26] reported that poly(methyl methacrylate) nanoparticles were successfully synthesized via differential microemulsion polymerization process using ammonium persulfate (APS) as initiator and SDS as surfactant. The effect of surfactant concentration was investigated on the particle size and polymer content. A particle size of less than 20 nm in diameter has been achieved with low surfactant concentration (5.5% based on monomer weight) under mild reaction condition.

Norakankorn et al. [27] studied the preparation of nanosized poly(methyl methacrylate) initiated by 2,2'-azoisobutyronitrile via differential microemulsion polymerization. The polymer particles with a molecular weight of around 1×10^6 and a particle size of about 20 nm can be achieved using mild conditions. The surfactant

amount in a typical condition was also used as low as 1/130 of the monomer amount in weight.

Yuan et al. [28] investigated the synthesis of poly(methyl methacrylate) nanoparticles using differential microemulsion polymerization. At a very low surfactant concentration (3 wt% based on monomer weight), a particle size of polymer emulsion was less than 20 nm and high monomer conversion (95%) and molecular weight (1.3×10^5) were observed.

The synthesis of polymer nanoparticles via differential microemulsion polymerization using an extremely low surfactant concentration can be achieved with high monomer conversion and high polymer content. In addition, DMP is suitable for a green commercial industry because of the absence of organic solvents under mild reactions.

1.4 Silica Surface Modification

One of the most popular inorganic nano-fillers in composite preparation is silica which is used for many applications such as adsorbents, catalyst supports, etc. Furthermore, silica nanoparticles are frequently used as reinforcing fillers in rubbers and polymers for improving their mechanical properties [29]. However, silica nanoparticles have a tendency to form agglomerates because of the large quantity of hydroxyl groups on the silica surface and the high surface energy and polarity, resulting in inferior compatibility and less stability between the silica and polymer matrix. Therefore, the silica surface is usually modified to improve adhesion between the silica filler and the polymer.

Generally, silica surface modification can be carried out by either physical or chemical methods. For physical methods, electrostatic and other types of Van der Waals interactions are the main driving forces in preliminary surface modification of silica. The process commonly involves surfactants or macromolecules to adsorb onto silica surface resulting in a polar group of surfactants is adsorbed to the silica surface by an electrostatic interaction. Thus, the physical attraction between the silica particles within the agglomerates is decreased and this procedure is easy for the silica particles to become incorporated into the polymer matrix [30, 31]. For instance, the presence of stearic acid adsorbed on the silica surface to reduce the agglomeration of silica

nanoparticles and the interaction between the filler and polymer matrix [32]. The surface of silica nanoparticle was modified with cationic surfactant cetyltrimethylammonium bromide (CTAB) to present the good dispersion stability and improve the interaction between silica and the polymer emulsion [33]. However, both of these physical interactions are in nature which led to be weak compared to chemical reactions.

Therefore, chemical treatment of the nanoparticle surface is necessary to improve compatibility and dispersion of the filler in the polymer matrix. Chemical system involve modification either with modifying agents or by grafting polymers. Silane coupling agents are usually used to treat the silica surface because of their unique bifunctional structure. They have hydrolyzable ends, which are capable of reacting with the silanol groups on the surface of silica through hydrolysis and polycondensation to form siloxane linkages (Si-O-Si bonds), and an organofunctional end, which has the ability to initiate the desired chemical reactions [34]. $RSiX_3$ stand for the general structure of the coupling agents, where the X represents the hydrolyzable groups, which are typically ethoxy, methoxy, or chloro groups. The organo, R, group can have a variety of functionalities depending on the requirements of the polymer.

Table 1.1 Typical silane coupling agents used for surface modification of silica nanoparticles [35].

abbreviation	name	chemical struture
APMDES	aminopropyl methydiethoxysilane	$H_2N(CH_2)_3(CH_3)Si(OC_2H_5)_2$
APMDMOS	(3-acryloxypropyl)methydimethoxysilane	$CH_2=CHCOO(CH_2)_3(CH_3)Si(OCH_3)_2$
APTES (APTS, APTEOS, APrTEOS)	3-aminopropyltriethoxysilane	$H_2N(CH_2)_3Si(OC_2H_5)_3$
APTMS (APTMOS, APrTMOS)	3-aminopropyltrimethoxysilane	$H_2N(CH_2)_3Si(OCH_3)_3$
APTMS (APTMOS)	(3-acryloxypropyl)trimethoxysilane	$CH_2=CHCOO(CH_2)_3Si(OCH_3)_3$
APTMS (APTMOS)	aminophenyltrimethoxysilane	$H_2NPhSi(OCH_3)_3$
TESPT	bis(triethoxysilylpropyl)tetrasulfane	$(C_2H_5O)_3Si(CH_2)_3S_4(CH_2)_3Si(OC_2H_5)_3$
DDS	dimethyldichlorosilane	$(CH_3)_2SiCl_2$
GPS (GPTS, GOTMS, GPTMOS, KH560)	3-glycidoxypropyltrimethoxysilane, 3-glycidyloxypropyltrimethoxysilane	$CH_2(O)CHCH_2O(CH_2)_3Si(OCH_3)_3$
ICPTES	3-isocyanatopropyltriethoxysilane	$OCN(CH_2)_3Si(OC_2H_5)_3$
MMS	methacryloxymethyltriethoxysilane	$CH_2=C(CH_3)COOCH_2Si(OC_2H_5)_3$
MPS (MPTMS, MPTS, MAMSE, MATMS, MSMA, TPM, MEMO, KH570)	methacrylic acid 3-(trimethoxysilyl) propyl ester, 3-(trimethoxysilyl)propyl methacrylate, 3-methacryloxypropyltrimethoxysilane	$CH_2=C(CH_3)COO(CH_2)_3Si(OCH_3)_3$
MPTES	methacryloxypropyltriethoxysilane	$CH_2=C(CH_3)COO(CH_2)_3Si(OC_2H_5)_3$
MPTS	mercaptopropyl triethoxysilane	$SH(CH_2)_3Si(OC_2H_5)_3$
MTES	methyltriethoxysilane	$CH_3Si(OC_2H_5)_3$
PTMS	phenyltrimethoxysilane	$PhSi(OCH_3)_3$
VTES	vinyltriethoxysilane	$CH_2=CHSi(OC_2H_5)_3$
VTS	vinyltrimethoxysilane	$CH_2=CHSi(OCH_3)_3$

The functional group X reacts with hydroxyl groups on the silica surface, while the alkyl chain may react with the polymer chain. Hydrophobic silica can be obtained. Some typical silane coupling agents used for surface modification of nanosilica are listed in Table 1.1 [35].

Silane coupling agents have been used to improve the hydrophobic nature of surface in chemical surface modification [36, 37]. Sun et al. [38] described the mechanism of silane treatment in three models of grafting as illustrated in Figure 1.2. The first molecule of silane couple agent is grafted onto the silica surface, and other molecules are condensed on the one which has been grafted as explain the first model. Model II is geometrically impossible which assumes that the silane forms three siloxane bonds. The last model is more realistic which involves the grafting reaction of the silane and condensation reaction. Moreover, Lin et al. [39] reported that 3-glycidoxypropyl trimethoxysilane was successfully grafted onto the silica surface and Haldorai et al. [40] revealed that silica surface was modified by methacryloxypropyl trimethoxysilane (MPTMS) which is capable of copolymerizing with styrene and provides a reactive C=C bond. The ideal result of surface treatment is to break down the agglomeration of silica nanoparticles, to produce nanostructural composites and to achieve the homogeneity of the nanosilica in the polymer latex.
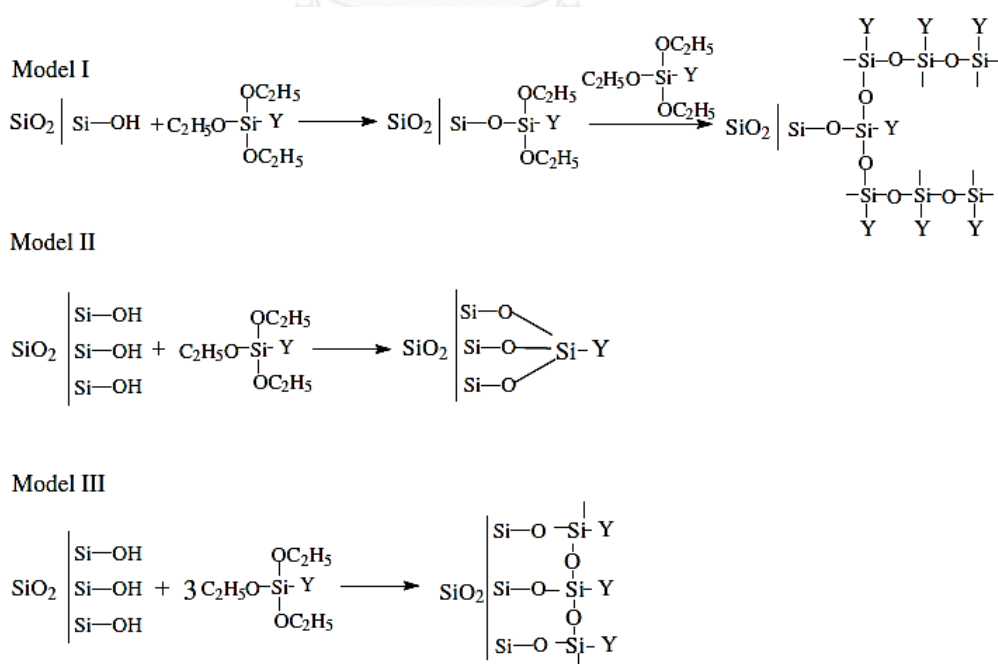
Figure 1.2 Grafting and polycondensation mechanism of silane coupling agent on silica particles, with Y is the organic functional group [38].

1.5 Polymer-Silica Nanocomposites

Nanocomposite materials are composed of the properties of the inorganic particles and an organic polymer; their combined effects have more potential for many applications in mechanical, optical and/or gas barrier engineering [10, 41, 42]. Nanocomposites often use special properties of nano-fillers to improve the properties of materials which the small fillers leads to a dramatic increase in interfacial area as compared with traditional composites. The interfacial area makes a significant volume fraction of interfacial polymer with properties different from the bulk polymer at low loadings [43, 44]. Silica is an important inorganic nano-fillers in composite preparation and widely used as effective reinforcement component in improving mechanical properties of polymers. Therefore, polymer/silica nanocomposites have received much attention in recent years and have been employed in many applications.

The traditional process of preparing polymer/silica composites is direct mixing of the silica into the polymer. Generally, the mixing can be done by melt and solution blending. The effective dispersion of the silica nanoparticles in the polymer matrix is the main difficulty in the mixing method due to the agglomeration of silica. Melt blending is usually used because of its efficiency, operability, and environmental containment. Nevertheless, it is difficult to prepare a homogeneous dispersion of nanoparticles in a polymeric latex as a result of the strong agglomerated tendency of nanoparticles. Thus, nanoparticle filled polymers occasionally contain a number of loosened clusters of particles and present properties even worse than conventional particle/polymer systems [45].

Pérez et al. [46] investigated the styrene-butadiene rubber (SBR)/silica nanocomposites prepared by melt blending. The addition of silica in the process resulted in increasing the glass transition temperature (T_g) and thermal resistance while the modulus and tensile strength slightly increased because of the adhesion of the nano-filler in the rubber nanocomposites. Moreover, the polymer and polymer blend such as polystyrene (PS) [47], polyethylene (PE) [48, 49] and polypropylene (PP) [46, 50] filled with silica have been reported. Solution blending is a liquid-state powder processing method that provides a good molecular level of mixing and is widely used in material preparation. Some limitations of melt mixing can be overcome when both of the polymer and the nanoparticles are well dissolved or dispersed in solution. However, a

high solvent amount and a high cost depending on the solvent and its recovery are required. Many polymers show good mixing with silica using this method [51, 52].

The synthesis of polymer/silica nanocomposites via direct mixing causes to physisorption, which is a relatively weak interaction and it is sensitive to chemical reagents and temperature resulting in easy desorption. Hence, various chemical methods could be applied to produce polymer/silica nanocomposites providing strong covalent bonds with functional groups. Grafting polymer onto the silica surface is one of the effective processes methods to increase the hydrophobicity of the silica particles and to improve interfacial interactions in nanoparticles resulting in better compatibility and dispersion of silica fillers in the polymer matrix. It can be noted that modification of nanoparticles through graft polymerization was very productive to prepare nanocomposites as a result of an increase in hydrophobicity of the nanoparticles that is useful to the filler/matrix miscibility, and an improved interfacial interaction yielded by the molecular entanglement between the grafting polymer on the nanoparticles and the polymer latex [53, 54]. Grafting polymer onto a silica surface by polymerization is characterized by many benefits, such as simple, low cost, easy control and widely applicability.

Lee et al. [55] investigated that polystyrene (PS)/silica composite particles have been successfully synthesized via surfactant-free emulsion polymerization and the incorporation of silica particles provided an enhancement in the thermal stability due to the strong interaction between silica and the polystyrene molecules. According to Kongsinlark et al. [18], monodispersed polyisoprene (PIP)-SiO_2 nanoparticles were produced (20-60 nm) via differential microemulsion polymerization (DMP) and exhibited reduced nano-SiO_2 aggregation in the PIP matrix and the surfactant concentration used was around 3% based on monomer weight and PIP-SiO_2 has been used as an effective nano-filler in a NR latex. In addition, from synthesis of poly(methyl methacrylate) (PMMA)/SiO_2 particles via emulsion polymerization, PMMA polymer could be grafted on the silica surface (37% grafting) and the silica particles became of lower aggregation [56].

Interestingly, RAFT emulsion polymerization has been applied to synthesize the nanacomposites with an inorganic particle and organic polymer. For 6-azidohexyl methacrylate polymerization mediated by 4-cyanopentanoic acid dithiobenzoate

anchored nano-silica, the surface-initiated RAFT polymerization combined with click reactions provided a way to modify the surface of nanoparticles with various functional polymers [57]. Generally, the surface of silica was functionalized with methyl methacrylate groups for improving the dispersion of silica. Recently, poly(methyl methacrylate)/silica nanocomposites have been synthesized via RAFT polymerization, and showed the best improvement of mechanical and thermal properties at 7 wt% silica in the nanocomposites [42]. Alternatively, the hydroxyl group on the silica surface could also be modified by the condensation reaction of 3-glycidyloxypropyl trimethoxysilane and 2-butyric acid dithiobenzoate as RAFT agent and then the RAFT agent anchored on the surface of silica nanoparticles could effectively react with the styrene via RAFT polymerization. These polystyrene-silica composites exhibited good controlled molecular weight and a narrow PDI (less than 1.1) [58].

1.6 Mechanical Properties of Polymer Nanocomposites

One of the important motivations for adding inorganic fillers to polymers matrix is the improve of their mechanical performance; the mechanical properties of polymer nanocomposites being a major concern [59]. The mechanical behavior of a polymer could be characterized by its stress–strain properties. A tensile method is broadly used to evaluate the mechanical properties of the nanocomposite products, and accordingly tensile strength, modulus and the elongation at break are three main variable obtained. These parameters was investigated with different silica content.

Bikiaris et al. [60] reported the properties of isotactic polypropylene-SiO_2 nanocomposites with untreated and surface-treated silica nanoparticles prepared by melt compounding. The mechanical properties after nanoparticle addition were slightly improved. A maximum in mechanical properties presented at 2.5 wt% silica content of both untreated and surface-treated silica. The silica amount higher than 2.5 wt% in the polymer latex resulted in decreased mechanical properties. This can be explained that the increased tendency of silica nanoparticles resulted to agglomerate at higher concentrations.

Hong et al. [61] studied that poly(methyl methacrylate) (PMMA) was introduced onto the silica surface by particle pretreatment using silane coupling agent (γ-methacryloxypropyl trimethoxy silane, KH570) followed by solution

polymerization. By adding silica nanoparticles into PMMA, the tensile strength and tensile modulus of silica reinforced PMMA films increased up to 95.8% and 193.2% in comparison with neat PMMA film.

Zhu et al. [62] reported the preparation of the core–shell poly(methyl methacrylate) (PMMA)-SiO_2 nanoparticles in an aqueous solution by suspension–dispersion–polymerization (SDP). The PMMA-SiO_2 nanoparticles were subsequently used as filler in a poly (vinyl chloride) (PVC) matrix. The results demonstrated that the addition of PMMA-SiO_2 into PVC latex led to increased tensile strength and elongation at break using very low (5 wt%) filler content.

Buhin et al. [63] studied the influence of monomer ratio, butyl acrylate (BA), and methyl methacrylate (MMA) as well as silica nanofiller morphology (pyrogenic and colloidal) and the properties of polyacrylate film (PA) synthesized by in situ emulsion polymerization. It was found that the colloidal silica nanofiller (10%) in poly(BA-co-MMA) 50/50 systems significantly increased strength at break and slightly decreased elongation at break compared to neat PA matrix. Thus, the addition of higher amounts of colloidal silica improved mechanical properties.

Rubber is a high molecular weight polymeric material, with high elongation and excellent resilience possessing low tensile strength and modulus and poor creep characteristics resulting to the limits for rubber applications. Silica is one of the reinforcing substances used, so fillers as silica are usually added to rubber in order to improve the mechanical properties of the composites. The use of silica particles, instead of carbon black, has proven to be of interest for rubber reinforcement [64].

Gauthier et al. [65] reported silica-filled styrene-butadiene rubber (SBR) by varying filler amount and surface treatment of silica. The use of coupling agents promoted the covalent bond between rubber and fillers to reduce the amplitude of the non-linear phenomenon resulting in improved tensile strength of the rubber.

Suzuki et al. [66] investigated the effect of rubber/filler interactions on the stress-strain behavior for silica filled styrene-butadiene rubber (SBR) vulcanizates. The rubber/filler interactions were controlled by the modification of the silica surface using several kinds of silane coupling agents. A chemical structure of bis-(3-triethoxysilylpropyl)-tetraslufide (TESPT) produced a strong chemical bonding between SBR and silica, which enhanced the tensile stress at a larger strain.

Furthermore, in the case of mono-functional coupling agents, the tensile stress at a larger strain decreased with an increase in the length of the alkyl chains in the coupling agents. The results explained that monofunctional coupling agents with long alkyl units worked as a plasticizer for rubber molecules.

Peng et al. [67] studied the preparation of natural rubber/silica (NR/SiO$_2$) by combining self-assembly and latex-compounding techniques. The SiO$_2$ nanoparticles were homogenously distributed in the NR matrix. The incorporation of silica nanoparticles into the elastomer latex led to a significant improvement in the mechanical properties of the elastomer. The tensile strength, tensile modulus as well as tear strength of the resulting nanocomposite markedly increased at SiO$_2$ content (2.5–4 wt%).

Liu et al. [68] reported the properties of styrene–butadiene rubber (SBR) filled with silica powder prepared by solution polymerization which was modified by three silane coupling agents of 3-methacryloxypropyl trimethoxy silane (MEMO), [3-(2-aminoethyl)aminopropyl] trimethoxy silane (AMMO), and bis[3-(triethoxysilyl) propyl] disulfide (TESPD). SBR filled with silica powder modified by MEMO showed better filler dispersion and mechanical properties in tensile strength, modulus at 300%, hardness and tear strength as compared with unfilled SBR and SBR filled with unmodified silica powder.

Chuayjuljit et al. [69] studied the polystyrene (PS)-encapsulated nanosilica used as a filler in the NR matrix. The properties of NR, tensile strength and modulus at 300% strain were found to be increased by the incorporation of PS-encapsulated silica at 9 phr, whereas the elongation at break deteriorated with the incorporation of PS-encapsulated silica nanoparticles.

1.7 Thermal Stability of Polymer Nanocomposites

Thermal properties are the properties of materials that change with temperature. The thermal analysis have many techniques (such as DSC, TGA, DTA, DMA/DMTA, etc.) to examine the properties of samples. TGA/DTA and DSC are the most widely used methods to determine the thermal properties of polymer nanocomposites. TGA can describe the thermal stability, the onset of degradation, and the percent silica incorporated in the polymer nanocomposites and DSC can be efficiently used to

determine the thermal transition behavior of polymer/silica nanocomposites. Normally, the incorporation of nanosized inorganic particles into the latex would enhance the thermal stability by acting as a superior insulator and mass transport barrier to the volatile products generated during decomposition [70].

Li et al. [71] reported the thermal degradation kinetics and morphology of natural rubber/silica (NR/SiO_2) nanocomposites. The nanocomposite with a SiO_2 content of 4 wt% was prepared by incorporating latex compounding with self-assembly methods. The SiO_2 particles are homogenously dispersed throughout the NR latex as spherical nano-clusters with an average size of 75 nm. The thermal stability of the nanoparticles is significantly improved in comparison to unfilled NR. The initial, peak and final degradation temperatures of the nanocomposite increased 17.9 °C, 17.0 °C, and 14.9 °C, respectively, over the host NR. At a given degradation temperature, the degradation rate and frequency factor of the nanocomposite are lower than those of unfilled NR because of a significant retarding effect of the SiO_2 particles. The significantly improved thermal stability of the nanocomposite is attributed to the addition of SiO_2 nanoparticles into the NR matrix which the silica and NR molecular chains strongly interact through various effects. Hence, the diffusion of degradation products from the NR latex to the gas phase is slowed down. Consequently, the nanocomposite has a more complex degradation and better thermal stability than those of unfilled NR.

Shang et al. [72] investigated the compatibility of soluble polyimide (PI)/SiO_2 composites induced by the coupling agent γ-glycidyloxypropyl trimethoxysilane (GOTMS). The PI/SiO_2 composites present higher thermal stabilities in comparison with pure PI. The thermal decomposition temperature (T_d) of a composite increased with its silica content and were higher than that of the unfilled PI. The T_g of the composites increased with increasing silica content. It can be noted that the coupling agent strengthened the interaction between the organic polymer matrix and the inorganic mineral particles caused an increased restricting strength of silica on the PI. Moreover, the coupling agent reduced the agglomeration of silica particles and thereby greatly increased the interfacial area at a given silica content. In addition, the reduced agglomeration of silica particles resulted in an increase in the cross-linking density. All

of these parameters led to a higher T_g for the PI/SiO$_2$ composites with a coupling agent than for pure PI.

Wang et al. [73] studied the natural rubber/silica (NR/SiO$_2$) nanocomposite with a SiO$_2$ content of 2 wt% prepared by the combining similar dissolve mutually theory with latex compounding techniques. The silica surface was modified with the silane-coupling agent before polymerization. The core-shell structure silica-poly(methyl methacrylate) (SiO$_2$-PMMA) nanoparticles were formed by grafting polymerization of MMA on the modified silica surface and then NR/SiO$_2$ nanocomposite was prepared by blending SiO$_2$-PMMA and PMMA-modified NR (NR-PMMA). The core-shell SiO$_2$-PMMA particles (60-100 nm) are well dispersed in latex at a suitable SiO$_2$/MMA ratio of 1:0.3, and the thickness of PMMA shell is about 25$-$ 35 nm. Furthermore, the dispersion of SiO$_2$-PMMA nanoparticles has been improved by grafting PMMA on both nano-SiO$_2$ and NR molecule chains. Based on the excellent dispersion of SiO$_2$-PMMA nanopaticles, T_g and thermal ageing resistances of nanocomposite are considerably enhanced.

1.8 Membrane Separation

Polymer-nanoinorganic particles composite membranes with inorganic nanopartices embedded in a polymer matrix present an interesting approach for improving the physical and chemical, as well as separation properties of membranes, since they possess characteristics of both organic and inorganic membranes such as good mechanical strength, thermal stability, permeability, selectivity, and so on. Much research and development are still needed to develop hybrid membranes for material science applications. [74]. In particular, silica nanoparticles are one of the most useful materials and are used as inorganic filler in practical preparation. Since the polymer/silica nanocomposites not only have improved physical properties such as the mechanical properties and thermal properties of the materials, but also exhibit some unique properties, which have attracted strong interest in many industries. Besides common plastic and rubber reinforcement, one potential and practical application of this nanocomposite is in membrane separation.

Pervaporation is one of the most interesting areas in membrane research and this process has been shown to be a necessary component for chemical separations. It
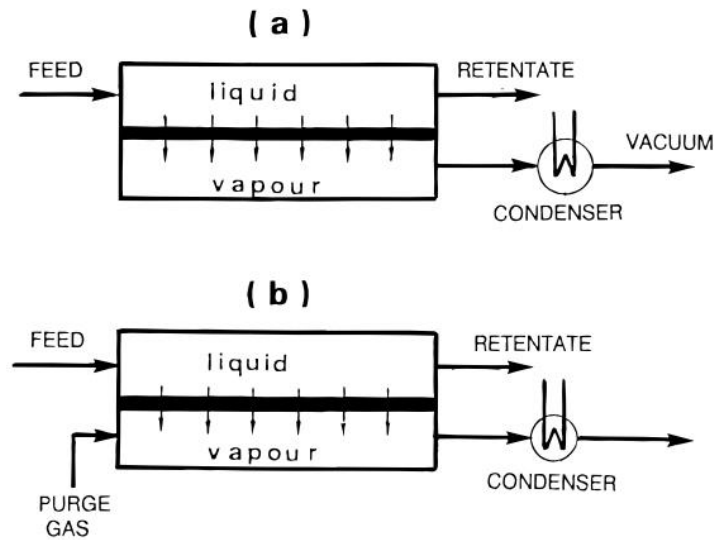
Figure 1.3 Schematic diagram of the pervaporation process (a) vacuum pervaporation,
(b) purge gas pervaporation [75].

is a relatively new membrane separation process that has elements in common with reverse osmosis and membrane gas separation. Figure 1.3 exhibits the pervaporation process, the liquid mixture to be separated (feed) is placed in contact with one side of a membrane and the permeated product (permeate) is removed as a low pressure vapor from the other side. The permeate vapor could be condensed and collected as desired. The chemical potential gradient across the membrane is the driving force for the mass transport. The driving force is created by applying either a vacuum pump or an inert purge (air or steam) on the permeate side to maintain the permeate vapor pressure lower than the partial pressure of the feed liquid. Nevertheless, vacuum pervaporation is used as the standard process and is the most widely useful mode of operation [75].

Because of the complicated penetrants-membrane interactions, it is difficult to formulate a single explanation for the complex transport process. There are two approaches to describe mass transport in pervaporation: the solution-diffusion model and the pore flow model. The solution-diffusion model as shown in Figure 1.4a, this model is accepted by the majority of membrane researchers. The pervaporation mechanism consists of three steps: i) sorption of the permeant from the feed liquid to the membrane, ii) diffusion of the permeant in the membrane, and iii) desorption of the permeant to the vapor phase on the downstream side of the membrane. For the pore flow model (Figure 1.4b), it is supposed that there are a bundle of straight cylindrical
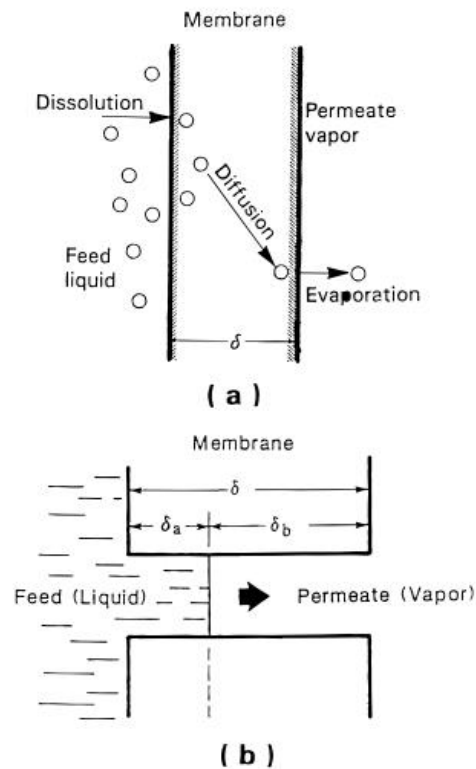
Figure 1.4 Schematic representation of the pervaporation transport mechanism
(a) solution-diffusion model, (b) pore flow model [75].

pores on the membrane surface. The mass transport by the pore flow model also consists
of three steps: i) liquid transport from the pore inlet to a liquid-vapor phase boundary,
ii) evaporation at the phase boundary, and iii) vapor transport from the boundary to the
pore outlet.

Nowadays, many research and development have been associated with organic-
inorganic nanocomposites for membrane preparation in order to achieve a good
separation. According to Liu et al. [76], silica nanoparticles in chitosan-silica complex
membranes used in pervaporation dehydration of ethanol-water mixtures served as
spacers between the polymer chains to provide extra space for water permeation, so as
to bring about high permeation rates within the complex membranes. Guo et al. [77]
reported that the addition of silica nanoparticles to chitosan would enhance the
selectivity and permeation flux of the complex membrane. A poly(vinyl alcohol)
(PVA)-SiO$_2$ nanocomposite membrane with the incorporation of silica particles into
PVA showed a high performance in pervaporative dehydration of an ethylene glycol
(EG) aqueous solution. The PVA-SiO$_2$ nanocomposite membrane exhibited desirable

changes in the morphology and crystalline structure of the membranes, and the thermal stability and stability of the membranes in EG aqueous solution were significantly enhanced.

Recently, Jadav et al. [78] studied a convenient synthesis method of polyamide nanocomposite membranes using silica nanoparticles. The nanocomposite membranes exhibited superior thermal stability than the pure polyamide membranes and the best membrane performance in terms of separation efficiency and productivity flux was observed in the membrane with a certain amount of silica loading. Zhao et al. [79] investigated that the polyelectrolyte complex (PEC)/SiO_2 nanohybrid membranes exhibited very high performance in iso-propanol dehydration as compared with other polymeric hybrid membranes. The selectivity of the membranes is slightly higher than that of pristine PEC membranes because of the fine dispersion of SiO_2. Besides, the incorporation of SiO_2 also improves the processability and mechanical properties of PEC. Sun et al. [80] reported the pervaporation of ethanol-water mixtures using organophilic nano-silica filled polydimethylsiloxane (PDMS) composite membranes. The solubility selectivity and the diffusion selectivity increased with an increase in organophilic silica concentration. Moreover, the composite membranes showed striking advantages in the total flux and separation factor as compared with unfilled PDMS membrane.

1.9 Objective and Scope of Dissertation

The principle objective of this research is to investigate the synthesis of polystyrene (PS)-SiO_2 and polyisoprene (PIP)-SiO_2 via RAFT emulsifier-free emulsion polymerization. Moreover, the preparation of poly(methyl methacrylate) (PMMA)-SiO_2 and poly(styrene-*co*-methyl methacrylate) (poly(ST-*co*-MMA))-SiO_2 via differential microemulsion polymerization are also studied. One approach is to improve the compatibility and dispersion of silica nanoparticles in the polymer emulsion. The focus on mechanical and thermal properties of natural rubber filled with the nanocomposites is also included.

In Chapter I, the concepts of RAFT polymerization and microemulsion polymerization are reviewed. The different techniques for modification of silica surface and synthesis of polymer/silica nanocomposites with historical and tutorial approaches

are reported. The overview of principal concepts of nanocomposites for different applications is also described.

In Chapter II, the experimental procedures for the synthesis of polymer-silica nanocomposites with good dispersion and high efficiency are reported as well as the preparation of polymer-silica nanoparticles filled natural rubber are presented. The various techniques are applied for characterization of nanocomposites and natural rubber products.

In Chapter III, the synthesis of PS-SiO$_2$ nanoparticles via RAFT emulsifier-free emulsion polymerization and the effect of macro-RAFT agent to initiator ratio on monomer conversion, particle size, particle size distribution, grafting efficiency and silica encapsulation efficiency are presented. The mechanical properties, thermal properties and oil swelling resistance of natural rubber filled with the PS-SiO$_2$ nanocomposites are also reported.

In Chapter IV, the RAFT emulsifier-free emulsion polymerization of PIP-SiO$_2$ nanoparticles using water-soluble initiators are investigated. The effect of initiator types and macro-RAFT agent to initiator ratio on monomer conversion, particle size, particle size distribution, grafting efficiency and silica encapsulation efficiency are studied. The mechanical and thermal properties of PIP-SiO$_2$ as nano-filler in natural rubber latex are also reported.

In Chapter V, the preparation of PMMA-SiO$_2$ nanoparticles via differential microemulsion polymerization are presented. The effects of process variables on monomer conversion, particle size, particle size distribution, grafting efficiency and silica encapsulation efficiency are investigated. A nanocomposite membrane from natural rubber latex and PMMA-SiO$_2$ emulsion was also studied for mechanical and thermal properties and pervaporation of water-ethanol mixtures.

In Chapter VI, the synthesis of poly(ST-*co*-MMA)-SiO$_2$ nanoparticles via differential microemulsion polymerization and the effect of process variables are studied. The mechanical and thermal properties and pervaporation performance (water-ethanol mixtures) of NR/poly(ST-*co*-MMA)-SiO$_2$ membranes are also studied.

In Chapter VII, the conclusions resulting from this study and recommendations for future work are summarized.

CHAPTER II

EXPERIMENTAL AND CHARACTERIZATION

2.1 Materials

2.1.1 Synthesis of Polystyrene-SiO_2 Nanocomposites

Nano-SiO_2 (Aerosil 200) with an average particle size of 12 nm was supplied by Degussa (Thailand). Vinyl trimethoxysilane (VTS, Sigma-Aldrich) was used as coupling agent. An ammonia solution (25% NH_4OH, Fisher Scientific) was used as catalyst for silica surface modification. Styrene (ST, $\geq$99%, Sigma-Aldrich) was washed with 5 wt% aqueous sodium hydroxide (NaOH, $\geq$98%, Sigma-Aldrich) to remove the inhibitor and dried over anhydrous magnesium sulfate ($MgSO_4$, $\geq$98%, EMD). Sodium styrene sulfonate (NaSS, Sigma-Aldrich), 4-cyanopentanoic acid dithiobenzoate (RAFT agent, Sigma-Aldrich) and sodium bicarbonate ($NaHCO_3$, pH value buffer, $\geq$99%, EMD) were used without further purification. 4,4'-azobis(4-cyanopentanoic acid) (ACP, initiator, Sigma–Aldrich) was purified by recrystallization from methanol (MeOH, Fisher Scientific). Hydroquinone (Sigma–Aldrich) was used to quench the reaction. The product was washed with methyl ethyl ketone (MEK, Sigma–Aldrich) to remove residual monomer and homopolymer. Deionized water was also used in all experiments.

2.1.2 Synthesis of Polyisoprene-SiO_2 Nanocomposites

Nano-SiO_2 (Aerosil 200) with an average particle size of 12 nm was supplied by Degussa (Thailand). The vinyl trimethoxysilane (VTS, Sigma-Aldrich) was used as coupling agent. An ammonia solution (25% NH_4OH, Fisher Scientific) was used as catalyst for silica surface modification. Isoprene monomer (IP, Sigma-Aldrich), sodium styrene sulfonate (NaSS, Sigma-Aldrich) and 4-cyanopentanoic acid dithiobenzoate (RAFT agent, Sigma-Aldrich) were used without further purification. 4,4'-azobis(4-cyanopentanoic acid) (ACP, Sigma–Aldrich) and 2,2'-Azobis(2-methylpropionamidine) dihydrochloride (V50, Wako Pure Chemical Industries, Ltd.) were used as water-soluble initiators. The methyl ethyl ketone (MEK, QRёC) was used for the rubber

coagulation. The product was washed with petroleum ether (PE, J.T.Baker) to remove residual monomer and homopolymer. Deionized water was also used in all experiments.

2.1.3 Synthesis of Poly(Methyl Methacrylate)-SiO$_2$ Nanocomposites

Nano-SiO$_2$ (Aerosil 200, particle size of 12 nm) was supplied by Degussa (Thailand). Vinyl trimethoxysilane (VTS, $\geq$98%, Sigma-Aldrich) and ammonia solution (25 wt% NH$_4$OH, QRëC) was used for silica surface modification. Methyl methacrylate (MMA, $\geq$99%, Sigma-Aldrich) was washed with 10 wt% aqueous sodium hydroxide (NaOH, $\geq$98%, QRëC) to remove the inhibitor and dried over anhydrous magnesium sulfate (MgSO$_4$, $\geq$98%, EMD). Ammonium persulfate (APS, $\geq$99%, Ajax Finechem), sodium dodecyl sulfate (SDS, $\geq$99%, Sigma-Aldrich), 1-pentanol (C$_5$H$_{11}$OH, Ajax Finechem), and sodium bicarbonate (NaHCO$_3$, $\geq$99%, EMD) were used as received. Deionized water was also applied for all polymerization processes.

2.1.4 Synthesis of Poly(Styrene-*co*-Methyl Methacrylate)-SiO$_2$ Nanocomposites

Commercial nano-SiO$_2$ (Aerosil 200) with average particle size of 12 nm was supplied by Degussa (Thailand). Vinyl trimethoxysilane (VTS, $\geq$98%) and ammonia solution (25 wt% NH$_4$OH) were used for silica surface modification. Styrene (ST, $\geq$99%, Sigma-Aldrich) and Methyl methacrylate (MMA, $\geq$99%, Sigma-Aldrich) were washed with 10 wt% aqueous sodium hydroxide (NaOH, $\geq$98%, Sigma-Aldrich) to remove the inhibitor and dried over anhydrous magnesium sulfate (MgSO$_4$, $\geq$98%, EMD). Ammonium persulfate (APS, $\geq$99%), sodium dodecyl sulfate (SDS, $\geq$99%), 1and sodium bicarbonate (NaHCO$_3$, $\geq$99%) were used as received. Deionized water was also applied for all polymerization processes.

2.1.5 Pre-Vulcanization of Natural Rubber Composites

Polystyrene-SiO$_2$, polyisoprene-SiO$_2$, poly(methyl methacrylate)-SiO$_2$ and poly(styrene-*co*-methyl methacrylate)-SiO$_2$ nanocomposites were used as nanofiller in pre-vulcanized natural rubber composites. Natural rubber (NR) latex with a total solid content of 60 wt% dry rubber content (DRC), zinc oxide (ZnO), zincdiethyl

dithiocarbamate (ZDEC) as vulcanization accelerators and sulfur as vulcanizing agent were purchased from the Rubber Research Institute of Thailand.

2.2 Surface Modification of Nanosilica

Modified nano-SiO_2 was prepared according to the literature [18]. First, 5 g of nano-silica were dispersed in 150 mL of water with sonication in an ultrasonic bath for 1 h and then the solution was stirred at 500 rpm for 30 min. 0.15 g of VTS were added dropwise into the dispersed solution after that 25 wt% aqueous ammonia solution was fed to adjust the pH of the solution to around 10. The solution was stirred for 30 min at room temperature, and then heated up to the reaction temperature of 90 °C, while stirring was maintained at 550 rpm. The reaction was allowed to proceed for an
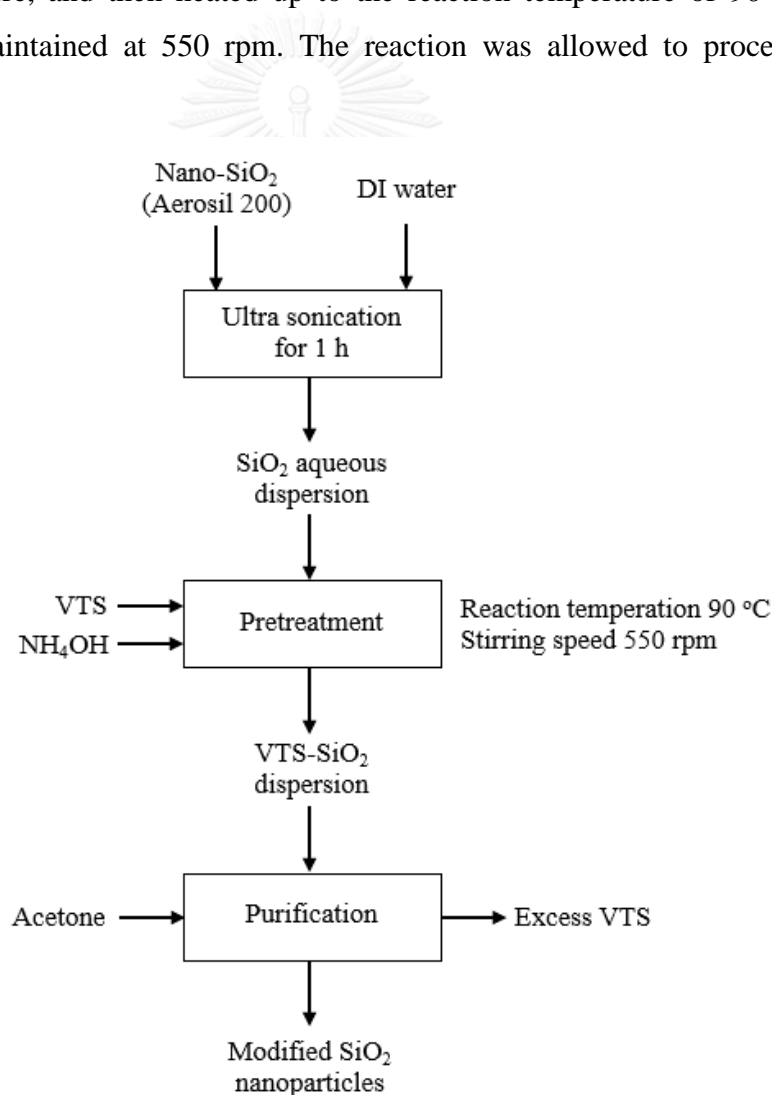
Figure 2.1 The schematic diagram of silica surface modification.

additional 24 h. After that the suspension was dried at 110 °C until constant weight was attained to obtain the modified nano-SiO_2. Later, the modified nano-SiO_2 was extracted with acetone for 24 h to remove any free VTS. Finally, VTS-SiO_2 was dried in an oven at 55 °C until constant weight was reached. The schematic diagram of silica surface modification is presented in Figure 2.1.

2.3 Synthesis of Polystyrene-SiO₂ Nanocomposites

2.3.1 Preparation of poly(styrenesulfonate-sodium): macro-RAFT agent

The macro-RAFT agent was prepared in a three-necked flask. Typically, NaSS (3 g, 14.5 mmol), ACP initiator (22.8 mg, 0.08 mmol) and RAFT agent (116.2 mg, 0.4 mmol) were dissolved in 18 mL of deionized water. Then the solution was stirred and deoxygenated by bubbling nitrogen through the solution for 30 min. After that it was immersed in an oil bath at 70 °C and the polymerization was allowed to proceed for 6 h using a magnetic stirrer. After completion of the polymerization, the solution was precipitated with an excess of methanol. Then the precipitated product was centrifuged and dried in a vacuum oven at 40 °C for 24 h. The obtained macro–RAFT agent was characterized.

2.3.2 Emulsifier-free emulsion polymerization of styrene (PS-co-RAFT) using macro-RAFT agent

PS-co-RAFT synthesis was carried out in a three-necked flask. Typically, the macro-RAFT agent and ACP initiator were dissolved in 30 mL of deionized water. The initiator concentration was kept constant at 1 wt% relative to styrene for all reactions. The weight ratio of macro-RAFT agent to initiator ([R]:[I]) was varied at 2:1, 4:1, 6:1, 8:1 and 10:1. The solution was charged into the flask and deoxygenated by bubbling nitrogen through the solution for 30 min. Then, the solution was immersed in an oil bath at 75 °C and ST monomer (3 g) was fed into the solution. When the addition of the monomer was completed, the solution was stirred for 8 h using a magnetic stirrer.

The PS-co-RAFT emulsion was obtained, then particle size and particle size distribution (PSD) were measured. Samples were quenched by using hydroquinone (0.01 wt% solution in water). To measure the monomer conversion gravimetrically and

the resulting emulsion was dried and the product was washed with MEK to remove residual monomer and homopolymer. The samples were dried at room temperature until constant weight was reached. The monomer conversion was determined using a gravimetric method and calculated using Eq. (2.1):

$$\text{Monomer conversion (\%)} = (W_2/W_1) \times 100$$

(2.1)

where W_1 and W_2 are the weights of monomer reacted and monomer charged, respectively.

The total number of latex particle in the system (N_p) and the number of polymer chains per particle (N) were calculated according to the following equations:

$$N_p = \frac{6\rho_0 V X_m}{\rho \pi D^3}$$

(2.2)

$$N = \frac{4}{3} \frac{\rho \pi (D/2)^3 N_A}{M_n}$$

(2.3)

where ρ_0 is the density of styrene (0.909 g/cm³ at 25 °C), V is the total volume of styrene, X_m is polymerization conversion, ρ is the density of polystyrene (1.05 g/cm³ at 25 °C), D is the diameter of particle, N_A is 6.02×10^{23} mol⁻¹, and $\overline{M_n}$ is the number-average molecular weight [28].

2.3.3 Synthesis of polystyrene-silica nanoparticles (PS-co-RAFT-SiO₂) using a macro-RAFT agent

PS-co-RAFT-SiO₂ synthesis was carried in a three-necked flask. Typically, 0.3 g of modified nano-SiO₂ were dispersed in 15 mL of deionized water using an ultrasonic bath for 1 h. Then, modified nano-SiO₂, macro-RAFT agent, ACP and NaHCO₃ and deionized water were charged into the flask. After that the solution was deoxygenated by bubbling nitrogen through the solution for 30 min. Then, the solution was immersed in an oil bath at 75 °C and ST monomer (3 g) was fed into the solution.

When the addition of the monomer was completed, the solution was stirred for 8 h, finally the emulsion was obtained. The schematic diagram of PS-co-RAFT-SiO$_2$ synthesis is presented in Figure 2.2. The particle size and PSD of the PS-co-RAFT-SiO$_2$ emulsion were measured. The monomer conversion was determined using a gravimetric method (similar to that described in section 2.3.2) and calculated using Eq. (2.4):

$$\text{Monomer conversion } (\%) = \frac{(M_0 - M_1)}{M_2} \times 100 \qquad (2.4)$$

where M_0 is the mass of the composite particles, M_1 is the mass of the charged silica particles and M_2 is the mass of the charged monomer.
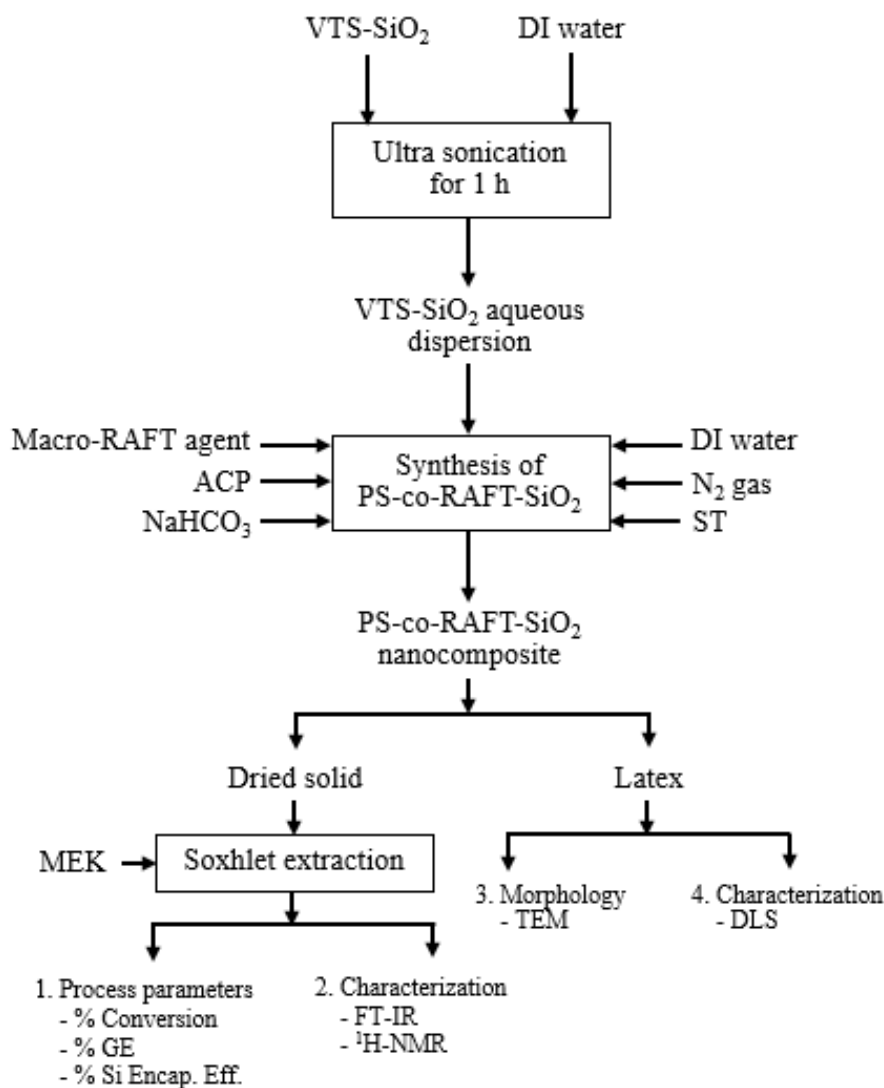
Figure 2.2 The schematic diagram of PS-co-RAFT-SiO$_2$ synthesis.

The PS-co-RAFT-SiO$_2$ was extracted using MEK in a soxhlet apparatus to remove the free polystyrene for 24 h and then the samples were dried to a constant weight. Grafting efficiency was determined using a gravimetric method. The polymer grafting efficiency was calculated using Eq. (2.5):

$$\text{Grafting efficiency (\%GE)} = (M_G/M_R) \times 100 \qquad (2.5)$$

where M_G and M_R are the mass of polymer in the composite sample and total mass of polymer formed, respectively.

An acid etching method was used to determine the silica encapsulation efficiency [18]. The composite latex was slowly added to an excess of HF solution. The resulting dispersion was dried and the weight percent of the residue was determined gravimetrically. The silica encapsulation efficiency was calculated using Eq. (2.6):

$$\text{Silica Encapsulation Efficiency (\%Si encap eff)} = (M_{ES}/M_S) \times 100 \qquad (2.6)$$

where M_{ES} and M_S are the mass of encapsulated silica and the total mass of SiO$_2$ in the system, respectively.

2.4 Synthesis of Polyisoprene-SiO$_2$ Nanocomposites

2.4.1 Synthesis of poly(styrenesulfonate-sodium): macro-RAFT agent

The macro-RAFT agent was synthesized according to the previous work [81]. Typically, NaSS (3 g, 14.5 mmol), ACP initiator (22.8 mg, 0.08 mmol) and RAFT agent (116.2 mg, 0.4 mmol) were dissolved in deionized water (18 mL). Then the solution was stirred and deoxygenated by bubbling nitrogen through the solution for 30 min. Afterwards it was immersed in an oil bath at 70 °C and the polymerization was proceeded for 6 h using a magnetic stirrer. After completion of the polymerization, the solution was precipitated with an excess of methanol. Then the precipitated product was centrifuged and dried in a vacuum oven at 40 °C until constant weight.

2.4.2 Emulsifier-free emulsion polymerization of isoprene (PIP-co-RAFT) using macro-RAFT agent

The synthesis of PIP-co-RAFT nanoparticles was carried out in a 300 mL Parr stainless steel reactor. Typically, the macro-RAFT agent and initiator were dissolved in deionized water (35 mL). The initiator concentration was kept constant at 1 wt% relative to isoprene for all reactions. The weight ratio of macro-RAFT agent to initiator ([R]:[I]) was varied at 1:1, 2:1, 3:1, 4:1 and 5:1. The solution was charged into the reactor equipped with an impeller stirrer, a thermocouple and a feeding tube. After that the solution was deoxygenated by a slow stream of nitrogen gas for 1 h at room temperature, while stirring was maintained at 300 rpm and then the system was heated up to 75 $^{\circ}$C. The feeding tube was filled with the isoprene (10 g) and connected with the reactor. The monomer was continuously fed into the reactor with a given rate of 0.3 mL/min that to be controlled with a needle valve. When the addition of the monomer was completed, the solution was aged for 15 h.

The PIP-co-RAFT emulsion was obtained, then particle size and particle size distribution (PSD) were measured. The PIP-co-RAFT latex was precipitated using excess MEK to produce the coagulated rubber. The coagulated rubber was filtered and dried in a vacuum oven at 40 $^{\circ}$C until constant weight was reached. The monomer conversion was determined using a gravimetric method and calculated using Eq. (2.1).

The emulsions were denoted as PIP-co-R1-ACP where R1 indicated the [R]:[I] ratio of 1:1 and ACP indicated the ACP initiator.

2.4.3 Synthesis of polyisoprene-silica nanoparticles (PIP-co-RAFT-SiO$_2$) using macro-RAFT agent

The nano-SiO$_2$ particles modified with VTS were prepared according to the literature [18]. PIP-co-RAFT-SiO$_2$ nanoparticles were synthesized in a 300 mL Parr stainless steel reactor. As a typically synthesis, 1 g of VTS-SiO$_2$ was dispersed in deionized water using an ultrasonic bath for 1 h. Then, VTS-SiO$_2$, macro-RAFT agent, initiator and deionized water (35 g) were charged into the reactor. The operational procedures for the reaction were similar to the synthesis of PIP-co-RAFT nanoparticles. The PIP-co-RAFT-SiO$_2$ emulsion was obtained, then the particle size and PSD were measured. The schematic diagram of PIP-co-RAFT-SiO$_2$ synthesis is shown in Figure

2.3. The latex was precipitated using excess MEK to produce the coagulated rubber. The coagulated rubber was filtered and dried in a vacuum oven at 40 °C until constant weight was reached. The monomer conversion was determined using a gravimetric method and calculated using Eq. (2.4).

The PIP-co-RAFT-SiO$_2$ nanoparticles were extracted using PE in a soxhlet apparatus to remove the free polyisoprene for 24 h and then the samples were dried to a constant weight. Grafting efficiency was determined using a gravimetric method. The polymer grafting efficiency was calculated using Eq. (2.5). An acid etching method was used to determine the silica encapsulation efficiency [81]. The composite sample was
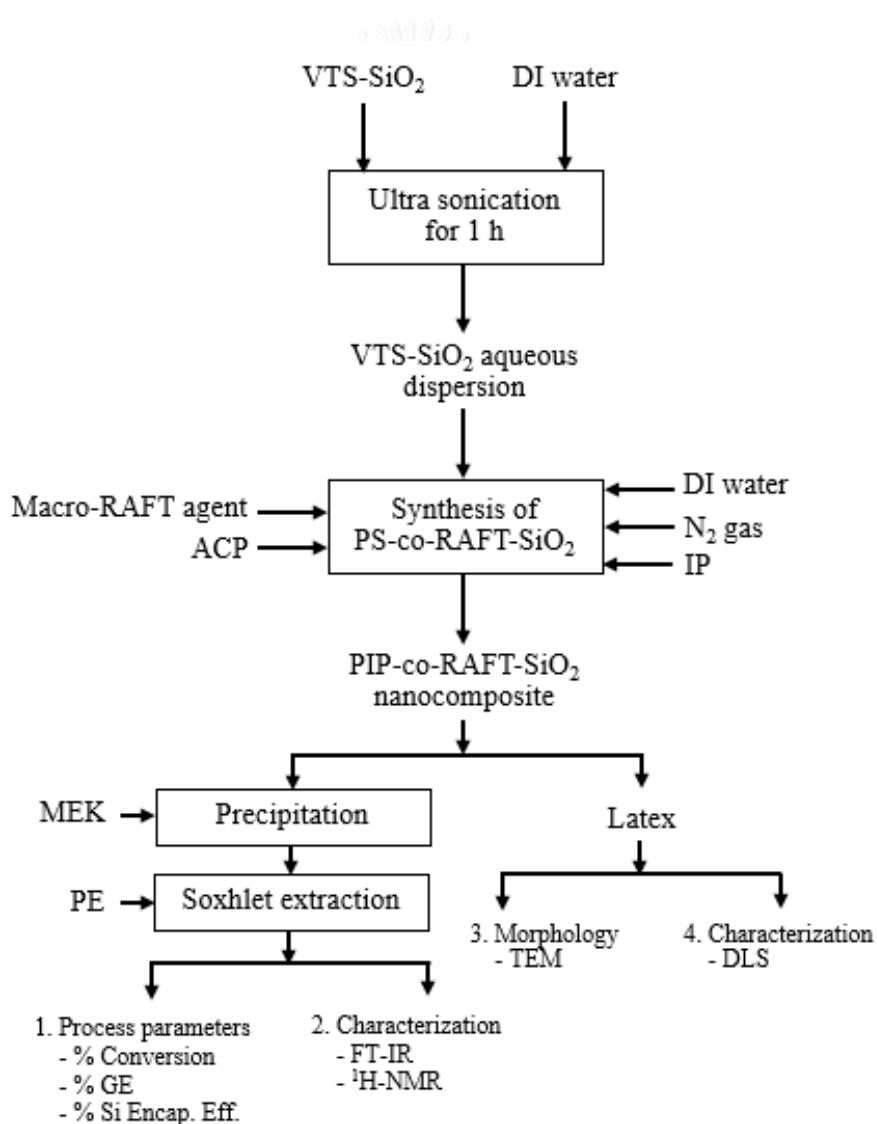
Figure 2.3 The schematic diagram of PS-co-RAFT-SiO$_2$ synthesis.

slowly added to an excess of HF solution. The resulting dispersion was dried and the weight percent of the residue was determined gravimetrically. The silica encapsulation efficiency was calculated using Eq. (2.6).

The nanocomposites were denoted as PIP-co-R1-ACP_Si where R1 indicated the [R]:[I] ratio of 1:1, ACP indicated the ACP initiator and Si indicated the modified nano-silica.

2.5 Synthesis of Poly(Methyl Methacrylate)-SiO$_2$ Nanocomposites

The nano-silica particles modified with VTS were prepared according to the literature [18]. PMMA-SiO$_2$ nanoparticles were prepared by differential microemulsion polymerization in a three-neck round-bottom flask equipped with magnetic stirrer and reflux condenser. As a typical synthesis, the modified SiO$_2$ was dispersed in deionized water with sonication in an ultrasonic bath for 1 h. Then, modified nano-SiO$_2$, SDS, APS, NaHCO$_3$ and deionized water (30 mL) were charged into the flask. Afterwards, the solution was deoxygenated by bubbling nitrogen gas for 30 min at room temperature. After that the solution flask was immersed in an oil bath at 75 ^{o}C, the mixture of MMA monomer (14 mL) and 1-pentanol (0.2 mL) was added very slowly with continuous monomer dropping for 1 h. Finally, the reaction temperature was raised to 80-85 ^{o}C for an additional hour. The PMMA–SiO$_2$ emulsion was obtained, then particle size and particle size distribution (PSD) were measured. The schematic diagram of PMMA-SiO$_2$ synthesis is shown in Figure 2.4. To measure the monomer conversion gravimetrically, the resulting emulsion was air-dried and the product was washed with acetone to remove residual monomer and free PMMA in the final product. The samples were dried in a vacuum oven at room temperature until constant weight was reached. Monomer conversion was calculated using Eq. (2.4).

An acid etching method was used to determine the silica encapsulation efficiency. The composite sample was gradually added to an excess HF solution. The resulting dispersion was dried and the weight percent of the residue was determined gravimetrically. The silica encapsulation efficiency was calculated using Eq. (2.6).
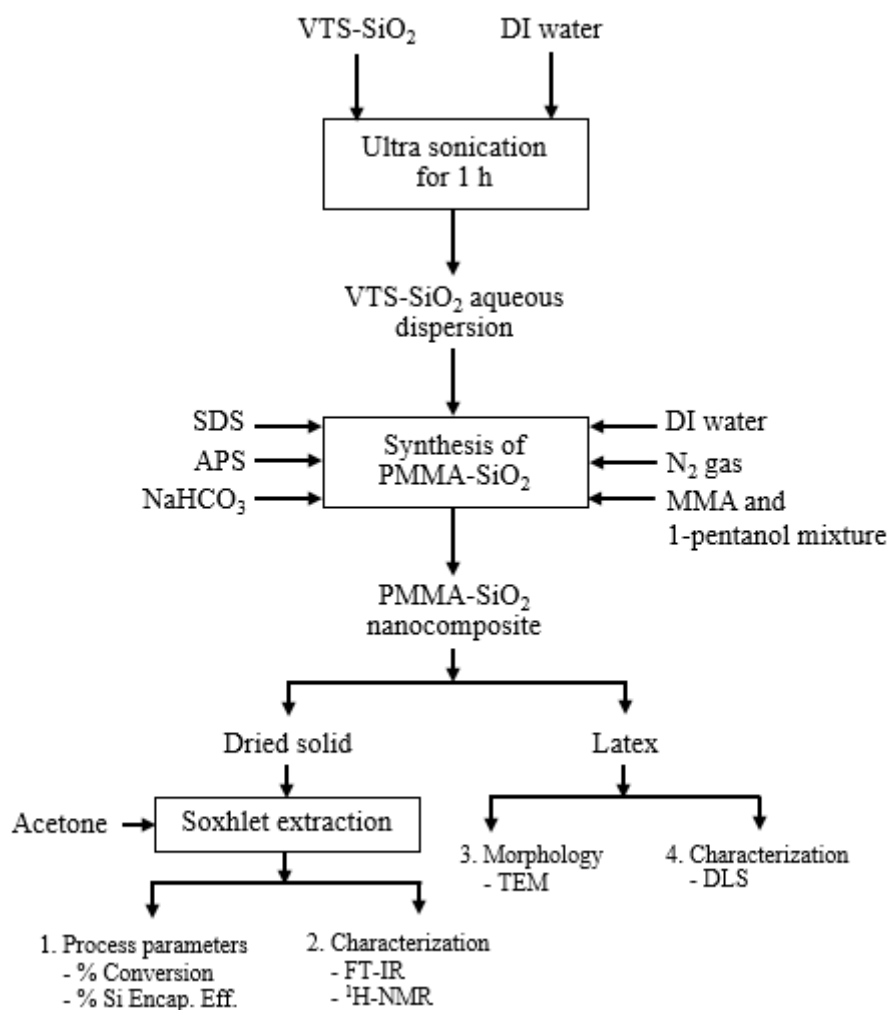
Figure 2.4 The schematic diagram of PMMA-SiO$_2$ synthesis.

2.6 Synthesis of Poly(Styrene-*co*-Methyl Methacrylate)-SiO$_2$ Nanocomposites

The nano-silica particles modified with VTS were prepared according to the literature [18]. Poly(ST-*co*-MMA)-SiO$_2$ nanoparticles were prepared by differential microemulsion polymerization in a three-neck round-bottom flask equipped with magnetic stirrer and reflux condenser. As a typical synthesis, the modified SiO$_2$ was dispersed in deionized water with sonication in an ultrasonic bath for 1 h. Then, modified nano-SiO$_2$, SDS, APS, NaHCO$_3$ and deionized water (30 mL) were charged into the flask. Afterwards, the solution was deoxygenated by bubbling nitrogen gas for 30 min at room temperature. After that the solution flask was immersed in an oil bath at 75 °C, the mixture of ST monomer (3 mL) and MMA monomer (3 mL) was added

very slowly with continuous monomer dropping for 30 min. When the addition of the monomer was completed, the solution was stirred for 2 h. The poly(ST-*co*-MMA)-SiO$_2$ emulsion was obtained, then particle size and particle size distribution (PSD) were measured. The schematic diagram of poly(ST-*co*-MMA)-SiO$_2$ synthesis is shown in Figure 2.5. To measure the monomer conversion gravimetrically, the resulting emulsion was air-dried and the product was washed with acetone to remove residual monomer in the final product. The samples were dried in a vacuum oven at room temperature until constant weight was reached. Monomer conversion was calculated using Eq. (2.4).
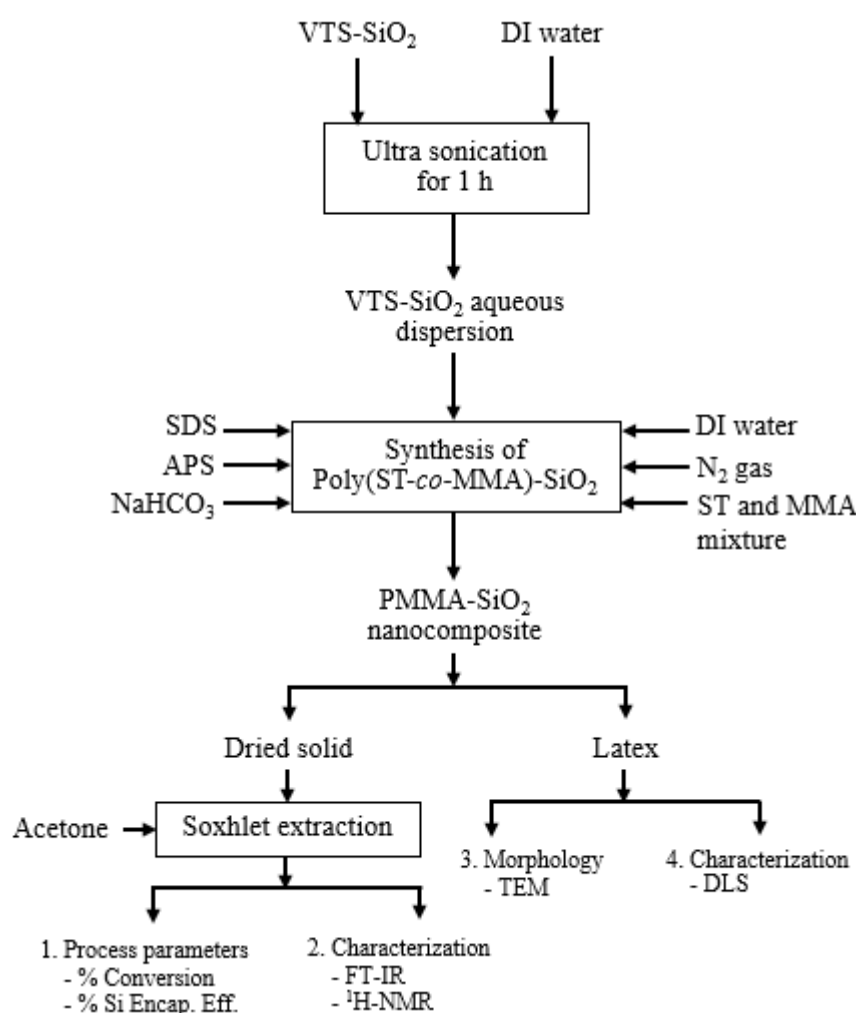
Figure 2.5 The schematic diagram of poly(ST-*co*-MMA)-SiO$_2$ synthesis.

An acid etching method was used to determine the silica encapsulation efficiency. The composite sample was gradually added to an excess HF solution. The resulting dispersion was dried and the weight percent of the residue was determined gravimetrically. The silica encapsulation efficiency was calculated using Eq. (2.6).

2.7 Preparation of NR/Polymer-SiO$_2$ Blends

i) Preparation of NR/PS-R-SiO$_2$ nanocomposites

For the preparation of the prevulcanized NR/PS-R-SiO$_2$ nanocomposite (PS-co-RAFT-SiO$_2$ was coded as PS-R-SiO$_2$), natural rubber (NR) latex with a total solid content of 60% was selected to blend with PS-co-RAFT-SiO$_2$ emulsion. The PS-co-R4-Si latex was dropped into NR latex at various weight ratios (NR:PS-R-SiO$_2$ = 100:0, 90:10, 85:15, 80:20, 75:25) under a stirring rate of 450 rpm for 30 min to form a good dispersion. Then, sulfur (1.5 phr), ZnO (2 phr) and ZDEC (1 phr) were dropped into the mixture and the system was heat up to 60 $^{\circ}$C with constant stirring at 300 rpm for 2 h. After that, the latex was cooled to room temperature and cast on a glass plate having dimensions of 9 cm x 9 cm x 3 mm. The cast film was dried at 70 $^{\circ}$C for 5 h. The composite sheet thickness was approximately 2.0 mm measured at five different points using a micrometer.

ii) Preparation of NR/PIP-R-SiO$_2$ nanocomposites

For the preparation of the prevulcanized NR/PIP-R-SiO$_2$ nanocomposite film (PIP-co-RAFT-SiO$_2$ was coded as PIP-R-SiO$_2$), the PIP-co-R3-ACP_Si and PIP-co-R4-V50_Si latex were selected to blend with NR latex with a total solid content of 60% at various weight ratio (NR/PIP-R-SiO$_2$ = 100/0, 90/10, 80/20,70/30) under a stirring rate of 450 rpm for 30 min to form a good dispersion. After that ZnO (2 phr), ZDEC (1 phr) and sulfur (1.5 phr) were dropped into the mixture, the system was heat up to 60 $^{\circ}$C with constant stirring at 350 rpm for 2 h. Then the nanocomposite latex was cooled to room temperature and cast on a glass plate (9 cm $\times$ 9 cm $\times$ 3 mm). The cast film was dried at 70 $^{\circ}$C for 5 h. The composite film thickness was approximately 2.0 mm measured at five different points using a micrometer.

iii) Preparation of PMMA-SiO$_2$ filled NR nanocomposite membranes

For the preparation of NR/PMMA–SiO$_2$ nanocomposite membrane, the PMMA–SiO$_2$ nanoparticle latex at 10 wt% silica loading was selected to blend with natural rubber (NR) latex (total solid content of 60%) at various weight ratios (NR/PMMA–SiO$_2$ = 100/0, 90/10, 80/20, 70/30, 60/40) under a stirring rate of 450 rpm for 30 min at room temperature to form a good dispersion. ZnO (2 phr), ZDEC (1 phr) and sulfur (1.5 phr) were dropped into the system, and then, the mixture was heated to 60 ^{o}C with constant stirring at 350 rpm for 2 h. Afterwards the nanocomposite latex was cast on a glass plate (9 cm × 9 cm × 3 mm) and dried at 70 ^{o}C for 5 h. The membrane thickness was approximately 0.2 mm measured at five different points using a micrometer. The appearance of NR/PMMA–SiO$_2$ membranes is shown in Figure 2.6.
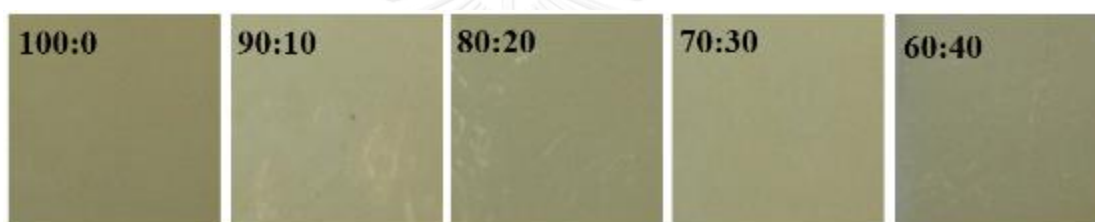
Figure 2.6 Appearance of NR/PMMA–SiO$_2$ nanocomposite membranes.

iv) Preparation of Poly(ST-*co*-MMA)-SiO$_2$ filled NR nanocomposite membranes

For the preparation of NR/Poly(ST-*co*-MMA)-SiO$_2$ nanocomposite membrane, the Poly(ST-*co*-MMA)-SiO$_2$ nanoparticle latex at 10 wt% silica loading was selected to blend with natural rubber (NR) latex (total solid content of 60%) at various weight ratios (NR/PMMA–SiO$_2$ = 100/0, 90/10, 85/15, 80/20, 75/25) under a stirring rate of 450 rpm for 30 min at room temperature to form a good dispersion. ZnO (2 phr), ZDEC (1 phr) and sulfur (1.5 phr) were dropped into the system, and then, the mixture was heated to 60 ^{o}C with constant stirring at 350 rpm for 2 h. Afterwards the nanocomposite latex was cast on a glass plate (9 cm × 9 cm × 3 mm) and dried at 70 ^{o}C for 5 h. The membrane thickness was approximately 0.2 mm measured at five different points using a micrometer.

2.8 Characterization

2.8.1 Particle Diameter Measurement

The particle size and size distribution of the latex were measured using a dynamic light scattering (DLS) technique at 25 $^{\circ}$C using a Nanotrac 150 particle size analyzer and reported as the number-average diameter (D_n).

2.8.2 ^{1}H NMR Spectroscopy

The microstructure of macro-RAFT agent and PS-*co*-RAFT was determined by ^{1}H Nuclear Magnetic Resonance (NMR) spectroscopy (Bruker 300 MHz spectrometer). The samples of macro-RAFT agent, PS-co-R2 and other copolymers were prepared in D_2O, $CDCl_3$ and DMSO-d_6, respectively. For PIP-co-RAFT, PMMA–SiO_2 and poly(ST-co-MMA)-SiO_2 nanoparticles were prepared by dissolving 20 mg dried sample in 1 mL of $CDCl_3$ at room temperature.

2.8.3 Fourier Transform Infrared Spectroscopy

Functional group analysis of nano-silica, modified nano-silica and PS-co-RAFT-SiO_2 was carried out using FTIR analysis (Thermo Nicolet 6700 spectrometer). Before analysis, the samples were ground with KBr powder and compressed to form pellets for FTIR analysis.

The chemical structure of VTS-SiO_2, PIP-co-RAFT-SiO_2, PMMA–SiO_2 and poly(ST-*co*-MMA)-SiO_2 nanoparticles was analyzed by FTIR spectroscopy (Perkin Elmer Spectrum RX I spectrophotometer). Infrared spectra were recorded in the region 4000–500 cm^{-1}, with a resolution of 0.5 cm^{-1}.

2.8.4 Morphological Study

The morphology and core-shell structure of PS-co-RAFT and PS-co-RAFT-SiO_2 were observed using a LEO 912 AB 100kV Energy Filtered Transmission Electron Microscope (EFTEM). The latex was first diluted 20 times with deionized water. Then, the diluted solution was dropped on a 400-mesh copper grid at room temperature and the excess solution was drawn off the grid with tissue paper. After that

the grid was stained with 1% OsO$_4$ for 2 min and the excess OsO$_4$ was drawn off with tissue paper.

The morphology of PIP-co-RAFT, PIP-co-RAFT-SiO$_2$, PMMA–SiO$_2$ and poly(ST-*co*-MMA)-SiO$_2$ nanoparticles was examined using a transmission electron microscope (TEM, JEOL JEM-2100) operating at an acceleration voltage of 80 kV. The sample latex was first diluted 20 times with deionized water and then, the diluted solution was dropped on a 400-mesh copper grid at room temperature. After that the grid was stained with 1% OsO$_4$ prior to analysis to obtain sufficient contrast.

Scanning electron microscopy (SEM, JSM-7610F) was used to investigate the fracture surface of NR/PMMA–SiO$_2$ nanocomposite membranes. The samples were fractured in liquid nitrogen and coated with gold by sputtering.

2.8.5 Thermogravimatic Analysis (TGA)

Thermogravimetric analysis (TGA) was performed with a thermal analysis instrument (Perkin-Elmer Pyris Diamond) to obtain the decomposition temperature (T_{id} and T_{max}). 10 mg of the samples were placed into a platinum pan. The temperature was raised under a nitrogen atmosphere from room temperature to 800 °C at a constant heating rate of 10 °C/min with a flow rate of nitrogen gas of 50 mL/min.

2.8.6 Differential Scanning Calorimetry (DSC)

Differential scanning calorimetry (DSC, Mettler Toledo 822e) was used to measure the glass transition temperature (T_g). A sample was cooled to -100 °C with liquid nitrogen and heated to 150 °C at a heating rate of 10 °C/min.

2.8.7 Dynamic Mechanical Thermal Analyzer (DMA)

Dynamic mechanical thermal analysis of NR/PIP-R-SiO$_2$ nanocomposite films was performed using a dynamic mechanical thermal analyzer (DMA, METTLER) in a shear mode. All samples were cut strips with dimension 4 mm × 4 mm × 2 mm. The temperature was run in the range of -80 °C to 25 °C at an oscillation frequency of 10 Hz with a heating rate of 5 °C/min. The storage modulus and the loss tangent (tan δ) curve were observed.

2.8.8 Gel Permeation Chromatography (GPC)

The molecular weight of the copolymers was measured using a Shimadzu LC solution GPC system (Japan) which consisted of a CBM 20 Alite system controller, LC-20AD solvent delivery unit, CTO-20A column oven and a RID-10A refractive index detector. Two columns were used for separation, which were Shodex GPC KF-806M (8.0 x 300 mm) and Shodex GPC KF-803L (8.0 x 300 mm) in series. The eluent was tetrahydrofuran (THF) with a flow rate of 1 mL/min and Shodex standard SM-105 (polystyrene standard) was used as standard. The samples were dissolved in THF (HPLC grade) and filtered through a 0.45 μm pore size filter. 20 μL samples were injected and the data was collected and analyzed by auto integration and calibration using a Shimadzu program.

2.8.9 Oil Swelling Resistance

The oil swelling resistance of NR/PS-R-SiO$_2$ composites was determined by swelling the specimens in motor oil (IRM 903 oil). The NR/PS-R-SiO$_2$ composites (30 × 5 × 2 mm) were weighed before and after immersion at room temperature for 70 h. The specimens were removed from the oil, quickly dipped in acetone and wiped lightly with tissue paper to remove the excess oil from their surface before weighing. The variation of apparent percentage of change was calculated by using Eq. (2.7):

$$\% \, \text{Swelling} = \frac{(M_2 - M_1)}{M_1} \times 100 \tag{2.7}$$

where M_1 and M_2 are mass of specimen before immersion and after immersion, respectively.

2.8.10 Swelling Ratio

The swelling ratio of the NR/PS-R-SiO$_2$ composites was determined according to ASTM D471. The sample (10 × 10 × 1 mm) was immersed in toluene for 7 d at ambient temperature [82]. The swelling ratio of the polymer (Q) was calculated according to Eq. (2.8):

$$Q = \frac{(W_2 - W_1)}{W_1} \tag{2.8}$$

where W_1 and W_2 are the weight of the sample before and after toluene immersion.

2.8.11 Crosslink Density

The crosslink density of the the NR/PS-R-SiO$_2$ composites was calculated using the Flory-Rehner equation [83, 84], as follows:

$$\eta_c = -\frac{\ln(1-V_r)-V_r-\chi V_r^2}{V_s(V_r^{1/3}-\frac{2V_r}{f})} \qquad (2.9)$$

where η_c is the crosslink density of the rubber (mol/cm^3), V_s is the molar volume of the toluene (106.2 cm^3/mol), χ is the polymer-solvent interaction parameter ($\chi = 0.3795$), f is the functionality of the crosslinks for the sulfur curing system ($f = 4$) and V_r is the volume fraction of rubber in the swollen gel, calculated according to Eq. (2.10):

$$V_r = -\frac{(\frac{W_1}{\rho_r}-\frac{W_f}{\rho_f})}{(\frac{W_1}{\rho_r}-\frac{W_f}{\rho_f})+(\frac{W_2-W_1}{\rho_s})} \qquad (2.10)$$

where W_f is the weight of filler in the rubber vulcanizates (g), ρ_r is the density of the rubber vulcanizates (g/cm^3), ρ_f is the density of silica particles from hydrophobic fumed silica (0.05 g/cm^3), and ρ_s is the density of toluene (0.862 g/cm^3) [83].

2.8.12 Contact Angle Measurement

The contact angle of water was measured using a Standard Goniometer (Ramé-Hart Model 200-F1). Water droplets were placed on NR/PMMA–SiO$_2$ and NR/Poly(ST-*co*-MMA)-SiO$_2$ composites and then, the dimensions of the droplets were examined using the software system. Each measurement was repeated three times and then evaluated for the final results.

2.9 Mechanical Properties of Vulcanized Rubber

The tensile properties of the NR/Polymer-SiO$_2$ nanocomposite were measured using a Universal Testing Machine (INSTRON 5566) at 500 mm/min of the cross-head speed according to ASTM D412. Test specimens were cut into dumbbell-type shape, and the average of three measurement of the three specimens was considered as the representative value.

2.10 Pervaporation of Water-Ethanol Mixture

The pervaporation process was carried out using a plate and frame module made of stainless steel as shown in Figure 2.7. The effective membrane area was 11.34 cm^2. The membranes (NR/PMMA–SiO$_2$ and NR/Poly(ST-*co*-MMA)-SiO$_2$) were put on a stainless steel porous support and contacted with the feed solution for 2 h by circulating the solution from a feed reservoir kept at room temperature. Then, the vacuum was applied to the permeate side and the pervaporation process was operated for an additional 3 h. Permeate was collected in cold traps while the liquid retentate was circulated back to the feed reservoir. The composition of permeate was determined using the calibration curve of the solution compositions versus their absorbance number.

The performance of the membrane for pervaporation was characterized from the total permeate flux, J (g/m^{2}h). Total permeate flux was calculated using Eq. (2.11):

$$J = W / (A \times t) \tag{2.11}$$

where W, A and t represent the total weight of permeate (g), the effective membrane area (m^2) and the operating time (h), respectively.
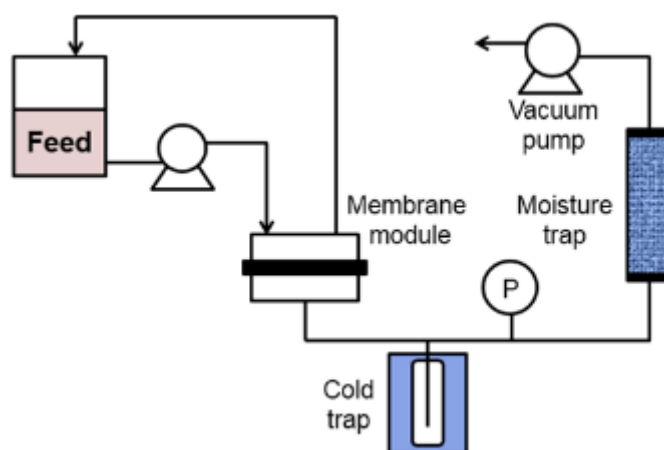
Figure 2.7 Schematics of pervaporation equipment.

CHAPTER III
SYNTHESIS OF POLYSTYRENE-SILICA NANOPARTICLES VIA RAFT EMULSIFIER-FREE EMULSION POLYMERIZATION

3.1 Introduction

Reversible addition-fragmentation chain-transfer polymerization (RAFT) has been advantageous and efficient because it can be readily applicable to a wide range of monomers and reaction conditions. The key of the RAFT polymerization process is the RAFT agent which is responsible for controlling chain growth. In the RAFT process, generally block copolymers are synthesized in 2 steps in which the first block is synthesized using a chain transfer agent (RAFT agent). Then, a well-defined block is used as a macromolecular chain transfer agent (macro-RAFT agent) to synthesize the next block. However, the RAFT mechanism lacks the ability for propagating chains under RAFT control. These problems are a result of the interaction between the RAFT agent and emulsifier. Therefore, RAFT emulsifier-free emulsion polymerization was investigated to find other stabilizers instead of emulsifiers. Furthermore, the RAFT agent was also developed with a water-soluble polymer. It is called a hydrophobic RAFT agent which can be successfully employed in emulsifier-free emulsion polymerization. However, nanocomposite materials have more potential for many applications in mechanical, optical, and/or gas barrier engineering. Silica is one of the most popular materials which are frequently used as reinforcing fillers in rubbers and polymers for improving their mechanical properties.

In this research work, the synthesis of PS-co-RAFT-SiO$_2$ core-shell nanoparticles via RAFT emulsifier-free emulsion polymerization was studied in depth for the effect of [R]:[I] ratio on particle size and core-shell morphology. Furthermore, PS-co-RAFT-SiO$_2$ nanoparticles as effective fillers in NR latex are rarely reported. For the emphasis on rubber application, oil resistance, the mechanical properties and thermal properties of NR/PS-R-SiO$_2$ composites were studied.

3.2 Characterization of PS-co-RAFT and PS-co-RAFT-SiO₂ Nanocomposites

The NMR spectra of the macro-RAFT agent and copolymers are shown in Figure 3.1. In the aromatic region, the macro-RAFT agent shows peaks A (6.4 ppm) and B (7.4 ppm) while the copolymer with low [R]:[I] ratio of 2:1 shows peak A and C (7.0 ppm). The copolymers at higher [R]:[I] ratio ([R]:[I] = 4:1 - 10:1) show all the peaks. It should be noted that the macro-RAFT agent takes part in the polymer backbone and could wrap over the core of polystyrene [20]. Moreover, Figure 3.2a shows the formation step of macro-RAFT agent and emulsifier-free emulsion polymerization of styrene. First of all, NaSS monomer reacted with the RAFT agent to form the macro-RAFT. On adding styrene, emulsifier-free emulsion polymerization of styrene took place in which polystyrene attached to the macro-RAFT agent.
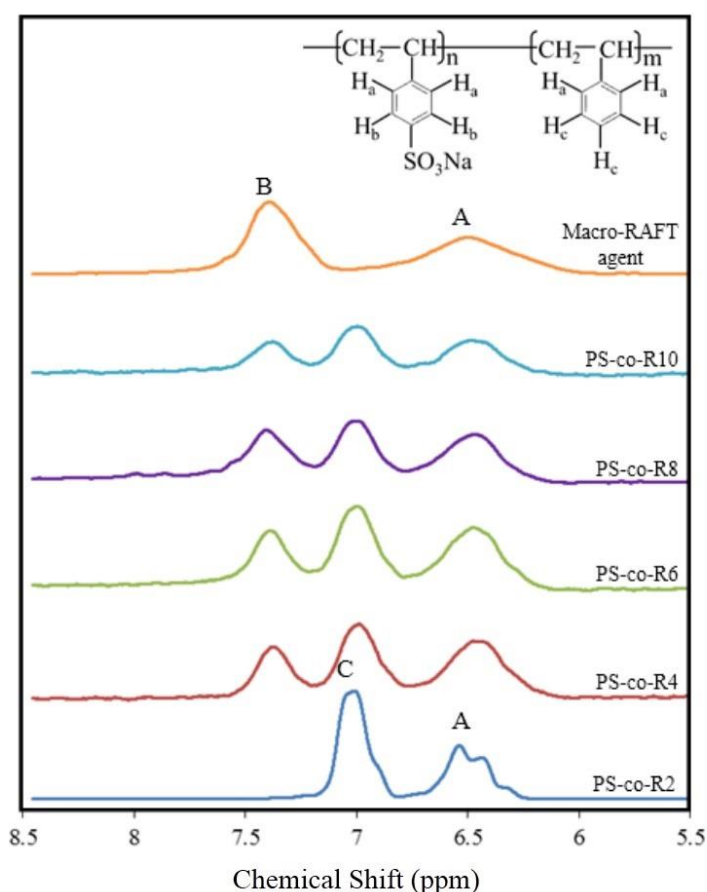
Figure 3.1 ^{1}H-NMR analysis of macro-RAFT agent, PS-co-R2 and all other copolymers.
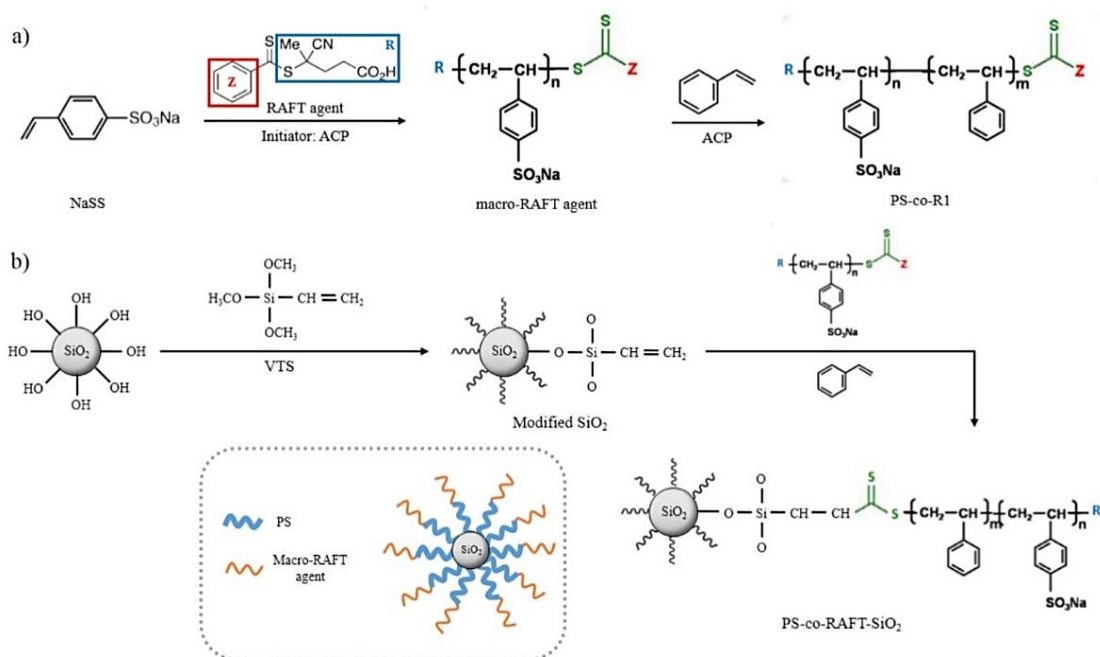
Figure 3.2 (a) Formation mechanism of emulsifier-free emulsion polymerization of styrene.

(b) The modification of silica particles and synthesis of polystyrene-silica nanoparticles (PS-co-RAFT-SiO$_2$).
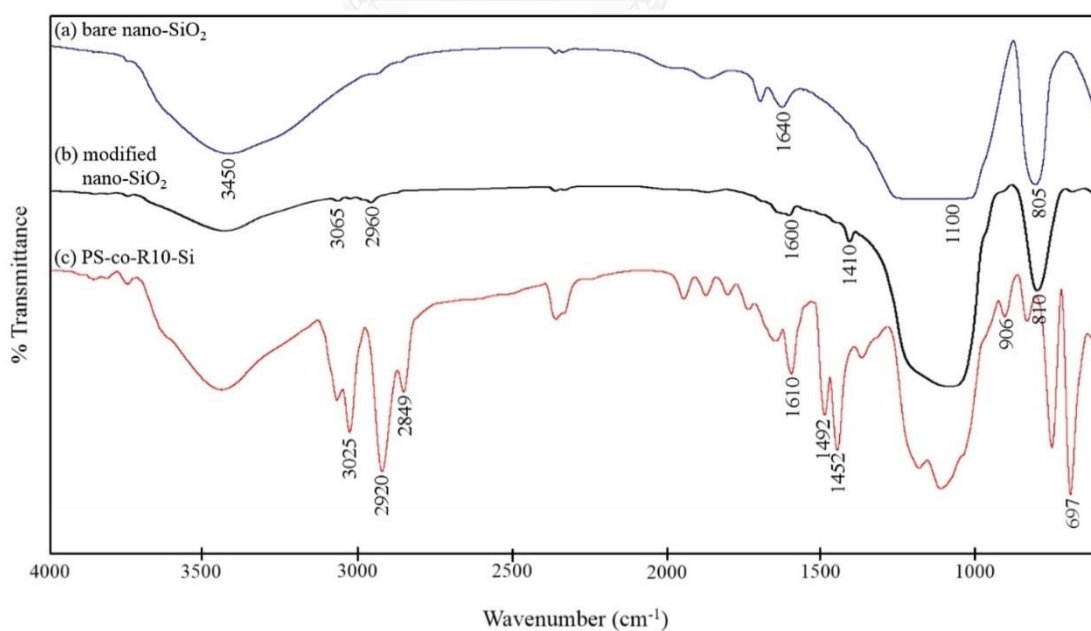
Figure 3.3 FT-IR spectra of (a) bare nano-SiO$_2$ (b) modified nano-SiO$_2$ and (c) PS-co-R10-Si.

Figure 3.3 shows the FT-IR spectra of bare nano-SiO$_2$, modified nano-SiO$_2$ and PS-co-R10-Si (at [R]:[I] ratio = 10:1). For bare nano-SiO$_2$, the most intensive absorption band at 1100 cm^{-1}, together with the less insensitive band at 805 cm^{-1} are ascribed to the vibration absorption of Si-O-Si groups. Furthermore, the absorbance at 1640 and 3450 cm^{-1} are attributed to the surface hydroxyl group (O-H) of silica. For modified nano-SiO$_2$, the absorption bands at 1110 and 810 cm^{-1} are assigned to Si-O-Si groups. The peaks at 3065 and 2960 cm^{-1} correspond to CH and CH$_2$ stretching of the VTS groups. The bands at 1600 cm^{-1} (C=C) and 1410 cm^{-1} (CH out of plain bending) are attributed to the double bonds of VTS. These results show that coupling agent can be bonded onto silica. PS-co-R10-Si has absorption peaks at 3025 (C-H arom), 1610 (C=C arom), 2920 and 2849 (-CH$_2$-CH$_2$), 1492 and 1452 (-C$_6$H$_5$), 906 and 697 (-CH=arom) cm^{-1} which are characteristic peaks of PS. These results show that the macro-RAFT agent can enter into the polymer backbone and styrene could be grafted onto SiO$_2$ via the macro-RAFT agent.

Furthermore, the proposed mechanism for the synthesis of PS-co-RAFT and PS-co-RAFT-SiO$_2$ is shown in Figure 3.2. For the synthesis of the macro-RAFT agent (Figure 3.2a), NaSS monomers reacted with the RAFT agent and the NaSS monomer slowly inserted into the RAFT agent molecules to form poly(styrenesulfonate-sodium) as the macro-RAFT agent. The macro-RAFT agent was used as an emulsifier in the polymerization. When ST monomer was added to the reaction, the ST monomer inserted into the macro-RAFT agents to yield PS-co-RAFT nanoparticles. The modification of silica particles and synthesis of PS-co-RAFT-SiO$_2$ were described in Figure 3.2b. The VTS coupling agents could be bonded onto the silica surface. The methoxy groups of silane were firstly catalyzed in aqueous solution to form silanol groups. The siloxane linkage between the silica surface and the silane agent was then produced through a polycondensation reaction. With the addition of macro-RAFT agent and ST monomer, the macro-RAFT agent attached to the silica surface and then the ST monomer attached to the macro-RAFT agent by successive addition (chain propagation) until all monomer in the reaction were consumed. Finally, the macro-RAFT agent and ST monomer were grafted onto modified silica to form PS-co-RAFT-SiO$_2$ structure and core-shell morphology.

3.3 Morphology of PS-co-RAFT and PS-co-RAFT-SiO₂ Nanocomposites

The morphology of PS-co-R2, PS-co-R10 and PS-co-R10-Si characterized by TEM are shown in Figure 3.4. The TEM image in Figure 3.4a (PS-co-R2) shows slightly aggregated spherical particles with a diameter of around 45 nm. This may be due to the occurrence of aggregation during the preparation of specimens [85]. Interestingly, Figure 3.4b (PS-co-R10) clearly shows the formation of a core-shell structure and the shell thickness of the particles is about 5 nm. The lighter black ring (shell) encloses the brighter spherical particle (core). It can be seen that the shell is PSS-Na and the core is PS from the nature of the PSS-Na (hydrophilic part) [20].
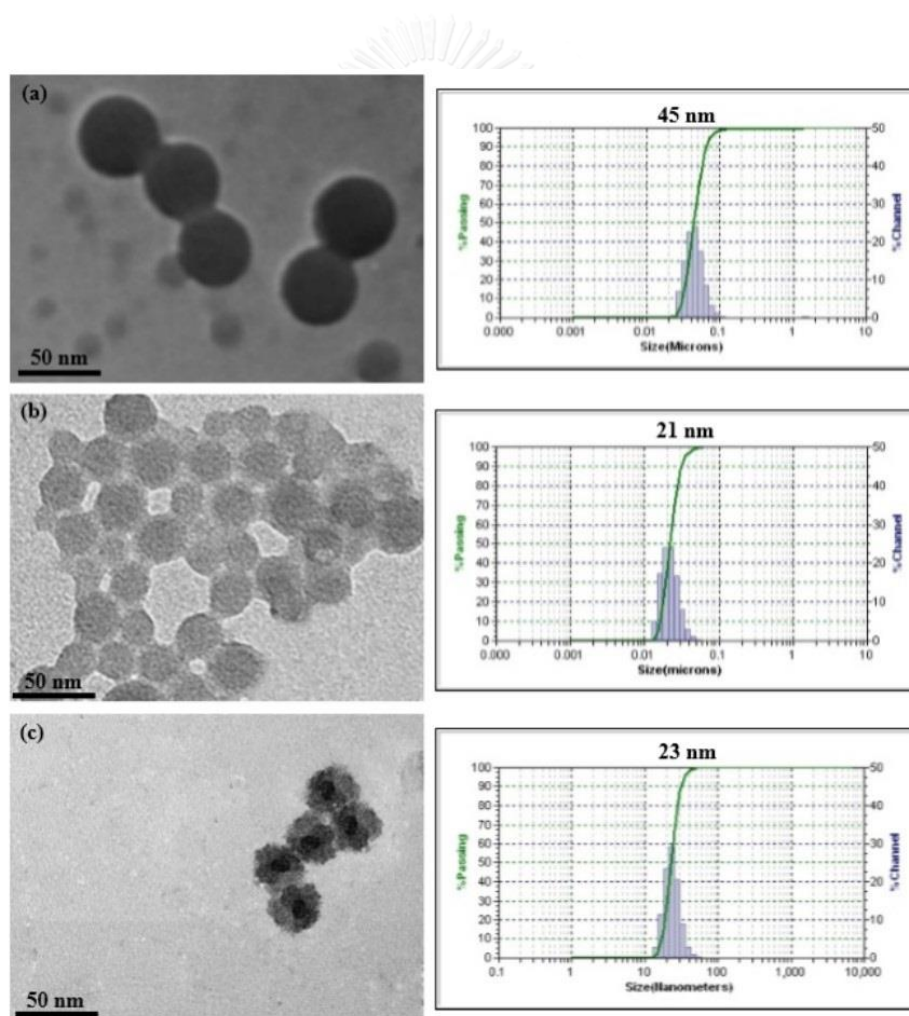
Figure 3.4 TEM micrographs and particle size distribution of (a) PS-co-R2 (at [R]:[I] = 2:1) (b) PS-co-R10 (at [R]:[I] = 10:1) and (c) PS-co-R10-Si (at [R]:[I] = 10:1, silica 10 wt% based on monomer).

However, Figure 3.4c (PS-co-R10-Si) also indicates the formation of a core-shell morphology but the shell is not spherical, since the polymer can spread on the surface of the grid in the dry state (for TEM analysis) [86]. Therefore, polystyrene could graft onto modified SiO_2, indicating that the RAFT emulsifier-free emulsion polymerization has successfully produced PS-co-RAFT-SiO_2 nanoparticles. Furthermore, a narrow PSD was achieved for all PS-co-RAFT and PS-co-RAFT-SiO_2 at all [R]:[I] ratio (Table 3.1 and 3.3).

3.4 Synthesis of PS-co-RAFT Nanocomposites

The particle size, particle size distribution (PSD), % total solid content and monomer conversion (%) of PS-co-RAFT are presented in Table 3.1. The particle size of PS-co-RAFT decreased with increasing the [R]:[I] ratio due to the RAFT agent amount representing the number of hydrophilic chains. The number of hydrophilic chains increased resulting in lower chain growth. Consequently, the particle size decreased with decreasing chain growth [11]. A particle size of 21-45 nm with PS-co-RAFT was achieved for polymerization at all [R]:[I] ratios. Moreover, the PSD values were found to be below 2, which was an indication that the polymerization had become controlled. The % total solid content was around 8.9-9.4, however, the monomer conversion was ≥99% for all [R]:[I] ratios. Figure 3.5 presents the effect of the [R]:[I] ratio on the characteristics of the PS-co-RAFT latex. It can be seen that at a high [R]:[I] ratio of 10:1, more transparent latex was produced.

Conversion versus reaction time for different ratios of [R]:[I] are presented in Figure 3.6. The plots exhibit three intervals. The first interval shows a very slow polymerization rate and low monomer conversion which lasts up to 1 h for PS-co-R2. However, for the other copolymers it lasts up to 2 h and during this period, particle formation commences. First, the initiator is fragmented into free radicals to initiate the polymerization of monomers. Then the oligoradicals react with the macro-RAFT agent to lead to chain extension and to form a copolymer. During this part of the polymerization, the macro-RAFT agent plays the role of a stabilizer as a surfactant. After that the polymerization rate becomes faster than during the first period. This

Table 3.1 Effect of [R]:[I] ratio on particle size, PSD, %total solid content and monomer conversion of PS-co-RAFT.

Name	[R]:[I][a]	Particle size (nm)	PSD	% Total solid content	Monomer conversion (%)
PS-co-R2	2:1	45.0	1.29	9.1	≥99
PS-co-R4	4:1	36.3	1.29	8.9	≥99
PS-co-R6	6:1	32.6	1.27	9.3	≥99
PS-co-R8	8:1	30.4	1.24	9.4	≥99
PS-co-R10	10:1	20.8	1.21	9.2	≥99

[a][R]:[I] = the ratio of macro-RAFT agent concentration to initiator concentration.
Condition: ACP = 30 mg, H_2O = 30 g, ST =3 g, Temp = 75 °C, Time = 8 h.

Table 3.2 Effect of macro-RAFT agent amount on molecular weight, Np and N.

Name	Particle size (nm)	$\overline{M}_w \times 10^{-5}$	$\overline{M}_n \times 10^{-5}$	$\overline{M}_w / \overline{M}_n$	$N_p \times 10^{18}$	N
PS-co-R2	45.0	4.24	1.65	2.56	5.99	182
PS-co-R6	32.6	3.02	2.02	1.49	15.74	57
PS-co-R10	20.8	12.26	3.38	3.62	60.61	9
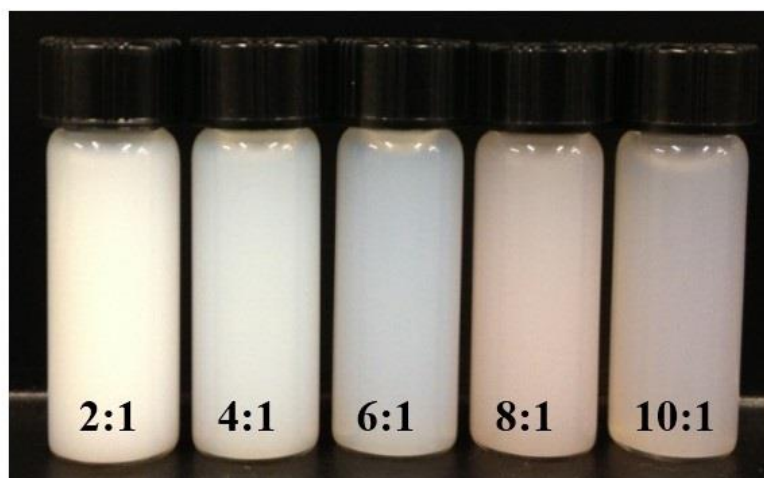
Figure 3.5 Effect of [R]:[I] ratio on characteristics of PS-co-RAFT emulsions.
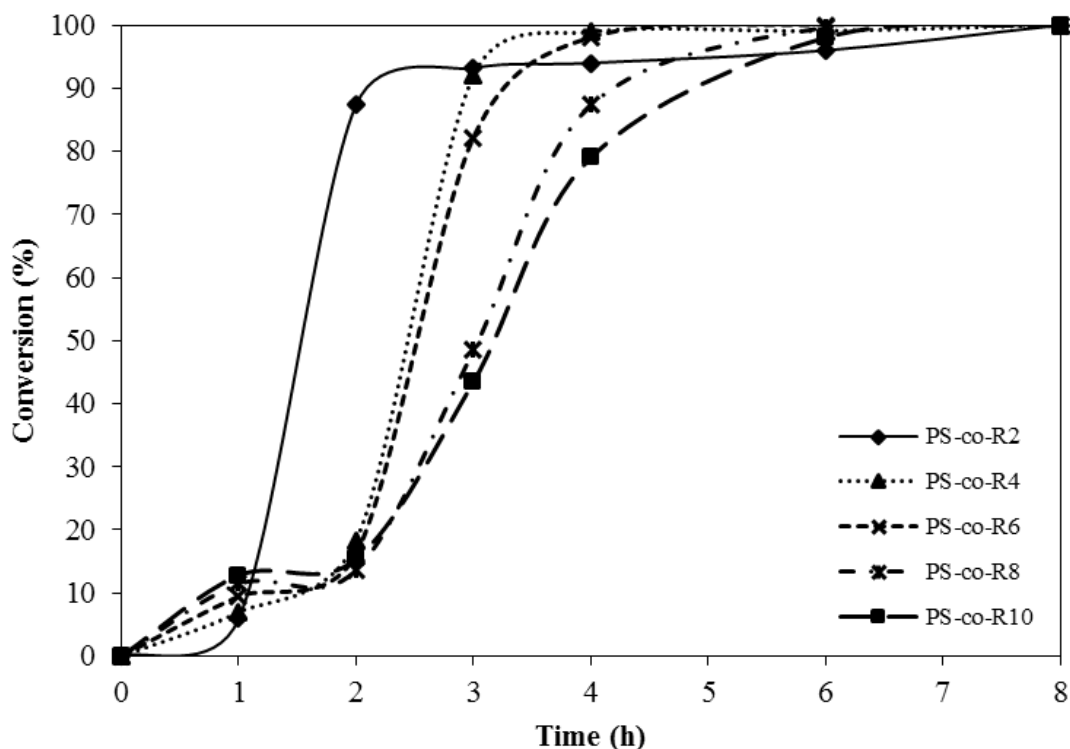
Figure 3.6 Conversion plots for surfactant free emulsion polymerization of styrene at different ratios of [R]:[I] varying from 2:1 to 10:1.

interval corresponds to propagation steps which last up to 2 h for PS-co-R2 and 3, 3, 4 and 4 h for [R]:[I] ratio = 4:1, 6:1, 8:1 and 10:1, respectively. After 6 h, the polymerization was almost complete. . It can be seen that the [R]:[I] ratio influences the overall polymerization. Moreover, the final conversions for all PS-co-RAFT reactions are ≥99% after 8 h. These results can be explained in that the macro-RAFT agent shows high performance for the polymerization [12, 20].

The molecular weight, the total number of latex particles in the system (Np) and the number of polymer chains per particle (N) of PS-co-RAFT nanocomposites are presented in Table 3.2. It was found that with an increase in the [R]:[I] ratio, the $\overline{M}_w$ increased from 4.24×10^5 to 12.26×10^5 and the $\overline{M}_n$ increased from 1.65×10^5 to 3.38×10^5. At low amount of macro-RAFT agent, the reaction sites could result the low molecular weights of PS-co-RAFT nanocomposites (PS-co-R2). However, the total number of latex particle in the system (Np) increased significantly with an increase in [R]:[I] ratio from 2:1 to 10:1. It could be noted that the macro-RAFT agent amount had

a pronounced effect on the particle formation (size and number). At low macro-RAFT agent concentration, the formation of PS-co-RAFT nanocomposites was in the particle nucleation period. On increasing the [R]:[I] ratio, more nucleation occurred in the water phase and a greater number of particles could be formed in the system [28]. Furthermore, the [R]:[I] ratio also affected the number of polymer chains per particle (*N*). The average number of polymer chains per particle decreased from 182 to 9 as the macro-RAFT agent amount was increased. This can be explained in that the high macro-RAFT agent amount produced the small particle size corresponding to the number of polymer chains in each particle [28].

3.5 Synthesis of PS-co-RAFT-SiO$_2$ Nanocomposites

The particle size, particle size distribution (PSD), % total solid content, monomer conversion (%), grafting efficiency (%GE) and silica encapsulation efficiency (%Si encap eff) of PS-co-RAFT-SiO$_2$ are presented in Table 3.3. The particle size of PS-co-RAFT-SiO$_2$ decreased on increasing the [R]:[I] ratio since the macro-RAFT agent amount influences the number of hydrophilic chains. The number of hydrophilic chains increased resulting in lower chain growth. Consequently, the diameter of latex particle decreased with a decrease in chain growth [11]. For the all [R]:[I] ratios, a particle size of 23-56 nm with PS-co-RAFT-SiO$_2$ was achieved. Furthermore, the PSD was below 2, indicating that the polymerization occurs under the good control. Nevertheless, the % total solid content was around 10.2-10.7 and the final monomer conversions were ≥99% for all polymerizations at various [R]:[I] ratios. In addition, the grafting efficiency decreased from 94% to 76% on increasing the [R]:[I] ratio since free PS (homopolymer) occurred rather than the encapsulation of SiO$_2$ within PS-co-RAFT at the high [R]:[I] ratio [20].

The effect of the [R]:[I] ratio on the characteristics of the PS-co-RAFT-SiO$_2$ latex is shown in Figure 3.7a. It indicates that with an increase in the [R]:[I] ratio, the diameter of latex particles exhibits a trend of decreasing and the latex becomes more transparent. However, the RAFT emulsifier-free emulsion polymerization of polystyrene on modified silica could provide PS-co-RAFT-SiO$_2$ nanocomposites with a monodispersion of silica in the latex resulting in a homogeneous composite emulsion. For the physical mixing of modified siliica with PS-co-RAFT latex (Figure 3.7b), it is

clearly seen that the system has a two-phase dispersion of modified silica and PS-co-RAFT latex because of the hydrophilic surface of the silica particle. The hydrophilic surface caused a heterogeneity, free polymer formation and silica agglomeration which cannot be broken down with high speed shearing or milling via mechanical mixing [87]. Therefore, the encapsulation of silica with PS-co-RAFT-SiO$_2$ could enhance the compatibility and dispersion of silica in the PS-co-RAFT-SiO$_2$ matrix, reduce the silica-silica interaction and result the homogeneity of silica in the PS-co-RAFT-SiO$_2$ latex.

Table 3.3 Effect of [R]:[I] ratio on particle size, PSD, %total solid content and monomer conversion of PS-co-RAFT-SiO$_2$.

Name	[R]:[I]^a	Particle size (nm)	PSD	% Total solid content	Monomer conversion (%)	%GE	%Si encap eff
PS-co-R2-Si^b	2:1	56.2	1.29	10.2	≥99	94.8	4.5
PS-co-R4-Si^b	4:1	38.7	1.23	10.5	≥99	88.4	26.6
PS-co-R6-Si^b	6:1	30.3	1.19	10.4	≥99	86.4	32.0
PS-co-R8-Si^b	8:1	26.6	1.19	10.6	≥99	87.5	52.2
PS-co-R10-Si^b	10:1	23.1	1.17	10.7	≥99	76.1	45.9

^{a}[R]:[I] = the ratio of macro-RAFT agent concentration to initiator concentration.
^{b}Silica amount = 10 wt% based on St.
Condition: ACP = 30 mg, H$_2$O = 30 g, ST =3 g, Temp = 75 °C, Time = 8 h.
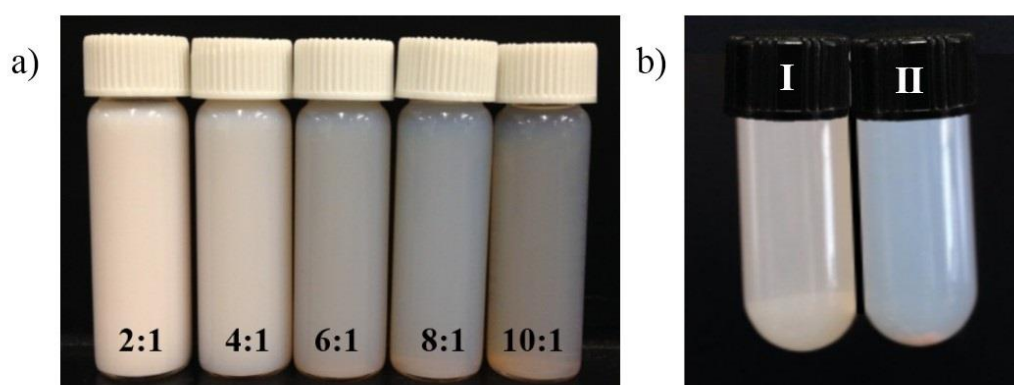
Figure 3.7 Effect of a) [R]:[I] ratio on characteristics of PS-co-RAFT-Si emulsions b) comparison between (I) silica mixed with PS-co-R10 and (II) silica encapsulated (PS-co-R10-Si).

3.6 Characteristics of NR/PS-R-SiO$_2$ Blends

The effect of PS-R-SiO$_2$ content on oil resistance, swelling ratio and crosslink density of NR/PS-R-SiO$_2$ blends are presented in Table 3.4. It was found that the oil resistance of the rubber blend was better than pure natural rubber and the oil resistance of rubber blend increased with increasing PS-R-SiO$_2$ content. It showed similar results as the blends of natural rubber with dichlorocarbene modified styrene-butadiene rubber and chloroprene rubber [88]. It can be explained in that the natural rubber was easily dissolved in oil because natural rubber and oil are of the same polarity [89]. Moreover, a consequence of the existing pressure involved between the rubber network and the oil acted to expand or shrink the rubber network. Thus, the composite filler could improve the swelling property of natural rubber. Therefore, the hybrid filler can improve the swelling property by increasing oil resistance. Additionally, with increasing PS-R-SiO$_2$ content, the swelling ratio tended to be decreased and crosslink density of NR/PS-R-SiO$_2$ blends increased due to network elasticity contributions. These crosslinks restricted extensibility of the rubber chains and made it more difficult for oil to diffuse into the gaps between rubber molecules. Therefore, the swelling resistance increased with increasing of crosslink density, indicating that the addition of PS-co-RAFT-SiO$_2$ composite enhanced the oil resistance of natural rubber.

Table 3.4 Effect of NR/PS-R-SiO$_2$ nanocomposites on oil resistance, swelling ratio and crosslink density.

NR/PS-R-SiO$_2$[a] (wt/wt)	SiO$_2$ content[b] (wt%)	% Swelling	Swelling ratio (Q)	Crosslink density (η_c x10^{-3}, mol/cm^3)
100/0	-	256	4.65	1.17
90/10	1.0	245	4.60	1.30
85/15	1.5	233	4.56	2.16
80/20	2.0	227	4.42	3.05
75/25	2.5	225	4.37	4.52

[a] PS-co-R4-Si was used as PS-R-SiO$_2$
[b] Silica content based on total rubber.

3.7 Mechanical Properties of NR/PS-R-SiO$_2$ Blends

PS-co-R4-Si nanocomposite was selected to blend with NR latex for mechanical testing. Mechanical properties of PS-R-SiO$_2$ filled NR were investigated in terms of tensile strength, modulus at 300% strain and elongation at break. The effects of PS-R-SiO$_2$ loading at NR:PS-R-SiO$_2$ ratio of 100:0, 90:10, 85:15, 80:20 and 75:25 (equivalent to 0%, 1%, 1.5%, 2% and 2.5% silica content in all nanocomposites, respectively) on mechanical properties of the composites are presented in Table 3.5. With the addition of PS-R-SiO$_2$ at 1 to 1.5%, the tensile strength of NR/PS-R-SiO$_2$ blends increased by 39.1% and 15.6% from the unfilled NR (19.2 MPa). This indicated that the PS-R-SiO$_2$ nanocomposites provide a reinforcing effect on the NR due to the homogeneous SiO$_2$ distribution. Nevertheless, the tensile strength of NR/PS-R-SiO$_2$ blends decreased by 12.0% and 17.7% with the addition of PS-R-SiO$_2$ at 2 to 2.5%. It can be explained in that the high loading leads to small aggregates of PS-R-SiO$_2$ and a lower the filler-rubber interaction.

The modulus at 300% strain of PS-R-SiO$_2$ filled NR at various blend ratios is presented in Table 3.5. The modulus at 300% strain of NR/PS-co-R4-Si blends increased with an increase in NR/PS-R-SiO$_2$ ratios. For the blend ratio of 75:25, the modulus at 300% strain of NR/PS-R-SiO$_2$ was found to increase to 2.9 MPa, compared with unfilled NR (1.3 MPa). This can be explained in that the stiffness of the PS-co-RAFT-SiO$_2$ nanocomposites effectively constrains the movement of the rubber chains and hence enhances the rigidity of the nanocomposites. For elongation at break of unfilled NR and filled NR as presented in Table 3.5, the unfilled NR exhibited the highest elongation at break (819%). NR rich compounds possessed the highest elongation at break due to NR crystallization which resulted upon stretching. With an increase in PS-R-SiO$_2$ amount, the % elongation at break decreases at 2-13% compared to the unfilled NR because of the addition of rigid and stiff silica fillers [90, 91]. However, elongation at break of NR/PS-R-SiO$_2$ was quite high due to the low PS-R-SiO$_2$ loading. It showed similar results as that of blends of natural rubber with styrene butadiene copolymer (SBR)-SiO$_2$ nanocomposites [87] and hydrogenated polybutadiene (HPB)-SiO$_2$ nanocomposites [90].

Table 3.5 Mechanical properties of NR/PS-R-SiO$_2$ nanocomposites.

NR/PS-R-SiO$_2$[a] (wt/wt)	SiO$_2$ content[b] (wt%)	Tensile strength (MPa)	300% Modulus (MPa)	Elongation at break (%)
100/0	-	19.2 ± 2.1	1.35 ± 0.07	819 ± 22
90/10	1.0	26.7 ± 0.6	1.76 ± 0.05	806 ± 20
85/15	1.5	22.2 ± 1.4	2.38 ± 0.06	739 ± 17
80/20	2.0	16.9 ± 0.8	3.03 ± 0.12	716 ± 26
75/25	2.5	15.8 ± 0.7	2.92 ± 0.11	710 ± 12

[a] PS-co-R4-Si was used as PS-R-SiO$_2$
[b] Silica content based on total rubber.

3.8 Thermal Properties of NR/PS-R-SiO$_2$ Blends

The initial decomposition temperature (T_{id}) and maximum decomposition temperature (T_{max}) of the unfilled NR and NR/PS-R-SiO$_2$ blends at different blend ratios are presented in Table 3.6 and Figure 3.8. Due to the low silica content, it slightly affected the decomposition temperature. It is obvious that the T_{id} of NR/PS-R-SiO$_2$ samples did not significantly change compared with unfilled NR. However, the T_{max} of NR/PS-R-SiO$_2$ composites increased from 386.3 $^{\circ}$C to 390.8 $^{\circ}$C with an increase in PS-R-SiO$_2$ loading (1-2.5 wt%). It can be noted that PS-R-SiO$_2$ nanoparticles could be uniformly dispersed in the NR phase resulting in high thermal stability of the nanocomposites [87]. Moreover, the NR and NR/PS-R-SiO$_2$ blends showed one-step polymer degradation and provided smooth weight loss curves. Similar results were earlier reported for NR/SBR-SiO$_2$ and NR/HPB-SiO$_2$ nanocomposites [87, 90].

Table 3.6 Thermal properties of NR/PS-R-SiO$_2$ nanocomposites.

NR/PS-R-SiO$_2$[a] (wt/wt)	SiO$_2$ content[b] (wt%)	T_{id} ($^{\circ}$C)	T_{max} ($^{\circ}$C)
100/0	-	356.1	383.3
90/10	1.0	357.0	386.3
85/15	1.5	356.6	386.1
80/20	2.0	356.0	389.6
75/25	2.5	354.0	390.8

[a] PS-co-R4-Si was used as PS-R-SiO$_2$
[b] Silica content based on total rubber.
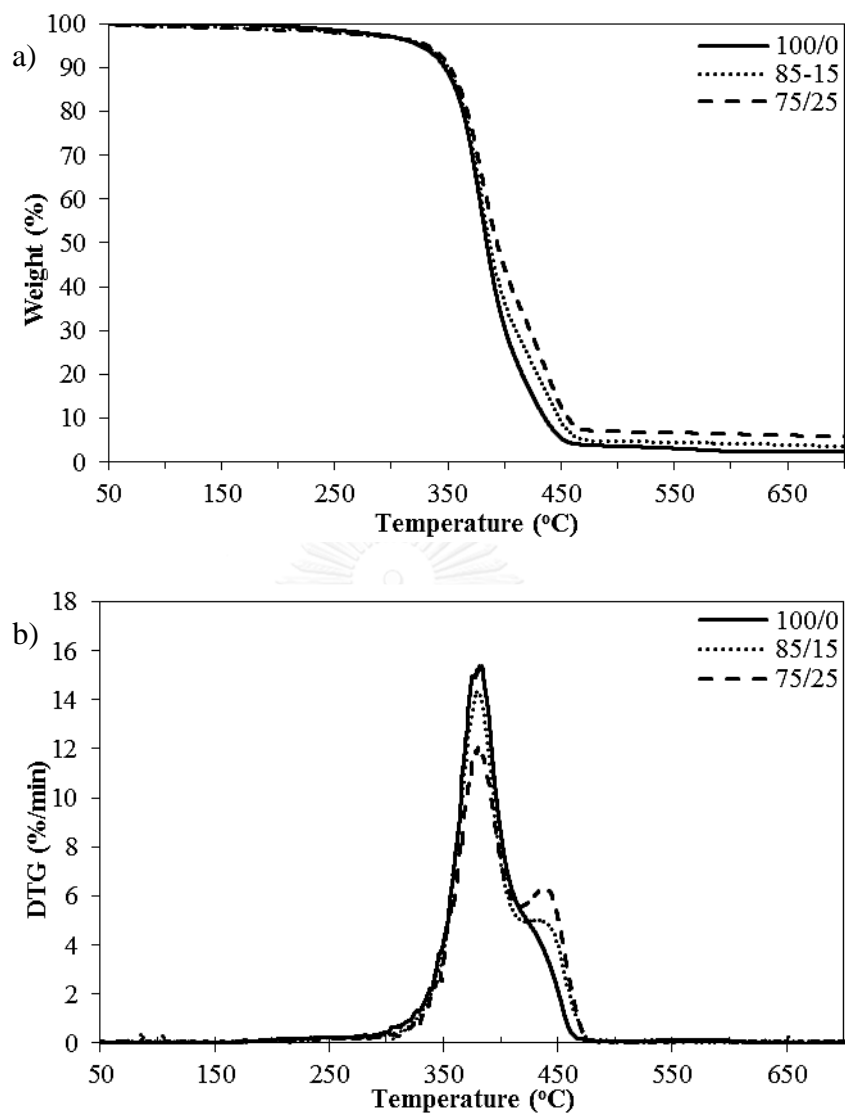
Figure 3.8 TGA and DTG curves of NR filled with PS-R-SiO$_2$ nanocomposites at various ratio (100/0, 85/15 and 75/25).

CHAPTER IV

RAFT EMULSIFIER-FREE EMULSION POLYMERIZATION OF POLYISOPRENE-SILICA NANOPARTICLES USING WATER-SOLUBLE INITIATORS

4.1 Introduction

Organic-inorganic nanocomposites consisting of polymers and nanoparticles are used in many applications such as coatings, membranes, optics, electronics and engineering. Silica is an important inorganic nano-fillers in composite preparation and widely used as effective reinforcement component in improving mechanical properties of polymers. Moreover, emulsion polymerization is an effective method because it provided environmental-friendly process, the heat of reaction was easily released during the polymerization and the viscosity of medium remained close to that of water during the polymerization. Furthermore, reversible addition-fragmentation chain-transfer (RAFT) polymerization is applicable to a wide range of monomers in a various conditions and does not require a catalyst. The key to success of RAFT polymerization process is the RAFT agent which is responsible for controlling chain growth. The original RAFT functionality is retained at the end of chain when diblock structures are formed using RAFT controlled polymerization. Therefore, water-soluble polymers were used for cooperating with the RAFT agent. This chemical structure was called the macro-RAFT agent which was achieved in the emulsifier-free emulsion polymerization. In the absence of emulsifier, the interaction between the RAFT agent and emulsifier was improved and it was also an environmentally desirable choice for preparation of polymer particles at low impurity content.

In this research work, the synthesis of PIP-co-RAFT-SiO$_2$ via RAFT emulsifier-free emulsion polymerization using macro-RAFT agent was studied in depth for the effect of initiator types and [R]:[I] ratio on particle size and core-shell morphology. PIP-co-RAFT-SiO$_2$ nanoparticles as effective fillers in NR latex was investigated, furthermore, NR/PIP-R-SiO$_2$ composites were focused on rubber application, the mechanical and thermal properties.

4.2 Characterization of PIP-co-RAFT and PIP-co-RAFT-SiO₂ Nanocomposites

The NMR spectrum of PIP-co-RAFT is shown in Figure 4.1. The PIP has the isomeric structures with *cis*-1,4, *trans*-1,4, 3,4 and 1,2 linkages representing the diene rubber properties. The ^{1}H-NMR spectroscopy is used to characterize the products of each structures and the ratio of structures are estimated from the integrated peak areas of these signal. The signals in the range of 5.6-5.9, 5.0-5.5 and 4.5-5.0 ppm are attributed to 1,4- PIP, 1,2- PIP and 3,4- PIP with the ratio of 93:3:4.

The FT-IR spectra of VTS-SiO₂ and PIP-co-RAFT- SiO₂ are shown in Figure 4.2. The modified nano-silica has the absorption bands at 1113 and 805 cm^{-1} which are assigned to Si-O-Si groups. The peaks at 2926 and 2850 cm^{-1} correspond to CH and CH₂ stretching of the VTS groups. The bands at 1634 cm^{-1} (C=C) and 1387 cm^{-1} (CH out of plain bending) are attributed to the double bonds of VTS. These results indicate that coupling agent could be bonded onto silica. For PIP-co-RAFT- SiO₂, the absorption bands at 2930 and 2860 cm^{-1} are related to the methylene and methyl stretching of PIP. Furthermore, the peaks at 1707 and 902 cm^{-1} correspond to the C=C stretching and CH wag of trisubstituted olefin of PIP, respectively. The bands at 1445 cm^{-1} and 1370 cm^{-1} are
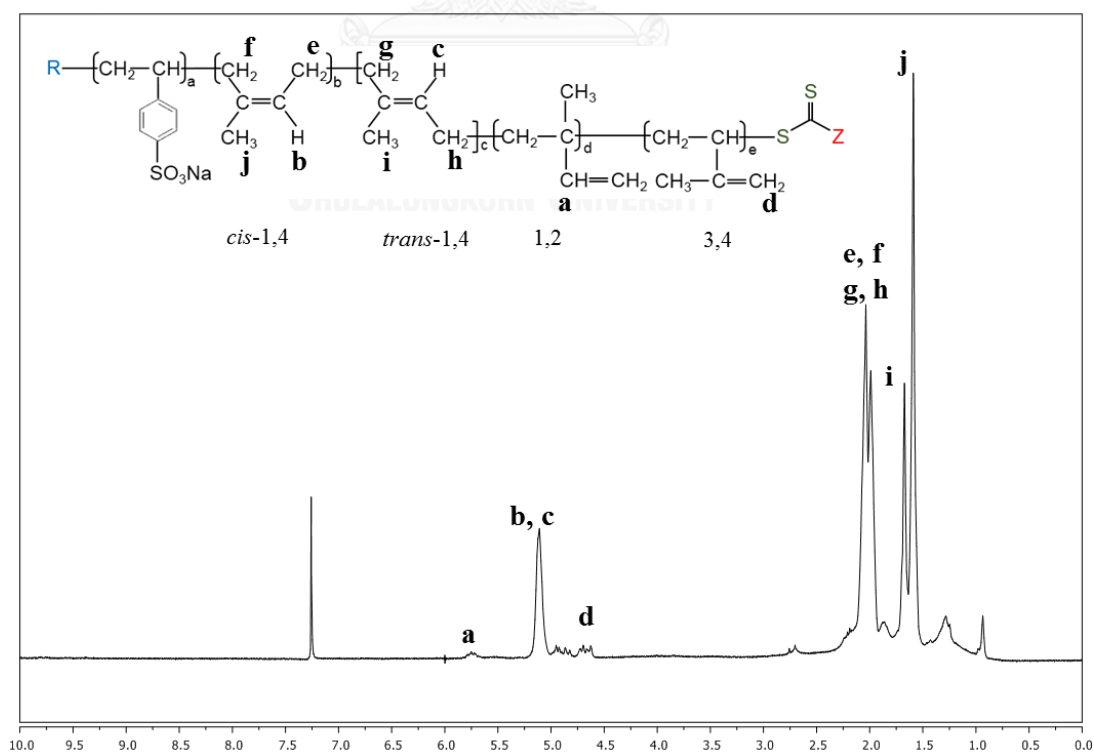
Figure 4.1 ^{1}H-NMR analysis of PIP-co-RAFT (PIP-co-R3-ACP) is carried out in CDCl₃.

attributed to the methyl deformation bands of polyisoprene. These results indicate that PIP was grafted onto the silica surface.

The synthesis of PIP-co-RAFT-SiO$_2$ as shown in Figure 4.3, the silica was firstly modified by VTS coupling agents to bond onto the silica surface. After that macro-RAFT agent and IP monomer were added into the polymerization. The macro-RAFT agent attached to the silica surface and then the IP monomer molecules slightly inserted into the macro-RAFT agent by chain propagation. Eventually, the macro-RAFT agent and IP monomer could be grafted onto the silica surface to produce PIP-co-RAFT-SiO$_2$ structure with core-shell morphology.
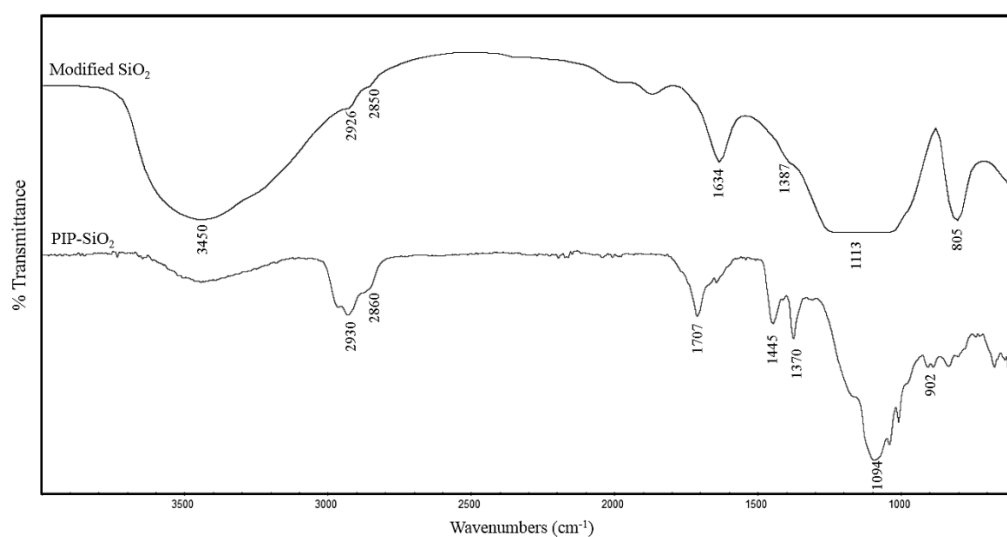
Figure 4.2 FT-IR spectra of VTS-SiO$_2$ (modified nano-silica) and PIP-co-RAFT-SiO$_2$ (PIP-co-R3-ACP-Si).
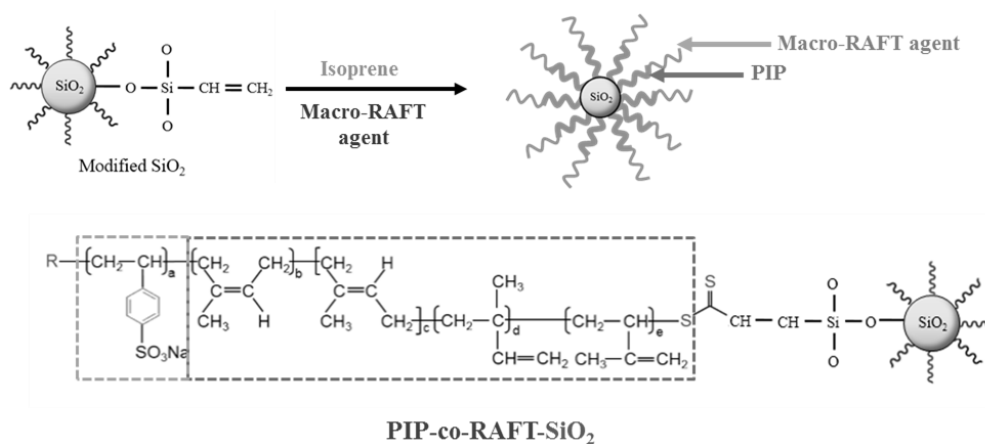
Figure 4.3 Proposed mechanism of polyisoprene-silica nanoparticles (PIP-co-RAFT-SiO$_2$) via RAFT emulsifier-free emulsion polymerization.

4.3 Morphology of PIP-co-RAFT and PIP-co-RAFT-SiO$_2$ Nanocomposites

The morphology of PIP-co-RAFT and PIP-co-RAFT-SiO$_2$ nanoparticles characterized by TEM are shown in Figure 4.4. The TEM image of PIP-co-R3-ACP (Figure 4.4a) presented the spherical PIP particles (without silica) with a diameter of around 37 nm. The micrographs of PIP-co-RAFT-ACP-SiO$_2$ and PIP-co-RAFT-V50-SiO$_2$ nanoparticles (Figures. 4.4b-4.4e) exhibited a core-shell structure which the darker area represented the nano-silica core region and the lighter area represented the PIP grafted onto the silica surface as the shell. Moreover, Figure 4.4 also shows that the nanoparticles are well-dispersed in the emulsion form and a narrow PSD is achieved for all PIP-co-RAFT and PIP-co-RAFT-SiO$_2$ nanocomposites at all [R]:[I] ratios. It can be noted that the RAFT emulsifier-free emulsion polymerization has successfully produced the PIP-co-RAFT and PS-co-RAFT-SiO$_2$ nanoparticles.
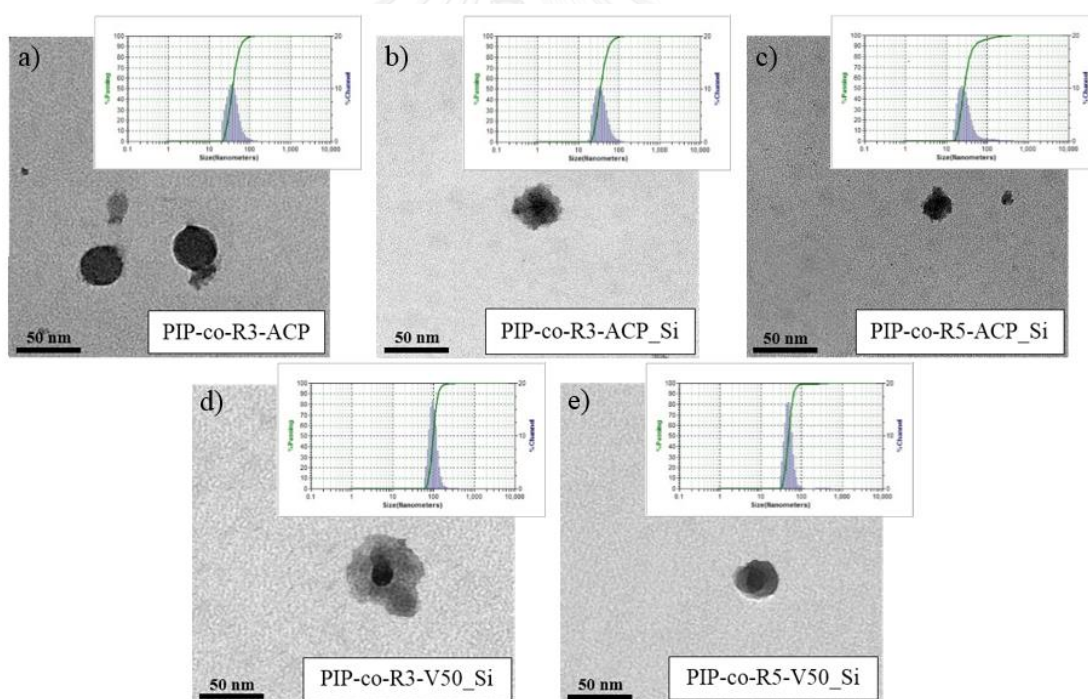
Figure 4.4 TEM micrographs of PIP-co-RAFT-ACP, PIP-co-RAFT-ACP-SiO$_2$ and PIP-co-RAFT-V50-SiO$_2$.

4.4 Synthesis of PIP-co-RAFT Nanoparticles

The particle size, particle size distribution (PSD), % total solid content and monomer conversion (%) of PIP-co-RAFT nanoparticles prepared using different initiators (ACP and V50) are presented in Table 4.1. For ACP initiators, the particle size of PIP-co-RAFT-ACP emulsion decreased with increasing the [R]:[I] ratio because of the macro-RAFT agent amount representing the number of hydrophilic chains. The number of hydrophilic chains increased resulting in lower chain growth. Therefore, the particle size decreased with decreasing chain growth. A particle size of 28-88 nm with PIP-co-RAFT-ACP latex was achieved for polymerization at all [R]:[I] ratios. For V50 initiators, the particle size of PIP-co-RAFT-V50 emulsion also decreased with increasing the [R]:[I] ratio. The polymerization was not attained at [R]:[I] ratio = 1:1 due to the coagulation of PIP-co-RAFT-V50 particles. The particle size of PIP-co-RAFT-V50 emulsion at the other [R]:[I] ratios was 59-184 nm. However, PIP-co-RAFT-ACP and PIP-co-RAFT-V50 nanocomposites at the same [R]:[I] ratio clearly showed the different particle size. PIP-co-RAFT-ACP nanoparticles presented the smaller size than PIP-co-RAFT-V50 nanoparticles. These could be caused by the different molecular structures of ACP and V50 initiators as illustrated in Figure 4.5. The dissociation properties of ACP and V50 initiators are weekly acidic (-COOH) and basic [-C(=NH)-NH$_2$], respectively. It can be said that the lone pair electron in the structure of V50 initiator gave the high reactivity. The V50 initiator was more active than the ACP initiator which initiator would react with monomer molecules at high reaction rate in the polymerization process, thus, there were nanoparticles with greater size in the PIP-co-RAFT-V50 emulsion.

Moreover, the PSD values were found to be below 2, indicating that the polymerization occurred under the good growth control. For the monomer conversion, it can be seen that the monomer conversion increased with an increase in [R]:[I] ratio. Due to the fact that macro-RAFT agent played the role of a stabilizer as an emulsifier, a higher macro-RAFT agent concentration may generate more chain growth which give more chain extension in the process resulting in a higher polymerization rate and monomer conversion. Nevertheless, PIP-co-R2-V50 and PIP-co-R3-V50 emulsion showed quite low conversion because the large particles might agglomerate and disturb in the polymerization.

The effect of the [R]:[I] ratio on the characteristics of the PIP-co-RAFT-ACP and PIP-co-RAFT-V50 latex are shown in Figures. 4.6a and 4.7a. For PIP-co-RAFT-ACP emulsion, it can be seen that more transparent latex was produced with increasing [R]:[I] ratio. On the other hand, the appearance of PIP-co-RAFT-V50 emulsions was less transparent due to the large particle size of latex.

Table 4.1 Effect of [R]:[I] ratio on particle size, % total solid content and monomer conversion (%) of PIP-co-RAFT.

Name	[R]:[I][a]	Particle size (nm)	PSD	% Total solid content	Monomer conversion (%)
ACP initiator					
PIP-co-R1-ACP	1:1	87.5	1.2	16.1	72.9
PIP-co-R2-ACP	2:1	54.0	1.3	17.0	77.3
PIP-co-R3-ACP	3:1	37.4	1.3	16.3	74.5
PIP-co-R4-ACP	4:1	36.3	1.4	17.8	81.0
PIP-co-R5-ACP	5:1	28.0	1.4	18.8	86.2
V50 initiator					
PIP-co-R1-V50	1:1	-[b]	-	-	-
PIP-co-R2-V50	2:1	184.3	1.1	7.4	31.8
PIP-co-R3-V50	3:1	165.9	1.1	10.0	44.4
PIP-co-R4-V50	4:1	61.5	1.2	19.8	85.5
PIP-co-R5-V50	5:1	58.6	1.1	18.6	81.8

[a] [R]:[I] = the ratio of macro-RAFT agent concentration to initiator concentration.
Condition: Initiator = 0.1 g, H_2O = 35 g, Isoprene = 10 g, Temp = 75 °C, Time = 15 h.
[b] "-" is coagulation of PIP-co-RAFT nanoparticles.
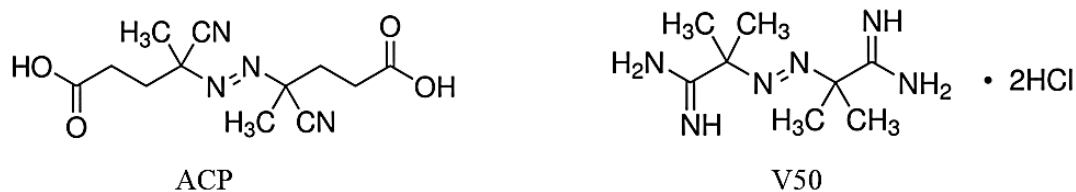
Figure 4.5 Chemical structure of ACP and V50 initiators
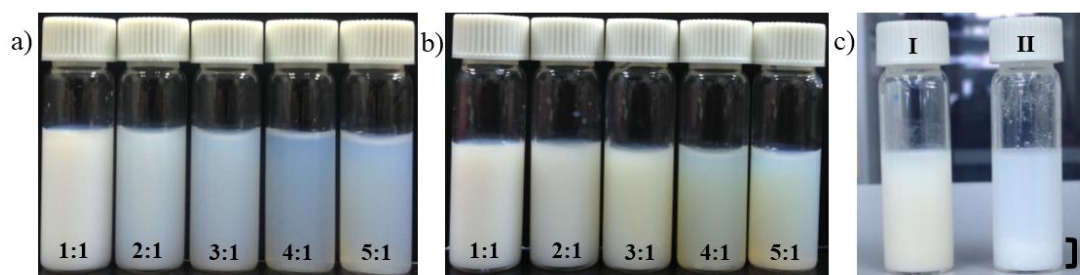
Figure 4.6 Effect of [R]:[I] ratio on characteristics of a) PIP-co-RAFT-ACP emulsions, b) PIP-co-RAFT-ACP-SiO$_2$ emulsions and c) comparison between PIP-co-R3-ACP-Si (silica encapsulated, I) and silica mixed with PIP-co-R3-ACP (II).
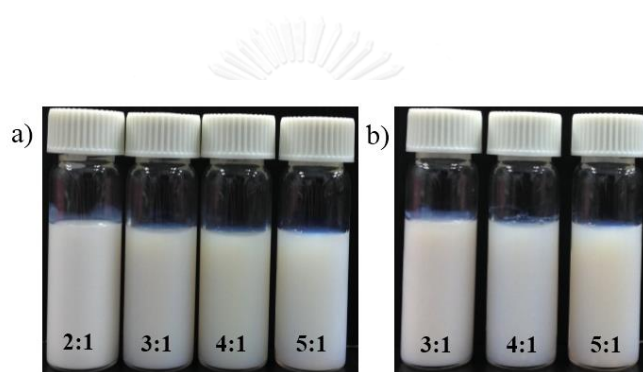
Figure 4.7 Effect of [R]:[I] ratio on characteristics of a) PIP-co-RAFT-V50 emulsions and b) PIP-co-RAFT-V50-SiO$_2$ emulsions.

4.5 Synthesis of PIP-co-RAFT-SiO$_2$ Nanoparticles

The particle size, particle size distribution (PSD), % total solid content, monomer conversion (%), grafting efficiency (%GE) and silica encapsulation efficiency (%Si encap eff) of PIP-co-RAFT-SiO$_2$ emulsion are presented in Table 4.2. The particle size of PIP-co-RAFT-SiO$_2$ nanocomposites decreased with an increase in the [R]:[I] ratio due to the fact that the macro-RAFT agent amount influenced the number of hydrophilic chains. The number of hydrophilic chains increased resulting in lower chain growth. Consequently, the diameter of particle decreased with a decrease in chain growth. For the all [R]:[I] ratios, a particle size of 25-73 nm with PIP-co-RAFT-ACP-SiO$_2$ latex was achieved. However, a particle size of 48-91 nm with PIP-co-RAFT-V50-SiO$_2$ emulsion was synthesized for the [R]:[I] ratios = 3:1, 4:1 and 5:1 due to the agglomeration of particles in the polymerization system at the other ratios

(1:1 and 2:1). Moreover, it was observed that PIP-co-RAFT-ACP-SiO$_2$ nanoparticles exhibited the smaller size than PIP-co-RAFT-V50-SiO$_2$ nanocomposites due to the different chemical structures of initiators used in the RAFT polymerization. The V50 initiator had more active structure than the ACP initiator, therefore, the PIP-co-RAFT-V50-SiO$_2$ nanoparticles showed a greater size in the system. Furthermore, the PSD was below 2, indicating that the polymerization had become controlled.

Nevertheless, PIP-co-RAFT-ACP-SiO$_2$ emulsion presented the monomer conversion increased from 64 to 91 % with increasing [R]:[I] ratio and the encapsulation of SiO$_2$ also increased from 18 to 74 % with increasing [R]:[I] ratio except [R]:[I] ratio = 5:1. It can be explained that the macro-RAFT agent as the role of a surfactant which absorbed on the silica surface and then provided the monomers into the chain growth resulting in a higher monomer conversion and silica encapsulation efficiency. However, the high macro-RAFT agent concentration had an effect on the polymerization process because macro-RAFT agent could inhibit the growth of polymer chain resulting in lower monomer conversion and silica encapsulation efficiency. In addition, the grafting efficiency showed quite high value (86-90 %). For PIP-co-RAFT-V50-SiO$_2$ synthesis, the monomer conversion showed the similar result as PIP-co-RAFT-ACP-SiO$_2$ synthesis but the encapsulation of SiO$_2$ decreased from 67 to 33 % with increasing [R]:[I] ratio because of the macro-RAFT agent and the reactivity of initiator. However, the grafting efficiency presented the high value (82-96 %).

The effect of the [R]:[I] ratio on the characteristics of the PIP-co-RAFT-SiO$_2$ latex is shown in Figures. 4.6b and 4.7b. It was found that PIP-co-RAFT-ACP-SiO$_2$ nanoparticles with an increase in the [R]:[I] ratio exhibited a trend of decreasing diameter of latex particles and the latex becomes more transparent. PIP-co-RAFT-V50-SiO$_2$ with an increase in the [R]:[I] ratio, it was not significantly changed transparency because of the large particle size of latex. However, the RAFT emulsifier-free emulsion polymerization of PIP on VTS-silica could provide PIP-co-RAFT-SiO$_2$ nanocomposites with a monodispersion of silica in the latex resulting in a homogeneous composite emulsion. For the physical mixing of VTS-siliica with PIP-co-R3-ACP latex (Figure 4.6c), it is clearly showed that there was a two-phase seperation of modified silica and PIP-co-RAFT emulsion in the system because of the hydrophilic silica

surface. The hydrophilic surface caused a heterogeneity, free polymer formation and silica agglomeration which cannot be broken down with high speed shearing or milling via mechanical mixing [87]. Therefore, the encapsulation of silica with PIP-co-RAFT-SiO$_2$ synthesis could enhance the compatibility and dispersion of silica in the PIP-co-RAFT-SiO$_2$ matrix, reduce the silica-silica interaction and result the homogeneity of silica in the PIP-co-RAFT-SiO$_2$ latex.

Table 4.2 Effect of [R]:[I] ratio on particle size, % total solid content, monomer conversion (%), %GE and %Si encap eff of PIP-co-RAFT-SiO$_2$.

Name	[R]:[I]^a	Particle size (nm)	PSD	% Total solid content	Monomer conversion (%)	%GE	%Si encap eff
ACP initiator							
PIP-co-R1-ACP-Si	1:1	73.1	1.5	14.8	64	86.4	18.3
PIP-co-R2-ACP-Si	2:1	44.1	1.5	17.1	77.1	90.4	50.4
PIP-co-R3-ACP-Si	3:1	37.5	1.2	19.2	84.2	82.5	55
PIP-co-R4-ACP-Si	4:1	27.2	1.5	21	91	89.1	73.5
PIP-co-R5-ACP-Si	5:1	24.8	1.5	19	86.8	89.2	61.8
V50 initiator							
PIP-co-R1-V50-Si	1:1	-^{b}	-^{b}	-^{b}	-^{b}	-^{b}	-^{b}
PIP-co-R2-V50-Si	2:1	-^{b}	-^{b}	-^{b}	-^{b}	-^{b}	-^{b}
PIP-co-R3-V50-Si	3:1	90.9	1.5	19.5	80.4	82.2	66.5
PIP-co-R4-V50-Si	4:1	66.1	1.4	22.1	96	91.4	56.6
PIP-co-R5-V50-Si	5:1	48.2	1.2	16.8	48.2	96.2	33.1

^{a} [R]:[I] = the ratio of macro-RAFT agent concentration to initiator concentration.
 Condition: Initiator = 0.1 g, H$_2$O = 35 g, Isoprene = 10 g, Silica = 1 g, Temp = 75 °C, Time = 15 h.
^{b} "-" is coagulation of PIP-co-RAFT-SiO$_2$ nanoparticles.

4.6 Mechanical and Thermal Properties of NR/PS-R-SiO$_2$ nanocomposites

PIP-co-R3-ACP-Si and PIP-co-R4-V50-Si nanocomposites were selected to blend with NR latex for mechanical and thermal testing. The effects of PIP-R-SiO$_2$ amount at NR/PIP-R-SiO$_2$ ratio of 100/0, 90/10, 80/20 and 70/30 (equivalent to 0%, 1%, 2% and 3% silica content in all nanocomposite films, respectively) on mechanical and thermal properties of the composites are presented in Table 4.3. The mechanical properties of PIP-R-SiO$_2$ filled NR were investigated in terms of tensile strength, modulus at 300% strain and elongation at break. For NR/PIP-R-SiO$_2$ nanocomposites with the addition of PIP-co-R3-ACP_Si emulsion, the tensile strength of blends (23.5-24.2 MPa) were higher than that of unfilled NR (17.9 MPa). This indicated that PIP-co-R3-ACP-Si nanocomposites provide a reinforcing effect on the natural rubber with a homogeneous dispersion of silica. Moreover, the modulus at 300% strain of samples with PIP-co-R3-ACP-Si loading was slightly increased from 1.11 to 1.24 MPa with an increase in NR/PIP-R-SiO$_2$ ratios. This can be explained in that these nanoparticles helped to increase the external force resistance because of the high interaction between the nano-fillers and the NR matrix. In additions, the elongation at break of blends increased from 871% to 972% with increasing PIP-co-R3-ACP_Si loading due to the flexible and elastic nature of polyisoprene.

Table 4.3 Mechanical properties of NR/PIP-R-SiO$_2$ nanocomposites.

NR/PIP-R-SiO$_2$ (wt/wt)	SiO$_2$ content[c] (wt%)	Tensile strength (MPa)	300% Modulus (MPa)	Elongation at break (%)
100/0	-	17.9 ± 0.7	1.11 ± 0.02	871 ± 32
ACP initiator[a]				
90/10	1.0	24.2 ± 2.1	1.19 ± 0.02	947 ± 08
80/20	2.0	23.5 ± 1.0	1.24 ± 0.01	972 ± 15
V50 initiator[b]				
90/10	1.0	18.4 ± 1.6	1.09 ± 0.01	889 ± 39
80/20	2.0	16.0 ± 1.2	1.19 ± 0.01	891 ± 34
70/30	3.0	15.1 ± 2.8	1.37 ± 0.08	935 ± 77

[a] PIP-co-R3-ACP-Si was used as PIP-co-R-SiO$_2$.
[b] PIP-co-R4-V50-Si was used as PIP-co-R-SiO$_2$.
[c] Silica content based on total rubber.

For NR/PIP-R-SiO$_2$ nanocomposites with the addition of PIP-co-R4-V50-Si latex, the tensile strength of blends at 1% silica loading (18.4 MPa) was slightly higher than the unfilled NR. However, the tensile strength of composites was decreased to 16.0 and 15.1 MPa with the addition of PIP-co-R4-V50-Si emulsion at 2-3% silica loading due to aggregation of PIP-R-SiO$_2$ nanoparticles and a lower the filler-rubber interaction. Furthermore, the modulus at 300% strain was gradually increased from 1.11 to 1.37 MPa and the elongation at break was increased from 871% to 935% with an increase in silica content from 0-3 wt%. These indicated that the nano-fillers increased the external force resistance with well dispersed fillers and the flexible and elastic properties of polyisoprene. Besides, the addition of PIP-co-R3-ACP-Si emulsion showed the better mechanical properties than the addition of PIP-co-R4-V50-Si emulsion. It can be noted that the particle size of PIP-R-SiO$_2$ fillers had an effect on tensile strength, modulus at 300% strain and elongation at break indicating that PIP-co-R3-ACP-Si (smaller particle size) was well-dispersed in the NR latex. Nevertheless, PIP-R-SiO$_2$ composites synthesized via RAFT polymerization could improve the mechanical properties of NR latex.

The initial decomposition temperature (T_{id}) and maximum decomposition temperature (T_{max}) of the unfilled NR and NR/PIP-R-SiO$_2$ blends at various blend ratios are presented in Table 4.4 and Figure 4.8. Because of the low silica content, it slightly affected the decomposition temperature. It is obvious that the T_{id} and T_{max} of NR/PIP-R-SiO$_2$ samples with the addition of PIP-co-R3-ACP-Si and PIP-co-R4-V50-Si latex did not significantly change compared with unfilled NR. Moreover, the NR and NR/PIP-R-SiO$_2$ blends showed one-step polymer degradation and provided smooth weight loss curves.

Table 4.4 Thermal properties of NR/PIP-co-R-SiO$_2$ nanocomposites.

NR/PIP-co-R-SiO$_2$ (wt/wt)	SiO$_2$ content[c] (wt%)	T_{id} (°C)	T_{max} (°C)
100/0	-	349.4	376.7
ACP initiator[a]			
90/10	1.0	348.7	375.6
80/20	2.0	348.8	376.7
V-50 initiator[b]			
90/10	1.0	348.9	377.0
80/20	2.0	348.6	376.6
70/30	3.0	348.8	377.3

[a] PIP-co-R3-ACP-Si was used as PIP-co-R-SiO$_2$.
[b] PIP-co-R4-V50-Si was used as PIP-co-R-SiO$_2$.
[c] Silica content based on total rubber.
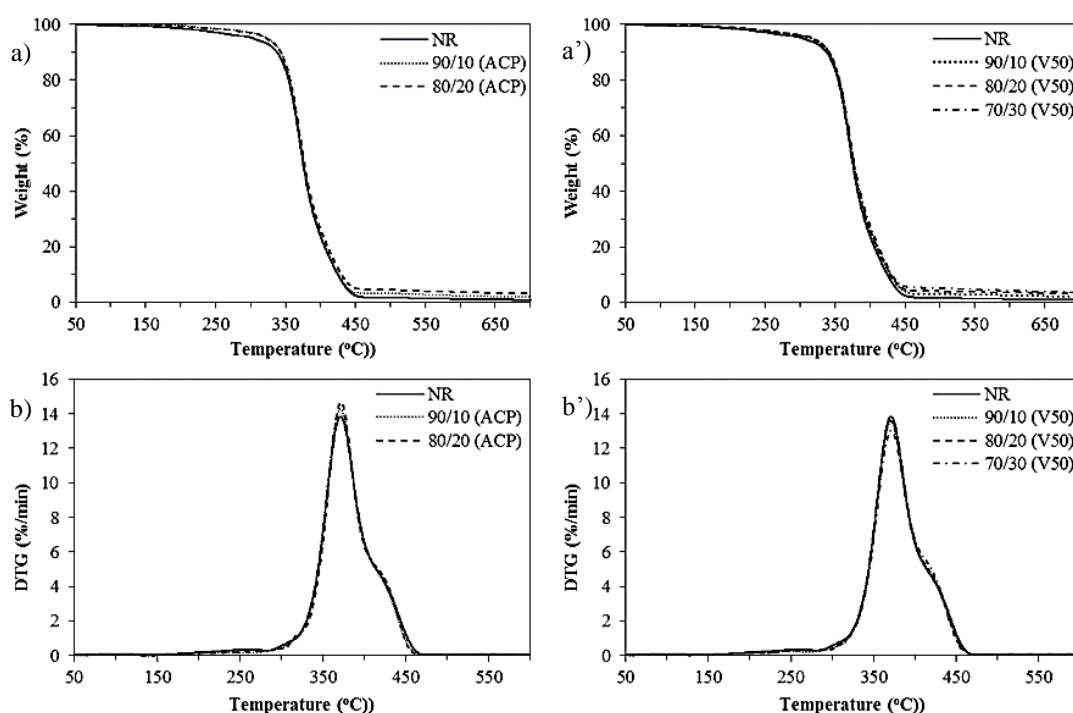
Figure 4.8 TGA curves of NR filled with PIP-R-SiO$_2$ nanocomposites at various ratio,
a) NR/PIP-co-R3-ACP-Si and a') NR/PIP-co-R4-V50-Si and DTG curves
of NR filled with PIP-R-SiO$_2$ nanocomposites at various ratio, b) NR/PIP-
co-R3-ACP-Si and b') NR/PIP-co-R4-V50-Si.

4.7 Dynamic Mechanical Properties of NR/PIP-R-SiO$_2$ Nanocomposites

The elastic modulus of a material and its mechanical dumping or energy dissipation characteristics as a function of frequency and temperature can be measured by DMA. The storage modulus (E') of the unfilled NR and NR/PIP-R-SiO$_2$ composites at different blend ratios are shown in Table 4.5 and Figure 4.9. It was observed that the E' values of all samples were decreased around the transition region which was a state after the onset of a sharp reduction in storage modulus because the mobility of the polymer chains increased with an increase in temperature. It can be noted that all samples have some elastic properties above their glass transition temperature (T$_g$). Moreover, the E' values of NR/PIP-R3-ACP-Si nanocomposites (at 20°C) at 1 and 2 wt% silica loading were 0.62 and 0.74 MPa. In the same way, the E' values of NR/PIP-R3-V50-Si films (at 20°C) at 1, 2 and 3 wt% silica content were 0.55, 0.60 and 0.79 MPa, respectively. It was found that the storage modulus of all NR/PIP-R-SiO$_2$ blends was higher than that of unfilled NR (0.53 MPa). It can be described that the addition of nano-filler led to decrease the stiffness and increase the ability to the damping capacity of the NR latex. Therefore, the addition of PIP-R-SiO$_2$ nanocomposites into the NR matrix could increase of the storage modulus resulting in the enhancement of stiffness and strength of NR.

The tan δ or loss tangent is determined from the ratio of dynamic loss modulus (E'') to storage modulus (E'). The tan δ of the unfilled NR and NR/PIP-R-SiO$_2$ composites at different blend ratios are shown in Table 4.5 and Figure 4.9. The NR/PIP-R-SiO$_2$ blends showed a lower internal fraction loss factor (tan δ) than vulcanized unfilled NR because of an increase in the homogeneity structure of the composite materials. Furthermore, the T$_g$ of NR/PIP-R3-ACP-Si (-38.8 to -37.6 ^{o}C) and NR/PIP-R3-V50-Si (-37.5 to -36.0 ^{o}C) was slightly higher than that of unfilled NR (-39.8 ^{o}C) because the addition of rigid particles gave a lower flexibility and mobility of the polymer chains.

Table 4.5 Dynamic Mechanical properties of NR/PIP-co-R-SiO$_2$ nanocomposites.

NR/PIP-co-R-SiO$_2$ (wt/wt)	SiO$_2$ content[c] (wt%)	E'$_{max}$ (MPa)	E'$_{20^oC}$ (MPa)	Tan δ	T$_g$ (°C)
100/0	-	732	0.53	2.44	-39.8
ACP initiator[a]					
90/10	1.0	814	0.62	2.36	-38.8
80/20	2.0	517	0.74	2.04	-37.6
V-50 initiator[b]					
90/10	1.0	584	0.55	2.36	-37.5
80/20	2.0	608	0.60	2.17	-36.9
70/30	3.0	591	0.79	2.06	-36.0

[a] PIP-co-R3-ACP-Si was used as PIP-co-R-SiO$_2$.
[b] PIP-co-R4-V50-Si was used as PIP-co-R-SiO$_2$.
[c] Silica content based on total rubber.
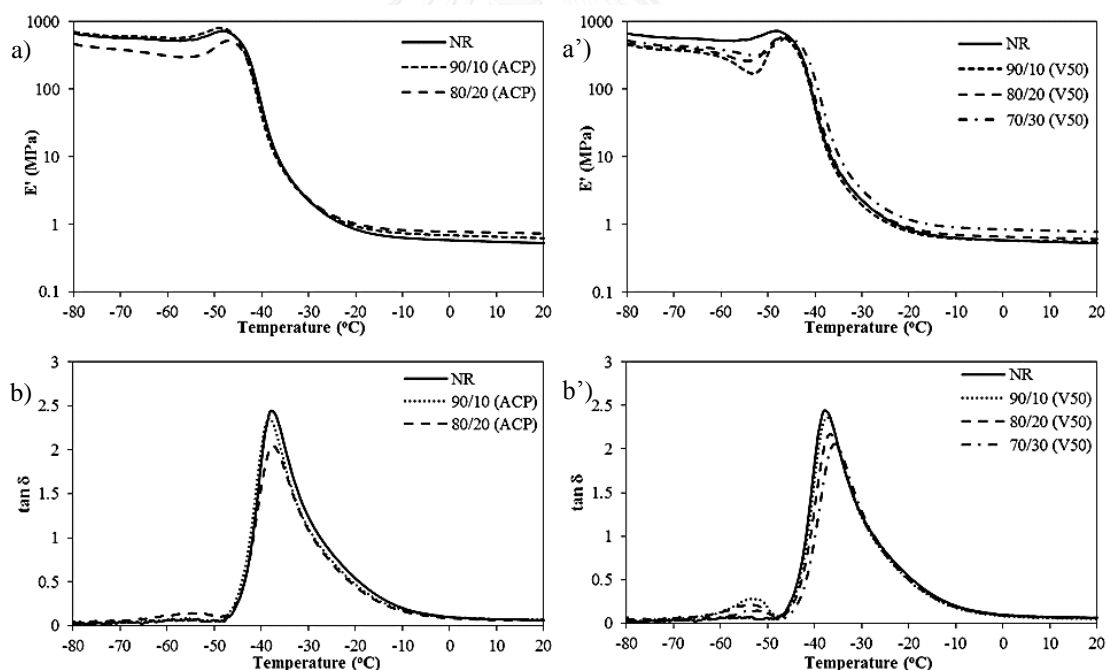
Figure 4.9 Temperature and NR/PIP-R-SiO$_2$ ratio dependence of storage modulus (E'), a) NR/PIP-co-R3-ACP-Si and a') NR/PIP-co-R4-V50-Si and temperature and NR/PIP-R-SiO$_2$ ratio dependence of loss tangent (tan δ), b) NR/PIP-co-R3-ACP-Si and b') NR/PIP-co-R4-V50-Si.

CHAPTER V

PREPARATION OF POLY(METHYL METHACRYLATE)-SILICA NANOPARTICLES VIA DIFFERENTIAL MICROEMULSION POLYMERIZATION AND PHYSICAL PROPERTIES OF NR/PMMA-SILICA HYBRID MEMBRANES

5.1 Introduction

The addition of inorganic fillers into polymer matrixes is well known as being a beneficial way to improve the polymer properties such as mechanical, thermal, optical and electrical properties. Polymer nanomaterials are widely used in many applications due to their good processability and properties. On the other hand, nanosilica is one of the most common inorganic fillers used in various fields as the silica is an effective reinforcement component in developing nanocomposites. Therefore, grafting of polymer chains onto silica nanoparticles is an effective methods to increase the hydrophobicity of the particles and to improve interfacial interactions in nanocomposites resulting in better compatibility and dispersion of silica particles in the polymer matrix. Besides common plastic and rubber reinforcement, one potential and practical application of this nanocomposite is in membrane separation. Pervaporation separates the liquid mixtures by the difference in the solubility and diffusivity of each liquid component within the membrane. In order to achieve a good separation, the membrane must contain the active sites that interact strongly with the separated species.

To produce inorganic-polymer hybrid particles, differential microemulsion polymerization (DMP) is a challenging process using low surfactant concentration and yields nano-size particles and high conversion. This led to the motivation of our research on preparation of PMMA-SiO_2 nanoparticles via DMP. The effect of silica loading and surfactant concentration on monomer conversion, silica encapsulation efficiency and particle size were investigated. The prevulcanized hybrid membrane of a natural rubber latex and PMMA-SiO_2 nanoparticles was prepared and tested for pervaporation of water-ethanol mixtures.

5.2 Characterization of PMMA-SiO$_2$ Nanoparticles

For the modified silica surface, the methoxy groups of the VTS coupling agent would be hydrolyzed and condensed with the silanol groups at the silica surface and then the MMA monomer was grafted on the silica surface. Figure 5.1 illustrates the FT-IR spectra of the VTS-SiO$_2$ and PMMA-SiO$_2$. For silica modified with VTS, the absorption bands at 1113, 805 and 470 cm^{-1} were assigned to the Si-O-Si groups. The absorption peaks at 3450, 2926 and 2850 cm^{-1} corresponded to OH, CH and CH$_2$ stretching of the VTS groups. The peaks at 1634 and 1387 cm^{-1} were attributed to C=C stretching and C-H out of plain blending of the VTS group, respectively. These results indicated that VTS silane coupling agents could be bonded with silanol groups of silica to introduce a double bond on the silica surface. For PMMA-SiO$_2$ nanocomposite, the absorption peaks at 2948, 1731 and 1449 cm^{-1} were assigned to CH, C=O and CH$_3$ stretching vibration of PMMA, respectively. All results obtained from FT-IR spectra confirmed that the silica nanoparticle has been successfully encapsulated by PMMA via DMP.

Additionally, Figure 5.2 presents ^{1}H-NMR spectra of PMMA-SiO$_2$ to identify the microstructure. The signal between 3.4-3.7 ppm corresponded to the protons of the methyl groups attached to the ester groups of the side chains. The peaks at 0.8 and 1 ppm referred to the protons of the methyl groups attached to the carbon of the backbone of the PMMA-SiO$_2$, and the peaks in the range of 1.6-2 ppm relate to the protons of the methylene groups from the backbone. The ^{1}H-NMR spectra confirmed that the PMMA was grafted onto the silica surface.
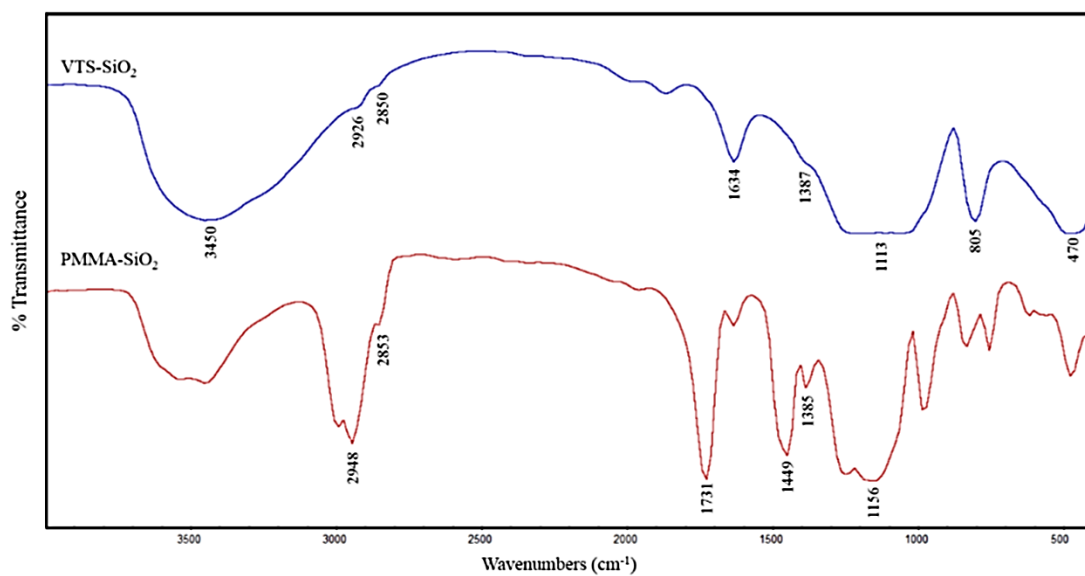
Figure 5.1 FT-IR spectra of VTS-SiO$_2$ (modified nano-silica) and PMMA-SiO$_2$
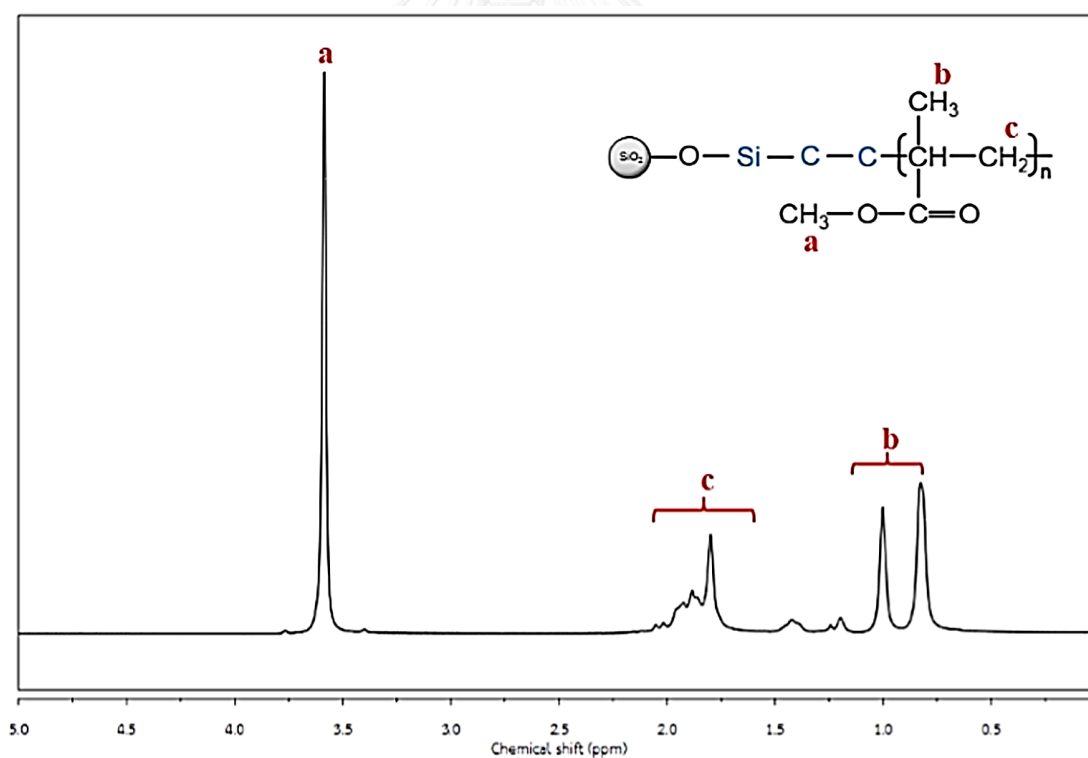
Figure 5.2 ^{1}H-NMR analysis of PMMA-SiO$_2$ is carried out in CDCl$_3$.
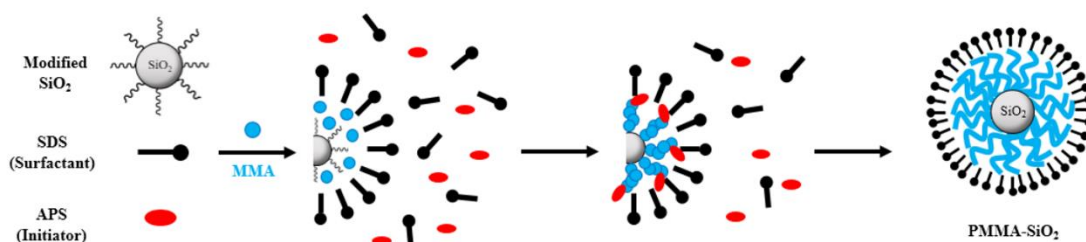
Figure 5.3 Formation mechanism of differential microemulsion polymerization of PMMA-SiO$_2$ nanoparticles.

The mechanism of PMMA-SiO$_2$ synthesis is proposed in Figure 5.3. The modified silica, SDS (surfactant) and APS (initiator) were dispersed in deionized water to form a homogeneous solution. The surfactant produced the micelles in the solution in which the hydrophilic parts turn toward the aqueous phase and the hydrophobic parts form the core of organic phase. For DMP, the MMA monomer was dropwise fed into the solution and the initiator decomposed into free radicals in the aqueous phase that produced reactive monomer radicals on the silica surface and monomer molecules. Then, these monomer radicals were reacted with the other monomers to form the oligomeric radicals to produce the growing chains until termination resulted in the PMMA-SiO$_2$ nanoparticles. Therefore, the PMMA could be grafted onto the silica surface with core-shell morphology.

5.3 Effect of parameters on PMMA-SiO$_2$ Preparation

For PMMA-SiO$_2$ synthesis using APS as initiator, the effect of initiator concentration on particle size and silica encapsulation efficiency is shown in Figure 5.4. It can be seen that the particle size and silica encapsulation efficiency did not significantly change over the range of low initiator concentration (0.61-1.61 wt%). This phenomenon can be explained by two steps. First, oligoradicals were generated in the aqueous phase. Second, oligoradicals could continue to form new particles via the nucleation process. Due to the fact that these two processes controlled the reaction in each step [28]. At a low initiator concentration, the oligoradicals could grow less into particles with a small change size resulting in the particle size of 44-46 nm. This showed the similar results as the synthesis of polybutadiene (PB)-SiO$_2$ nanoparticles using

potassium persulfate in which the particle size changed very slightly at the low initiator amount [90].

SDS was used as surfactant for encapsulation of nanosilica with PMMA at a concentration above the critical micelle concentration (CMC). The surfactant concentration had a significant effect on particle size and silica encapsulation efficiency as illustrated in Figure 5.5a. The particle size decreased from 50.0 to 33.7 nm with an increase in the surfactant concentration from 3.34 to 10.34 wt% based on monomer. For DMP, after nucleation, the particles could grow and collide with each other. At low surfactant concentration (or not enough), after collision, the particles would merge together and become larger ones. Therefore, the surfactant concentration increased resulting in a smaller particle size. Furthermore, the silica encapsulation efficiency increased from 75.3 to 98.7 % with an increase in the surfactant concentration. This is due to the surfactant being absorbed on the silica surface which then, provided the monomer swollen micelles resulting in the diffusion of hydrophobic monomer onto the silica surface [92]. On the other hand, at a higher surfactant amount, more surface of silica nanoparticles could be provided with monomer micelles which resulted in an increase in silica encapsulation efficiency. From the characteristics of the PMMA-SiO$_2$ latex as shown in Figure 5.5b, the diameter of latex exhibited a trend of decreasing diameter and more transparent latex was produced with increasing surfactant concentration. Similar results was observed for the synthesis of PB-SiO$_2$ nanoparticles [90] and styrene butadiene copolymer (SBR)-SiO$_2$ nanocomposites [87].
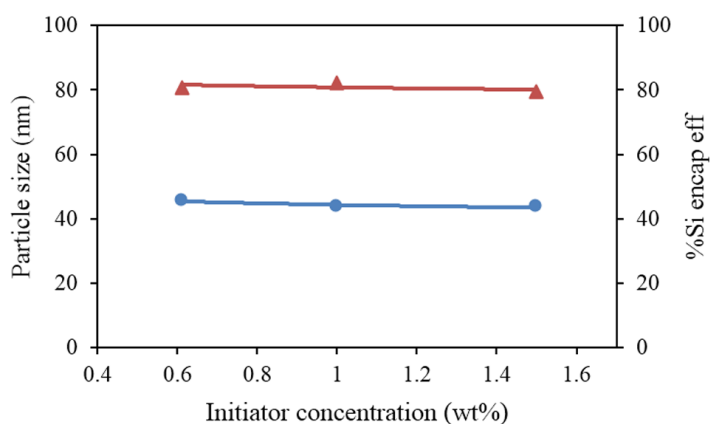
Figure 5.4 Effect of APS concentration on; (●) Particle size, (▲) %Si encap eff. Condition: M/H$_2$O = 0.4, SiO$_2$ = 5 wt%, SDS = 5.34 wt% base on monomer.
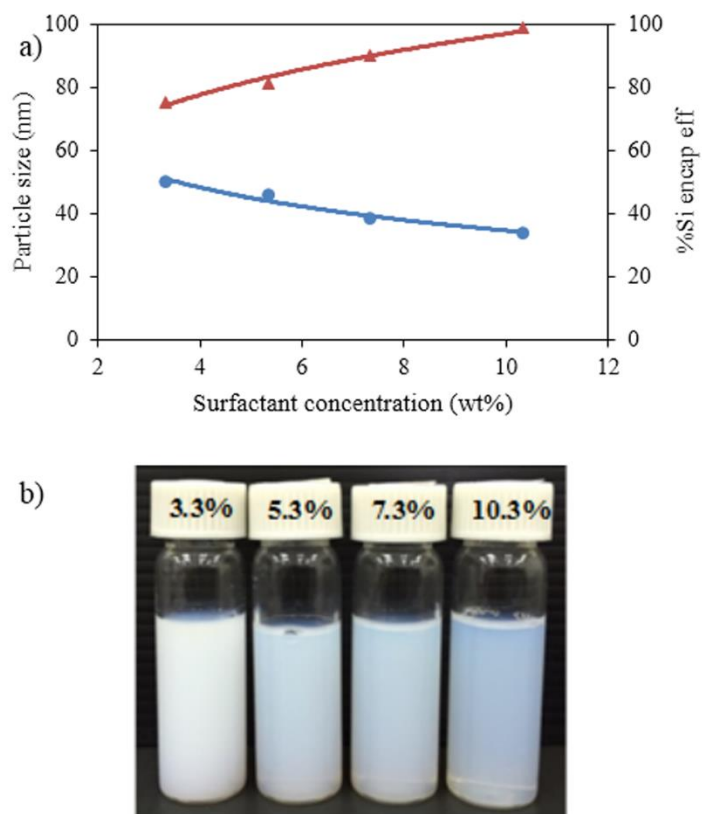
Figure 5.5 Effect of SDS concentration on; (●) Particle size, (▲) %Si encap eff and characteristic of latex. Condition: $M/H_2O = 0.4$, $SiO_2 = 5$ wt%, APS = 0.61 wt% base on monomer.
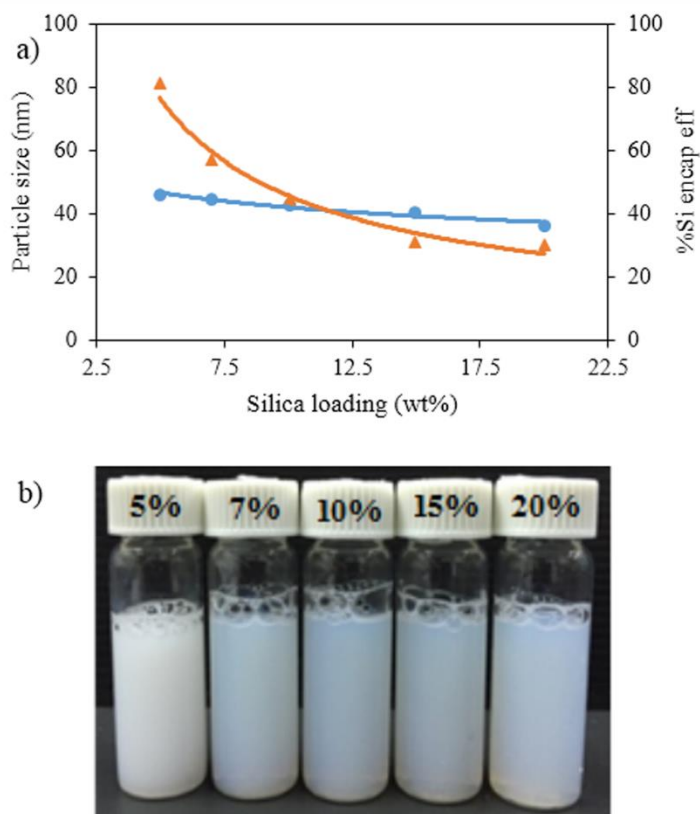
Figure 5.6 Effect of silica loading on; (●) Particle size, (▲) %Si encap eff and characteristic of latex. Condition: $M/H_2O = 0.4$, SDS = 5.34 wt%, APS = 0.61 wt% base on monomer.

Moreover, the effect of silica loading on particle size and silica encapsulation with PMMA is presented in Figure 5.6a. The silica loading did not significantly affect the particle size of PMMA-SiO$_2$. However, the silica encapsulation efficiency decreased from 81.1 to 29.7 % with an increase in the silica loading from 5 to 20 wt% based on monomer. Due to the fact that the high amount of silica loading led to an increase in silica aggregation and decreased the encapsulated silica resulting in a low silica encapsulation efficiency. It showed a similar result as PIP-SiO$_2$, PB-SiO$_2$ and SBR-SiO$_2$ nanocomposites [18, 87, 90]. From the characteristics of PMMA-SiO$_2$ nanoparicles as shown in Fig. 5.6b, the latex did not clearly show a change of appearance with an increase in silica loading. Nevertheless, the DMP of PMMA on modified nano-SiO$_2$ could provide PMMA-SiO$_2$ nanoparticles with a monodispersion of silica in the PMMA latex. Therefore, this novel method could enhance the

compatibility and dispersion of silica in the PMMA matrix, and reduce the silica-silica interaction resulting in a homogeneous PMMA-SiO$_2$ nanocomposite latex.

At the optimum condition (APS = 0.61 wt%, SDS = 5.34 wt%, SiO$_2$ = 10 wt%) for PMMA-SiO$_2$ synthesis by DMP, the high stability of the emulsion with a particle nano-size of 42.6 nm and silica encapsulation of 44.5 % were obtained for further blending with NR to form NR/PMMA-SiO$_2$ nanocomposite membranes.

5.4 Morphology of PMMA-SiO$_2$ Nanoparticles and NR/PMMA-SiO$_2$ Hybrid Membranes

The morphology of PMMA-SiO$_2$ nanocomposites with different surfactant concentrations characterized by TEM is illustrated in Figure 5.7. It was observed that the representative TEM micrographs exhibited a core-shell structure at different surfactant concentration, 3.34 wt%, 5.34 wt% and 10.34 wt%, respectively. The darker areas in the center of particle represented the silica core and the brighter areas represented the PMMA encapsulated onto the silica surface as the shell. Interestingly, the thickness of the shell decreased with increasing surfactant concentration. This can be explained in that with increasing surfactant concentration, the grafting efficiency showed a decreasing tendency resulting in a reduction in the PMMA shell thickness. Nevertheless, the nano-silica particles were well dispersed in the latex and a narrow PSD was achieved for all PMMA-SiO$_2$ nanocomposites. It can be concluded that the PMMA-SiO$_2$ nanocomposites with core-shell structure have been successfully prepared via DMP which was similar to the synthesis of PIP-SiO$_2$ [18], PB-SiO$_2$ [90] and SBR-SiO$_2$ [87] nanocomposites.

PMMA-SiO$_2$ emulsion at 10 wt% of silica loading was selected to blend with NR latex and the morphology of NR/PMMA-SiO$_2$ nanocomposites at various PMMA-SiO$_2$ loading in nanocomposite membranes was characterized by SEM. The cross-sectional morphology of NR/PMMA-SiO$_2$ membranes with various PMMA-SiO$_2$ loading (NR/PMMA-SiO$_2$ ratio of 100/0, 80/20 and 60/40, equivalent to 0%, 2% and 4% silica content) are shown in Figure 5.8. When the PMMA-SiO$_2$ nanocomposite emulsion was blended with the NR matrix, the SEM images of NR/PMMA-SiO$_2$ (Figures. 5.8b and 5.8c) show good compatibility between the PMMA-SiO$_2$ nanofiller and the NR matrix. This provided evidence that the stronger interaction between

PMMA-SiO$_2$ nanoparticles and NR latex resulted in a good-dispersion of nanoparticles in the NR/PMMA-SiO$_2$ composite membranes compared with pure NR membrane.
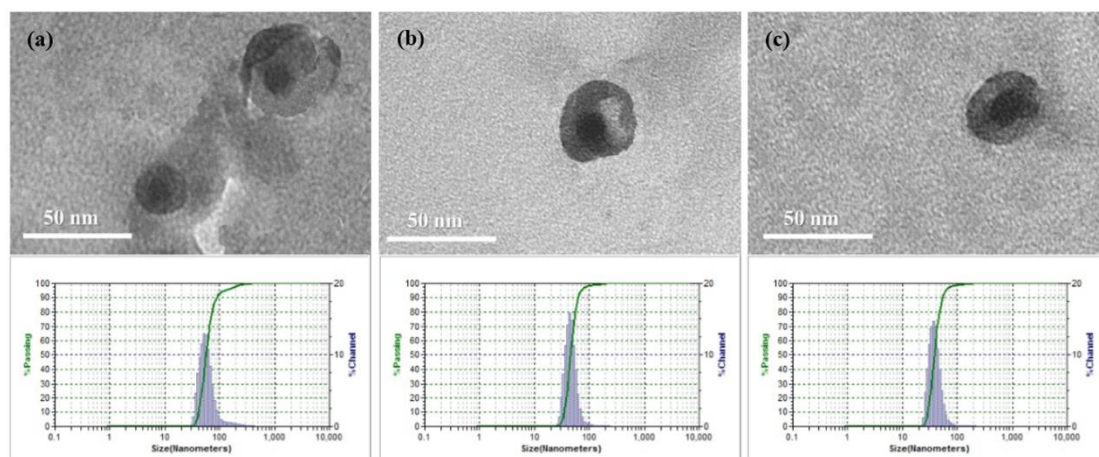
Figure 5.7 TEM micrographs and particle size distribution (PSD) of PMMA-SiO$_2$ with (a) SDS = 3.34 wt% (b) SDS = 5.34 wt% and (c) SDS = 10.34 wt%.
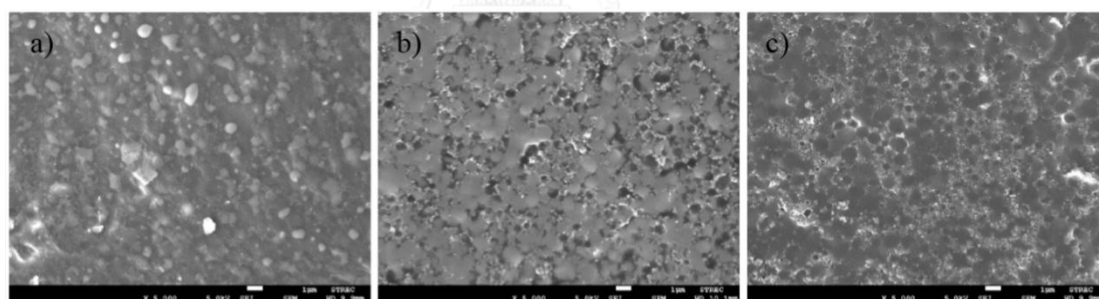
Figure 5.8 Cross-section SEM microscopy images of NR/PMMA-SiO$_2$ hybrid membranes with magnification of 5000x: a) pure NR, b) NR/PMMA-SiO$_2$ (80/20) and c) NR/PMMA-SiO$_2$ (60/40).

5.5 Thermal, Mechanical and Surface Properties of NR/PMMA-SiO₂ Hybrid Membranes

The effects of PMMA-SiO$_2$ loading at NR/PMMA-SiO$_2$ ratio of 100/0, 90/10, 80/20, 70/30 and 60/40 (equivalent to 0%, 1%, 2%, 3% and 4% silica content in all nanocomposite membranes, respectively) on thermal, mechanical and surface properties are summarized in Table 5.1. The T$_g$ of NR/PMMA-SiO$_2$ nanocomposite membranes (-63.1 to -63.8 ^{o}C) at different blend ratios were about the same value as that of unfilled NR (-63.8 ^{o}C) due to the low silica addition. The DSC thermograms of the nanocomposite membranes show a single T$_g$ because of the good dispersion of the PMMA-SiO$_2$ emulsion in the NR latex. The encapsulation of silica (core) and PMMA (shell) enhanced the good compatibility and dispersion of silica in the NR latex resulting in the homogeneity of NR/PMMA-SiO$_2$ nanocomposite.

The initial decomposition temperature (T$_{id}$) and maximum decomposition temperature (T$_{max}$) of the unfilled NR and NR/PMMA-SiO$_2$ nanocomposite membranes are presented in Table 5.1. The T$_{max}$ of NR/PMMA-SiO$_2$ nanocomposite increased from

Table 5.1 Thermal, mechanical and surface properties of NR/PMMA-SiO$_2$ nanocomposites membranes.

NR/PMMA-SiO$_2$[a] (wt/wt)	100/0	90/10	80/20	70/30	60/40
SiO$_2$ content[b] (wt%)	-	1.0	2.0	3.0	4.0
Thermal properties					
T$_g$ (^{o}C)	-63.8	-63.1	-63.6	-63.5	-63.8
T$_{id}$ (^{o}C)	353.9	361.9	362.0	360.7	360.9
T$_{max}$ (^{o}C)	382.7	393.7	394.5	394.8	395.2
Mechanical properties					
Tensile strength (MPa)	23.0 ± 1.0	24.0 ± 1.1	23.0 ± 0.1	11.1 ± 0.9	7.3 ± 1.1
300% Modulus (MPa)	1.04 ± 0.02	1.32 ± 0.03	2.04 ± 0.05	2.77 ± 0.11	4.97 ± 0.13
Elongation at break (%)	894 ± 16	877 ± 22	753 ± 12	593 ± 05	386 ± 33
Surface properties					
Contact angle in degree	107.8 ± 3.7	95.5 ± 4.7	83.1 ± 3.5	75.0 ± 2.3	68.9 ± 3.0
Water droplet					

[a] PMMA-SiO$_2$ preparation condition: M/H$_2$O = 0.4, SiO$_2$ = 10 wt%, SDS = 5.34 wt%, APS = 0.61 wt% base on monomer.
[b] Silica content based on total rubber.
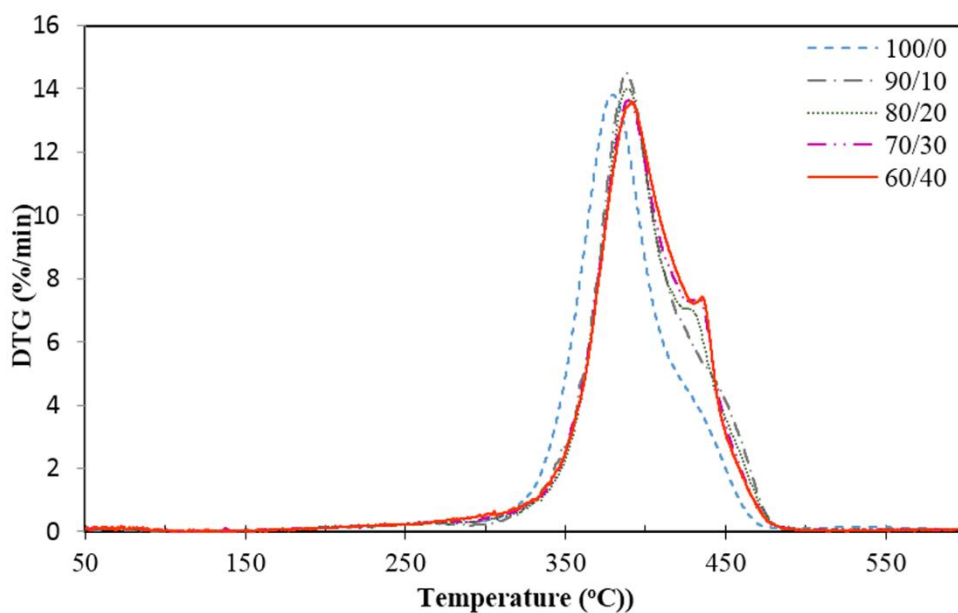
Figure 5.9 DTG curves for pure NR and NR/PMMA-SiO$_2$ nanocomposites.

393.7 to 395.2 $^{\circ}$C with an increasing PMMA-SiO$_2$ loading (1-2.5% SiO$_2$). This result implies that PMMA-SiO$_2$ nanoparticles could be uniformly dispersed in the NR latex resulting in the high thermal stability of the nanocomposite membranes [87]. From the DTG curves of the unfilled NR and NR/PMMA-SiO$_2$ nanocomposite membranes (Figure 5.9), the main thermal decomposition of NR matrix (C-C chain bonds rupture and hydrogen transfer) was observed. Moreover, the degradation curves of NR/PMMA-SiO$_2$ samples are slightly shifted to a higher temperature with the addition of PMMA-SiO$_2$ into the NR latex because of the intertwining between one PMMA chain on the silica surface and another PMMA chain on a NR molecule [67, 73, 93].

Mechanical properties of PMMA-SiO$_2$ filled NR were investigated in terms of tensile strength, modulus at 300% strain and elongation at break. From Table 5.1, the tensile strength of NR/PMMA-SiO$_2$ nanocomposite membranes with the addition of PMMA-SiO$_2$ at 10 wt% (1% SiO$_2$) was slightly higher than the unfilled NR (23.0 MPa). This indicated that the PMMA-SiO$_2$ nanoparticles provide a reinforcing effect on natural rubber with a uniform dispersion of silica. In contrast, the tensile strength of nanocomposite membranes was decreased with addition of PMMA-SiO$_2$ loading at 30-40 wt% (3-4% SiO$_2$) due to silica aggregation and the low interaction between NR and PMMA-SiO$_2$ nanoparticles.

From Table 5.1, the modulus at 300% strain of PMMA-SiO$_2$ filled NR significantly increased with increasing silica concentration. For the blend ratio of 60/40, the modulus at 300% strain of NR/PMMA-SiO$_2$ was increased to 5.0 MPa, compared with unfilled NR (1.0 MPa). This is due to the high modulus of PMMA polymer and the reinforcement effect of silica (rigid particle) which reduced the flexibility of rubber chains, thus the material with higher silica content also exhibited higher modulus [67, 94]. The elongation at break of the nanocomposite membranes was decreased with increasing PMMA-SiO$_2$ content. It was observed that the sample with 4% silica content presented a low elongation at break (386%) compared with unfilled NR (894%) due to the presence of PMMA polymer as a brittle thermoplastic and the low strain at break [95]. Besides, the addition of silica filler restricted the flexibility of the rubber chains [67]. For the blend ratio of 80/20, a small silica loading (2%) gave a remarkable enhancement in the mechanical properties of membrane.

The water contact angles of the PMMA-SiO$_2$ nanocomposite membranes with different PMMA-SiO$_2$ loading are also presented in Table 5.1. The water contact angles decreased with an increase of PMMA-SiO$_2$ loading in the NR matrix. This confirmed that the hydrophilic properties of the PMMA-SiO$_2$ emulsion had an effect on the hydrophilic membrane surface. Moreover, the high dispersion of silica particles in the membrane could intervene in the tight packing of polymer chains and the diffusion of water molecules through the membranes are also easier [80, 96]. When the PMMA-SiO$_2$ loading increased from 0 to 40 wt% (SiO$_2$ content = 0 − 4 wt%), the contact angle of the filled NR surface decreased from 107.8° to 68.9°. This result indicated that the reactive hydroxyl groups of the PMMA-SiO$_2$ nanoparticle exhibited an enhanced effect on the hydrophilic surface of the NR composite films.

5.6 Pervaporation Performance

The separation of an ethanol-water mixture via pervaporation through the NR/PMMA-SiO$_2$ hybrid membrane was performed. Pervaporation experiments were carried out using a mixture of ethanol-water at 20 vol% ethanol concentration. The effect of PMMA-SiO$_2$ content in membrane on the total permeate flux is presented in Fig. 5.10. An increase of PMMA-SiO$_2$ content from 10 to 40 wt% in the membrane leads to an increase of permeate flux from 1767 to 2511 g/m^{2}h. It can be explained that

a higher PMMA-SiO$_2$ content in the membrane gave more reactive hydroxyl groups resulting in a stronger interaction between water molecules and the membrane. Therefore, more water molecules can pass and diffuse through the membrane [87]. Since the PMMA-SiO$_2$ emulsion composed of PMMA homopolymer, free silica and PMMA encapsulated silica which PMMA was the hydrophilic polymer and silica particles had the hydrophilic groups (-OH) on the surface, adding PMMA-SiO$_2$ to NR latex can improve the hydrophilicity of membrane [96, 97]. These results are in according with a contact angle measurements as presented in Table 1. The water contact angle decreased with an increasing PMMA-SiO$_2$ loading in the composite membrane. This result indicated that the reactive hydroxyl groups of the PMMA-SiO$_2$ nanoparticles exhibited an enhanced effect on the hydrophilic surface of the composite film. Surprisingly, the results of the permeation measurement showed ≥ 99.9 vol% water concentration in the composition of the total permeate flux. These results indicated that the highly dispersed PMMA-SiO$_2$ has an active surface, which could change the membrane structure, resulting in easier permeation of water molecules.
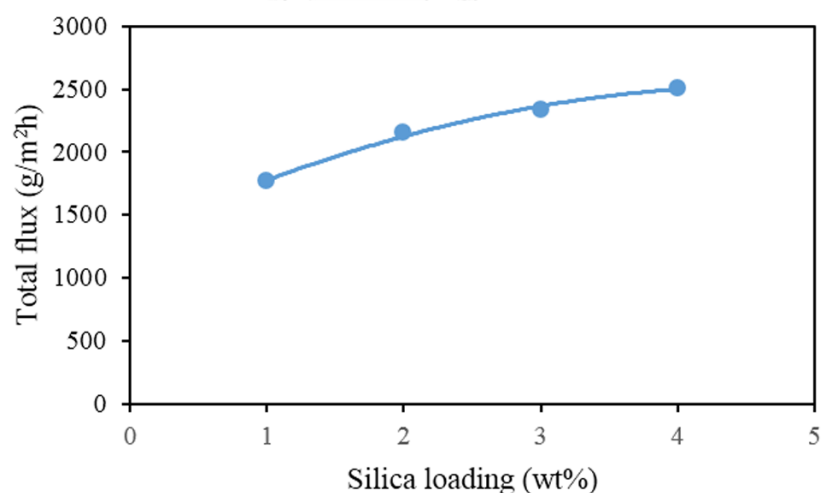
Figure 5.10 Effect of PMMA-silica content in membranes on total permeate flux at 80 vol% water concentration in feed.

NR/PMMA-SiO$_2$ hybrid membranes at PMMA-SiO$_2$ content of 20 wt% (2wt% silica) with good mechanical properties (tensile strength = 23.0 MPa, modulus at 300% strain = 2 MPa, elongation at break = 753%) was selected for separation of ethanol-water mixtures at various water concentrations (60-100%) via pervaporation experiments. Figure 5.11 shows the effect of feed compositions on the total permeate flux through the nanocomposite membranes. A significant increase in permeability was observed with increasing feed water concentration and the permeate flux has ≥99.9 vol% water concentration for all experiments. This result implies that the free volume in the membrane was increased with increasing feed water concentration resulting in highly permeate flux. Moreover, the volume of water molecule is smaller than that of ethanol molecule so the water molecule can permeate freely [87, 96]. It is interesting to note that the physical properties of NR/PMMA-SiO$_2$ hybrid membranes could be improved resulting in a high potential for future applications in membrane separation technology.
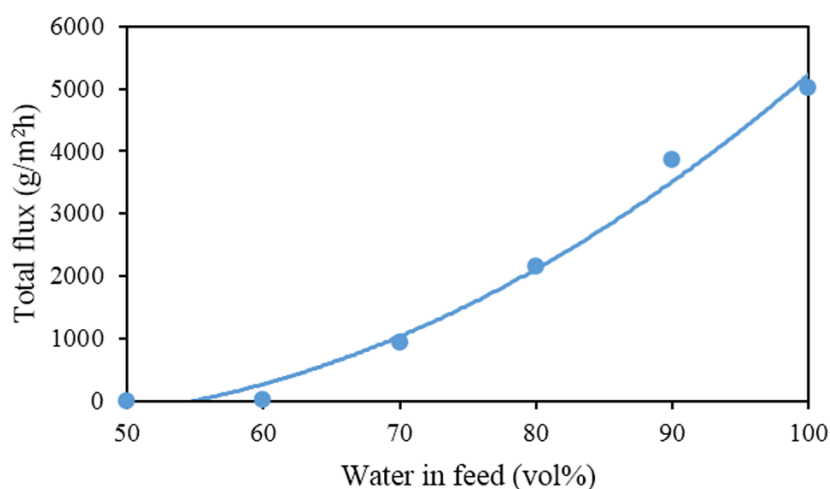
Figure 5.11 Effect of feed water concentration (vol%) on total permeate flux for NR/PMMA-SiO$_2$ nanocomposite membranes with PMMA-SiO$_2$ content of 20 wt%.

CHAPTER VI

PREPARATION OF POLY(STYRENE-*CO*-METHYL METHACRYLATE)-SILICA NANOPARTICLES VIA DIFFERENTIAL MICROEMULSION POLYMERIZATION AND PHYSICAL PROPERTIES OF NR/POLY(ST-*CO*-MMA)-SILICA HYBRID MEMBRANES

6.1 Introduction

In recent years, nanocomposite materials are becoming increasingly important due to their extraordinary properties based on the combined system of the different components. The combination of nanoscale inorganic species with organic polymers has a high potential for future applications. These materials have gained much interest because of the remarkable properties. Nanosilica, one of the most common inorganic material, shows many functional properties including effective reinforcement. However, difficulties of such an approach on polymer/silica composites are potential incompatibilities between silica and polymer due to the difference of polarity, stability and surface energy, resulting in phase separation. To avoid these problems, different methods can be applied and many chemical methods have been developed for the preparation of nanocomposites. However, the silica surface could be modified with silane coupling agents to improve adhesion between the silica particle and the polymer and emulsion polymerization also provides an effective way of synthesizing polymer/silica nanoparticles.

In this research work, poly(styrene-*co*-methyl methacrylate)/SiO$_2$ nanoparticles was synthesized via differential microemulsion polymerization. The influence of surfactant concentrations and silica loading on monomer conversion, particle size, as well as silica encapsulation efficiency was also investigated. The prevulcanized nanocomposite membranes of a natural rubber matrix and poly(styrene-*co*-methyl methacrylate)/SiO$_2$ nanoparticles was experimented in pervaporation process of water-ethanol mixtures. This research is important from an academic as well as an industrial point of view.

6.2 Characterization of Poly(ST-*co*-MMA)-SiO$_2$ Nanocomposites

The characterization of modified silica with VTS and poly(ST-*co*-MMA)-SiO$_2$ nanocomposites were performed using FT-IR spectra as shown in Figure 6.1. For the modified silica (Figure 6.1a), the absorption peaks at 1108, 809 and 471 cm^{-1} were attributed to the Si-O-Si groups. The absorption bands at 3435, 2922 and 2851 cm^{-1} corresponded to OH, CH and CH$_2$ stretching of the VTS groups. The peaks at 1630 and 1377 cm^{-1} were assigned to C=C stretching and C-H out of plain blending of the VTS group, respectively. These results indicated that the silane coupling agents could be bonded on the silica surface. For poly(ST-*co*-MMA)-SiO$_2$ nanoparticles (Figure 6.1b), the absorption peaks at 2947, 2851, 1731, 1449 and 1385 cm^{-1} were assigned to CH$_3$, CH$_2$, C=O, CH$_2$ bending and CH$_3$ bending of methacrylate group of MMA, respectively. The absorption bands in 3027, 1602 and 700 cm^{-1} corresponded to CH, C=C and CH out of plain bending of the aromatic group of ST, respectively. These results from FT-IR spectra confirmed that that poly(ST-*co*-MMA) could be grafted onto the silica surface.
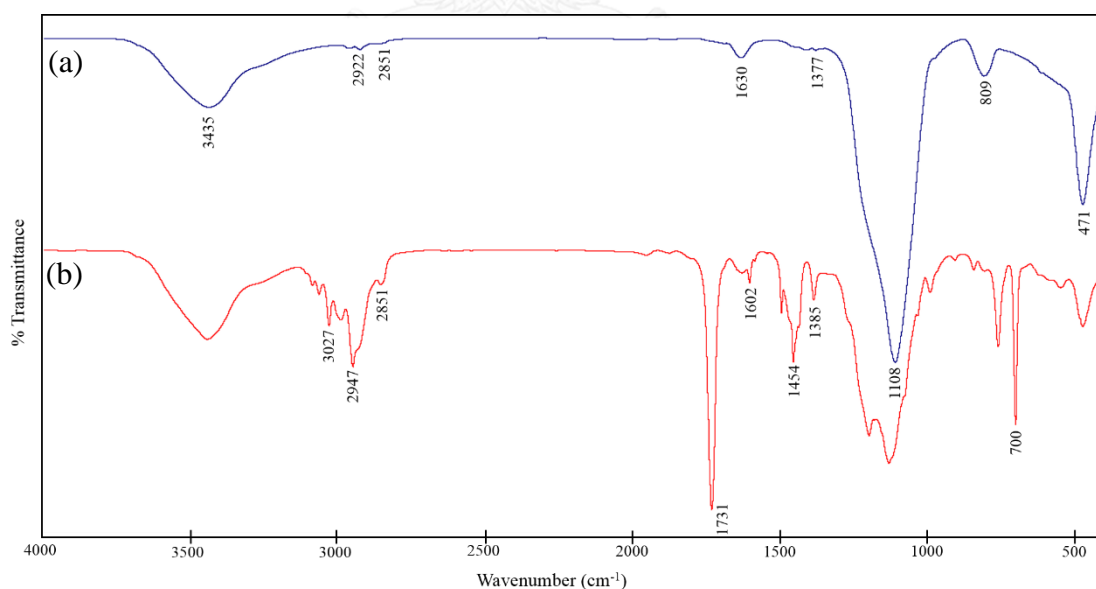
Figure 6.1 FT-IR spectra of (a) modified silica and (b) poly(ST-*co*-MMA)-SiO$_2$.

Additionally, ^{1}H-NMR spectra of poly(ST-*co*-MMA)-SiO$_2$ to identify the microstructure was shown in Figure 6.2. Phenyl protons of polystyrene was observed in the range of 7.0-7.2 ppm and methine protons of PS are found at 1.9 ppm. For PMMA, the signal between 2.8-3.6 ppm corresponded to the protons of the methyl groups attached to the ester groups of the side chains. The peaks in the range of 0.7-1.0 ppm referred to the protons of the methyl groups attached to the carbon of the backbone of the PMMA and the signal at 1.3 relate to the methylene protons of both PS and PMMA. The ^{1}H-NMR spectra indicated that the poly(ST-*co*-MMA) was grafted onto the silica surface.
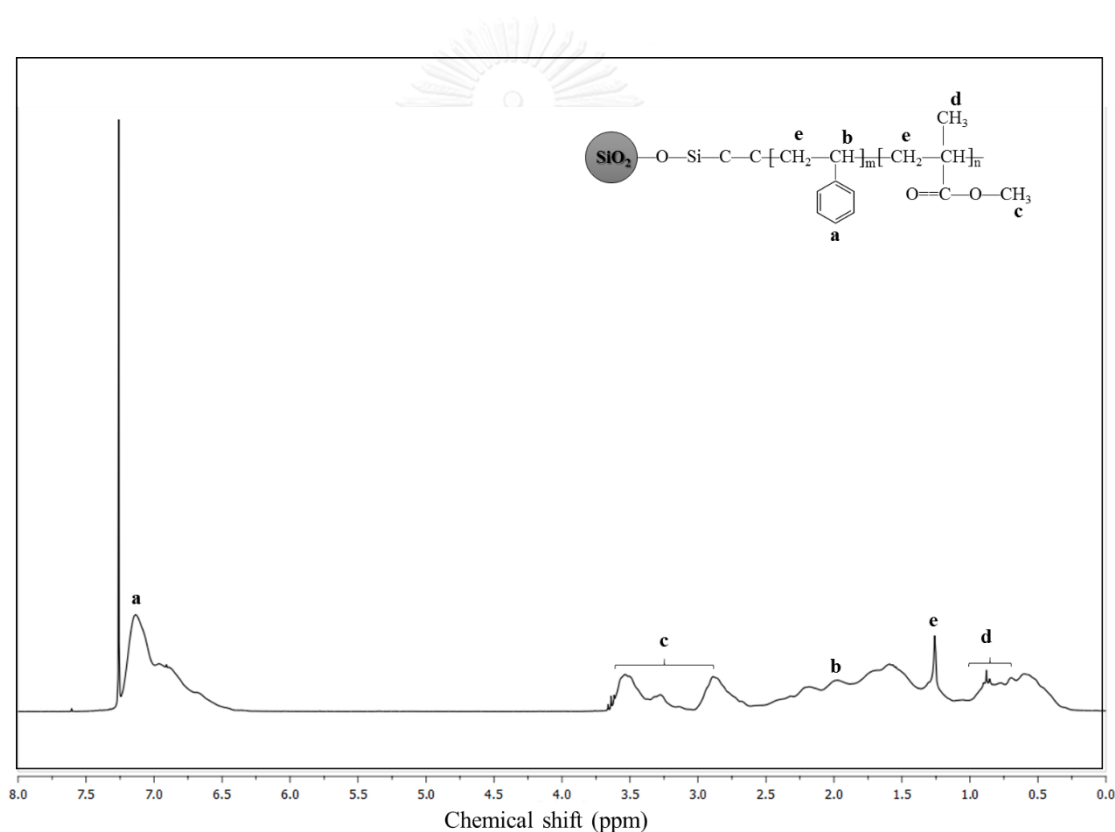
Figure 6.2 ^{1}H-NMR analysis of poly(ST-*co*-MMA)-SiO$_2$ is carried out in CDCl$_3$.

6.3 Effect of parameters on Poly(ST-*co*-MMA)-SiO₂ Preparation

SDS was used as emulsifier for encapsulation of silica with ST and MMA at a concentration above the critical micelle concentration (CMC). The surfactant concentration had a significant effect on particle size as shown in Figure 6.3a. The trend of particle size decreased with increasing the surfactant concentration from 1 to 5 wt% based on monomer. For these polymerization, the particles could grow and collide with each other after nucleation. At low surfactant concentration (or not enough), the particles would merge together and become larger ones after collision. Therefore, the surfactant concentration increased resulting in a smaller particle size. . From the characteristics of the poly(ST-*co*-MMA)-SiO₂ emulsion as illustrated in Figure 6.3b, the diameter of latex exhibited a trend of decreasing diameter and more transparent latex was produced with increasing surfactant amount.

Additionally, the effect of silica loading on particle size and silica encapsulation of poly(ST-*co*-MMA)-SiO₂ are exhibited in Figure 6.4a. The particle size decreased with an increasing in silica loading at 10wt%, however, the trend of particle size increased with increasing the silica content (15-20 wt%). It can be explained that the high silica loading led to increase the silica agglomerations resulting in large particles. Nevertheless, the silica encapsulation efficiency decreased with increasing the silica content. It can be noted that the high silica amount tend to an increase in silica aggregation and decreased the encapsulated silica resulting in a low silica encapsulation efficiency. From the characteristics of the poly(ST-*co*-MMA)-SiO₂ emulsion as illustrated in Figure 6.4b, the latex showed a change of appearance with an increase in silica loading (10-20 wt%). Therefore, this method could enhance the compatibility and dispersion of silica in the polymer matrix, and reduce the silica-silica interaction resulting in a homogeneous poly(ST-*co*-MMA)-SiO₂ emulsion.

At the optimum condition (SDS = 3 wt% and SiO₂ = 10 wt%) for poly(ST-*co*-MMA)-SiO₂ preparation, the high stability of the emulsion with a particle nano-size of 20.5 nm and high silica encapsulation were obtained for further blending with NR to form poly(ST-*co*-MMA)-SiO₂ nanocomposite films.
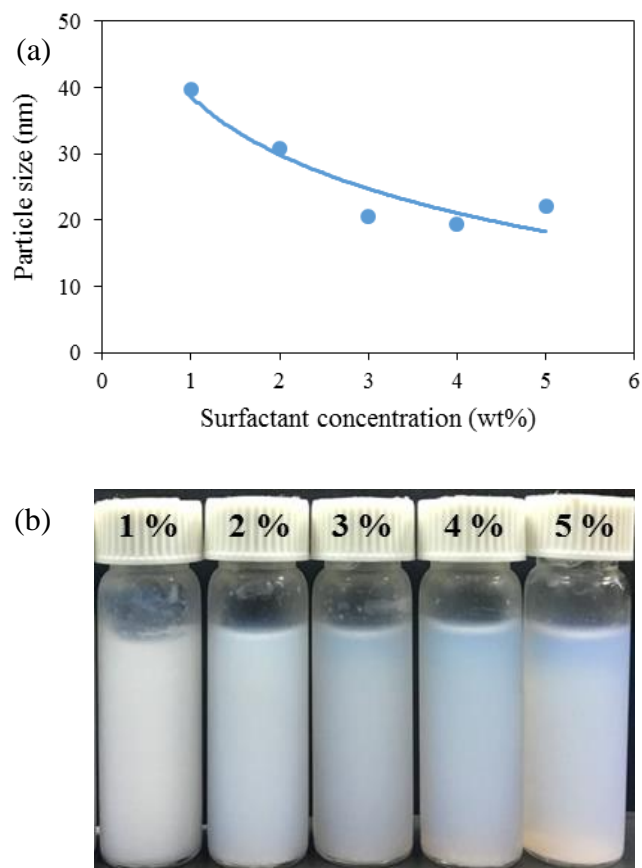
Figure 6.3 Effect of SDS concentration on particle size and characteristic of latex.
Condition: H_2O = 30 g, SiO_2 = 10 wt%, ST:MMA = 1, APS = 1 wt% base
on monomer.
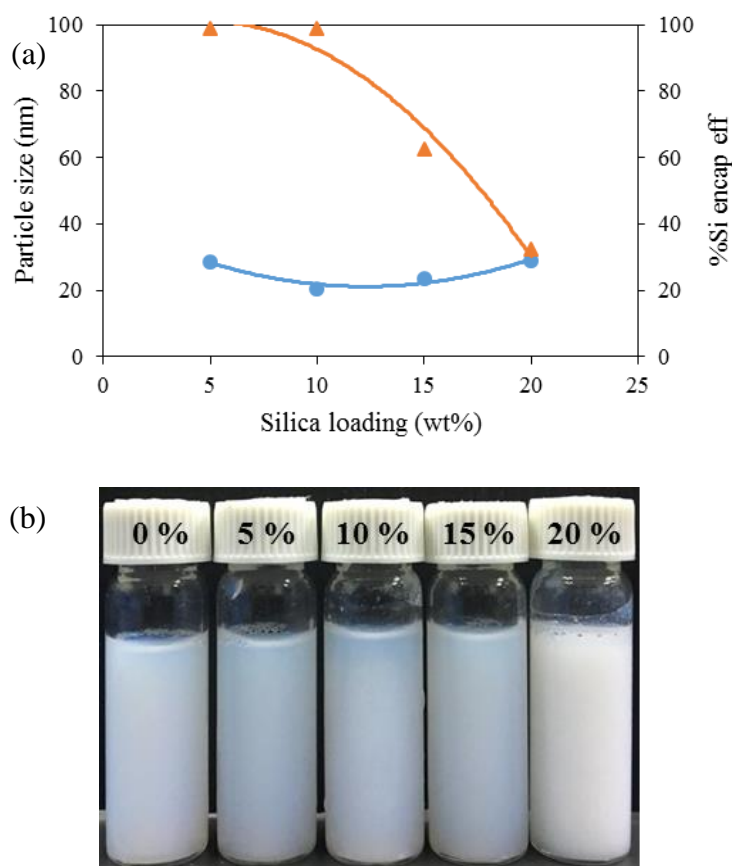
Figure 6.4 Effect of silica loading on; (●) Particle size, (▲) %Si encap eff and characteristic of latex. Condition: $H_2O = 30$ g, ST:MMA = 1, SDS = 3 wt%, APS = 1 wt% base on monomer.

6.4 Morphology of Poly(ST-co-MMA)-SiO₂ Nanoparticles and NR/Poly(ST-co-MMA)-SiO₂ Hybrid Membranes

The morphology of poly(ST-*co*-MMA)-SiO$_2$ nanocomposites with different silica loading characterized by TEM is presented in Figure 6.5. It was found that the TEM image of poly(ST-*co*-MMA) emulsion in Figure 6.5a shows spherical particles with a diameter of around 26 nm. Moreover, the other nanocomposites at different silica loading (5 and 10 wt%, Figure 6.5b and c) clearly shows the formation of a core-shell structure. The darker areas in the center of particle represented the silica core and the brighter areas represented the polymer encapsulated onto the silica surface as the shell. However, Figure 6.5d exhibits the agglomeration phenomenon of silica particles due to

the effect of more silica loading. It can be concluded that the poly(ST-*co*-MMA)-SiO$_2$ nanocomposites with core-shell structure have been successfully synthesized via DMP.

The proposed mechanism of poly(ST-*co*-MMA)-SiO$_2$ preparation is presented in Figure 6.6. The modified silica, SDS as surfactant and APS as initiator were dispersed in deionized water to form a homogeneous solution. The surfactant generated the micelles in the process in which the hydrophilic parts turn toward the aqueous phase and the hydrophobic parts form the core of organic phase. For DMP, the ST and MMA mixture was dropwise fed into the system and the initiator decomposed into free radicals in the aqueous phase that produced reactive monomer radicals on the silica surface and monomer molecules. Then, these radicals were reacted with the other monomers to form the oligomeric radicals to produce the growing chains until termination resulted in the poly(ST-*co*-MMA)-SiO$_2$ nanocomposits. Hence, the polymer can be grafted onto the silica surface with core-shell structure.
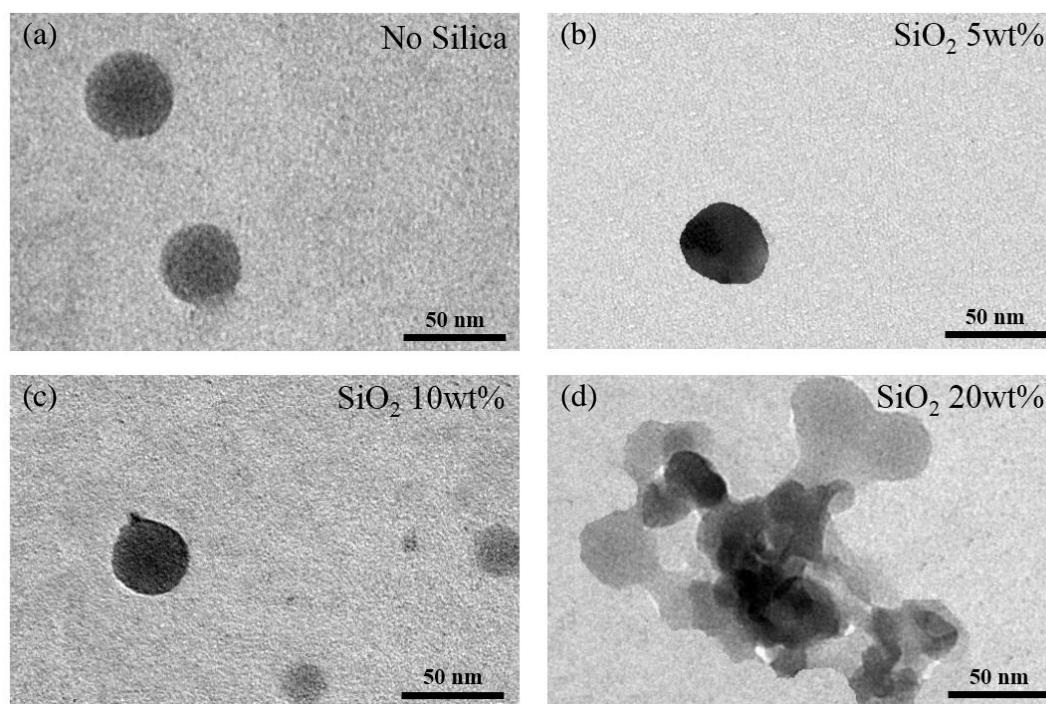
Figure 6.5 TEM micrographs of poly(ST-*co*-MMA) nanoparticles with different silica content.
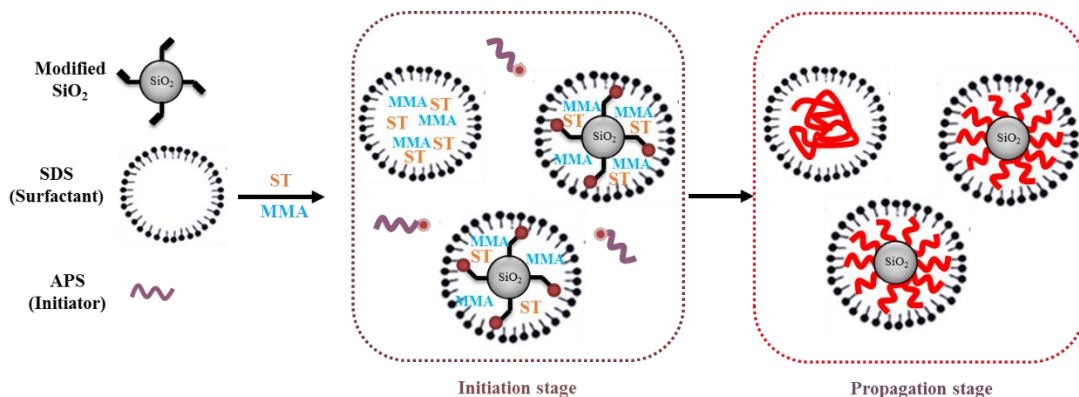
Figure 6.6 The proposed model for differential emulsion polymerization of poly(ST-*co*-MMA)-SiO$_2$ nanoparticles.

6.5 Thermal Properties of Poly(ST-*co*-MMA)-SiO$_2$ Nanoparticles

From thermogravimetric analysis (TGA) of the poly(ST-*co*-MMA) and poly(ST-*co*-MMA)-SiO$_2$ nanoparticles are presented in Figure 6.7, this investigation revealed the addition of silica has an effect on the thermal stability of poly(ST-*co*-MMA) particles. The decomposition temperature of poly(ST-*co*-MMA)-SiO$_2$ nanocomposite (402 °C) was higher than that of poly(ST-*co*-MMA) nanoparticle (406 °C). The silica addition can improve the degradation of polymer particles. Furthermore, the residual weight at the final process of poly(ST-*co*-MMA) filled silica is larger than that of the pure polymer because the silica loading in poly(ST-*co*-MMA)-SiO$_2$ cannot decompose.
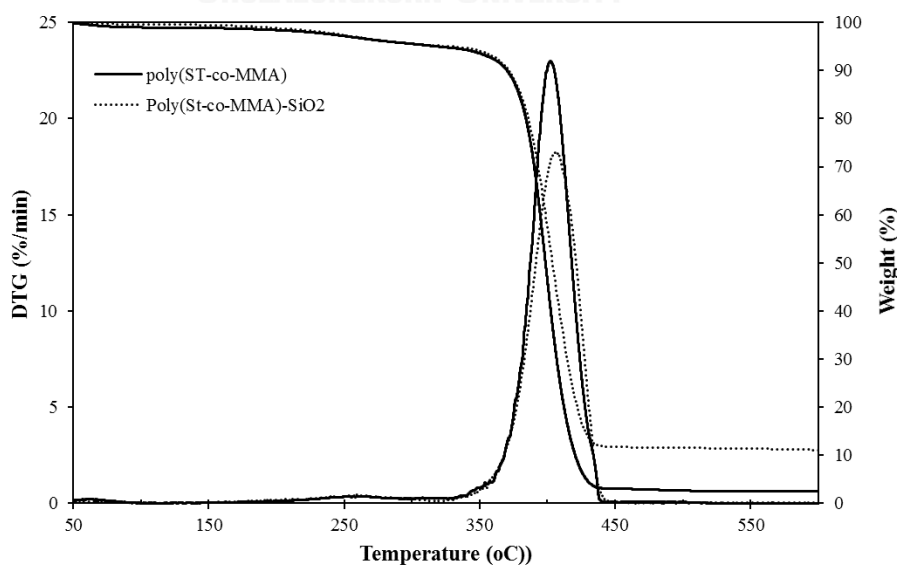
Figure 6.7 Thermograms of poly(ST-*co*-MMA) and poly(ST-*co*-MMA)-SiO$_2$.

6.6 Mechanical and Surface Properties of NR/Poly(ST-*co*-MMA)-SiO₂ Hybrid Membranes

Mechanical properties of poly(ST-*co*-MMA)-SiO$_2$ filled NR with different nanocomposite loading were investigated in terms of tensile strength, modulus at 300% strain and elongation at break (Table 6.1). The tensile strength of NR/poly(ST-*co*-MMA)-SiO$_2$ films with the various addition of nanocomposite emulsion were lower than the unfilled NR (20.6 MPa). It can be noted that the low tensile strength was due to the non-homogeneous sample. However, the modulus at 300% strain of nanocomposite films were increased to compared with unfilled NR (1.13 MPa) because the high modulus of polymer and the reinforcement effect of silica particles which reduced the flexibility of rubber chains, thus the materials with higher silica loading presented higher modulus. Besides, the elongation at break of the hybrid membranes were decreased with adding poly(ST-*co*-MMA)-SiO$_2$ content because of the presence of polymer as a brittle thermoplastic and the low strain at break.

Table 6.1 Mechanical properties of NR/poly(ST-*co*-MMA)-SiO$_2$ nanocomposites.
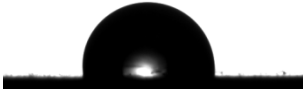
NR/poly(ST-*co*-MMA)-SiO$_2$[a] (wt/wt)	SiO$_2$ content[b] (wt%)	Tensile strength (MPa)	300% Modulus (MPa)	Elongation at break (%)
100/0	-	20.6 ± 5.5	1.13 ± 0.04	820 ± 24
90/10	1.0	8.1 ± 0.7	1.30 ± 0.04	707 ± 27
85/15	1.5	8.0 ± 0.3	1.17 ± 0.22	781 ± 39
80/20	2.0	6.2 ± 0.5	1.46 ± 0.07	700 ± 53
75/25	2.5	7.6 ± 0.8	1.66 ± 0.12	707 ± 47

[a] Poly(ST-*co*-MMA)-SiO$_2$ preparation condition: H$_2$O = 30 g, SiO$_2$ = 10 wt%, ST:MMA = 1:1, SDS = 3 wt%, APS = 1 wt% base on monomer.
[b] Silica content based on total rubber.

The water contact angles of the NR/poly(ST-*co*-MMA)-SiO$_2$ nanocomposite membranes with different polymer loading are presented in Table 6.2. The water contact angles decreased with an increase of polymer content in the NR latex. This confirmed that the hydrophilic properties of the polymer emulsion had an effect on the hydrophilic membrane surface. Furthermore, the high dispersion of silica particles in the membrane could intervene in the tight packing of polymer chains and the diffusion of water molecules through the membranes are also easier [80, 96]. When the poly(ST-*co*-MMA)-SiO$_2$ loading increased from 0 to 25 wt% (SiO$_2$ content = 0–2.5 wt%), the contact angle of the filled NR surface decreased from 94° to 50°. This result indicated that the reactive hydroxyl groups of the nanoparticle showed an enhanced influence on the hydrophilic surface of the NR composite films.

Table 6.2 Contact angle of NR/poly(ST-*co*-MMA)-SiO$_2$ nanocomposite membranes.

NR/poly(ST-*co*-MMA)-SiO$_2$[a] (wt/wt)	SiO$_2$ content[b] (wt%)	contact angle in degree	Water droplet
100/0	-	94.1 ± 3.9	
90/10	1.0	80.6 ± 1.1	
85/15	1.5	71.2 ± 2.7	
80/20	2.0	64.3 ± 2.3	
75/25	2.5	50.1 ± 2.7	

[a] Poly(ST-*co*-MMA)-SiO$_2$ preparation condition: H$_2$O = 30 g, SiO$_2$ = 10 wt%, ST:MMA = 1:1, SDS = 3 wt%, APS = 1 wt% based on monomer.
[b] Silica content based on total rubber.

6.7 Pervaporation Performance

The separation of an ethanol-water mixture via pervaporation through the NR/poly(ST-*co*-MMA)-SiO$_2$ hybrid membrane was performed. Pervaporation process was carried out using a mixture of ethanol-water at 20 vol% ethanol concentration. The effect of silica loading in membrane on the total permeate flux is shown in Table 6.3. It was found that an increase of poly(ST-*co*-MMA)-SiO$_2$ content in the membrane affected to a small increase of permeate flux. These results were in according with a previous contact angle measurements. It can be explained that a higher silica content in the membrane gave more reactive hydroxyl groups resulting in a stronger interaction between water molecules and the hybrid membrane. Therefore, more water molecules can pass and diffuse through the membrane. Unfortunately, the total flux of the pervaporation process was very low due to the membrane thickness.

Table 6.3 Effect of poly(ST-*co*-MMA)-SiO$_2$ content in membranes on total permeate flux at 80 vol% concentration in feed.

NR/poly(ST-*co*-MMA)-SiO$_2$[a] (wt/wt)	SiO$_2$ content[b] (wt%)	Total flux (g/m^{2}h)
90/10	1.0	-
85/15	1.5	9.8
80/20	2.0	10.5

[a] Poly(ST-*co*-MMA)-SiO$_2$ preparation condition: H$_2$O = 30 g, SiO$_2$ = 10 wt%, ST:MMA = 1:1, SDS = 3 wt%, APS = 1 wt% based on monomer.
[b] Silica content based on total rubber.

CHAPTER VII
CONCLUSIONS AND RECOMMENDATIONS

7.1 Conclusions

i) **Synthesis of Polystyrene-Silica Nanoparticles via RAFT Emulsifier-Free Emulsion Polymerization**

From emulsifier-free emulsion polymerization, PS-co-RAFT and PS-co-RAFT-SiO$_2$ nanoparticles were successfully prepared by using a macro-RAFT agent. For PS-co-RAFT synthesis, the [R]:[I] ratio has a great effect on particle size, molecular weight, the total number of latex particles in the system (N_p), the number of polymer chains per particle (N). PS-co-R10 exhibited high molecular weight, a large number of latex particles and a low number of chains per particle. The particle size of PS-co-RAFT (20-45 nm) and PS-co-RAFT-SiO$_2$ (23-56 nm) increased with decreasing the [R]:[I] ratio. Moreover, PS-co-RAFT-Si showed quite high grafting efficiency. TEM photographs of PS-co-R10 and PS-co-R10-Si clearly showed spherical particles with a core-shell morphology. The PS-R-SiO$_2$ composite could improve the swelling property of natural rubber. For mechanical properties of NR/PS-R-SiO$_2$ blends, the tensile strength and modulus of composites were higher than unfilled NR, indicating that the compatibility of NR and PS-R-SiO$_2$ could improve the thermal and mechanical properties of NR composites. The PS-R-SiO$_2$ could be used as effective nano-filler at low loading of 1-1.5 wt% in NR for the future applications in all rubber products with good physical properties. Thus, the synthesis of well-dispersed PS-R-SiO$_2$ via RAFT emulsion polymerization is of importance from an academic as well as an industrial point of view.

ii) **RAFT Emulsifier-Free Emulsion Polymerization of Polyisoprene-Silica Nanoparticles Using Water-Soluble Initiators**

The water-soluble initiators were successfully used in RAFT emulsifier-free emulsion polymerization of polyisoprene. The characteristics of PIP-co-RAFT and PIP-co-RAFT-SiO$_2$ nanoparticles prepared using ACP and V50 initiators were investigated. For PIP-co-RAFT preparation, the initiator types and the [R]:[I] ratio have an effect on

particle size and monomer conversion. The PIP-co-RAFT-ACP nanoparticles showed smaller size than the PIP-co-RAFT-V50 nanoparticles, however, the particle size of PIP-co-RAFT emulsion prepared using ACP (28-88 nm) and V50 initiator (59-184 nm) increased with decreasing the [R]:[I] ratio. For PIP-co-RAFT-SiO$_2$ preparation, the PIP-co-RAFT-ACP-SiO$_2$ nanoparticles also showed smaller size than the PIP-co-RAFT-V50-SiO$_2$ nanoparticles. Nevertheless, the particle size of PIP-co-RAFT-SiO$_2$ emulsion prepared using ACP (25-73 nm) and V50 initiator (48-91 nm) increased with decreasing the [R]:[I] ratio. Moreover, the PIP-co-RAFT-SiO$_2$ emulsion presented quite high grafting efficiency and a core-shell structure as confirmed that by TEM micrographs. For mechanical properties of NR/PIP-R-SiO$_2$ blends, the tensile strength, modulus and elongation at break of composites were higher than unfilled NR indicating that the compatibility of PIP-R-SiO$_2$ and natural rubber matrix could improve the mechanical properties of NR composites. The PIP-R-SiO$_2$ latex prepared using ACP initiator can be used as effective fillers at low silica content (1-2 wt%) in NR latex for the approaching applications in all NR products.

iii) Preparation of Poly(Methyl Methacrylate)-Silica Nanoparticles via Differential Microemulsion Polymerization and Physical Properties of NR/PMMA-SiO$_2$ Hybrid Membranes

PMMA–SiO$_2$ nanoparticles were synthesized via differential microemulsion polymerization. The silica loading, initiator and surfactant concentration had an effect on particle size and silica encapsulation efficiency of PMMA–SiO$_2$ nanocomposites. A high monomer conversion of 99.9% and PMMA–SiO$_2$ nanoparticles with a size range of 30–50 nm were obtained at a low surfactant concentration (5.34 wt%). TEM micrographs exhibited a core-shell morphology of PMMA–SiO$_2$ nanoparticles. The NR/PMMA–SiO$_2$ hybrid membranes were made from a green polymer and used for pervaporation of ethanol-water mixtures. For mechanical properties of NR/PMMA–SiO$_2$ membrane, the tensile strength and modulus of composites membrane were higher than unfilled NR. The membranes exhibited high permeate flux with increasing PMMA–SiO$_2$ content and feed water concentration, and high water selectivity for all experiments. Therefore, the PMMA–SiO$_2$ nanocomposites could be used as an effective material in future applications.

iv) Preparation of Poly(Styrene-*co*-Methyl Methacrylate)-Silica Nanoparticles via Differential Microemulsion Polymerization and Physical Properties of NR/Poly(ST-*co*-MMA)-Silica Hybrid Membranes

Poly(ST-*co*-MMA)–SiO$_2$ nanoparticles were successfully prepared by differential microemulsion polymerization. The surfactant concentration and silica amount had an effect on particle size and silica encapsulation efficiency of poly(ST-*co*-MMA)–SiO$_2$ latex. A high monomer conversion and poly(ST-*co*-MMA)–SiO$_2$ nanoparticles with a size range of 20–40 nm were obtained at a low surfactant concentration (1-5 wt%). TEM images showed a core-shell morphology of poly(ST-*co*-MMA)–SiO$_2$ emulsion. The NR/poly(ST-*co*-MMA)–SiO$_2$ membranes were made from a green polymer and used for pervaporation of ethanol-water mixtures. For mechanical properties of poly(ST-co-MMA)-SiO$_2$ filled NR, the modulus of composites membrane were higher than unfilled NR. The membranes had low performance in the pervaporation process, therefore, the NR/poly(ST-*co*-MMA)–SiO$_2$ membranes could be improved.

Comparison of nanoparticles and NR/Polymer-SiO$_2$ nanocomposites from emulsion polymerization is shown in Table 7.1.

7.2 Recommendations

Further research on the synthesis of new polymer-silica nanocomposites should be concerned with the following aspects:

The RAFT polymerization is a recent alternatives to synthesis the nanocomposites and PMMA can be easily adopted to individual purposes. Therefore, the incorporation of nanosilica via RAFT emulsifier-free emulsion polymerization could be potentially applied to produce PMMA-SiO$_2$ nanocomposites using various initiators.

The NR/PS-co-RAFT-SiO$_2$ and NR/PIP-co-RAFT-SiO$_2$ films showed an improvement in mechanical and thermal properties so these nanocomposite membranes could be further studied for ethanol-water separation by pervaporation process.

Table 7.1 Comparison of nanoparticles and NR/Polymer-SiO$_2$ nanocomposites from emulsion polymerization.

Polymerization	Monomer	Macro-RAFT agent[1] Surfactant[2]	Initiator	Nanoparticles particle size (nm)		Selected emulsion	NR/Polymer-SiO$_2$ nanocomposites			
				without SiO$_2$	with SiO$_2$		Silica loading (wt%)	Mechanical properties		
								TS (MPa)	M$_{300}$ (MPa)	EB (%)
RAFT emulsion	ST	PSS-Na[1]	ACP	20-45	23-56	PS-co-R4-Si	1	26.7 ± 0.6	1.76 ± 0.05	806 ± 20
RAFT emulsion	IP	PSS-Na[1]	ACP	28-88	25-73	PIP-co-R3-ACP-Si	1	24.2 ± 2.1	1.19 ± 0.02	947 ± 08
			V50	59-184	48-91	PIP-co-R4-V50-Si	1	18.4 ± 1.6	1.09 ± 0.01	889 ± 39
Differential microemulsion	MMA	SDS[2]	APS	-	30-50	PMMA-SiO$_2$ (SiO$_2$ = 10 wt%, SDS = 5.34 wt%)	2	24.0 ± 1.1	1.32 ± 0.03	877 ± 22
Differential microemulsion	ST + MMA	SDS[2]	APS	-	20-40	Poly(ST-co-MMA)-SiO$_2$ (SiO$_2$ = 10 wt%, SDS = 3 wt%, ST:MMA = 1:1)	N/A	N/A	N/A	N/A

REFERENCES

[1] Y.K. Chong, T.P.T. Le, G. Moad, E. Rizzardo, S.H. Thang, A more versatile route to block copolymers and other polymers of complex architecture by living radical polymerization: the RAFT process, Macromolecules 32(6) (1999) 2071-2074.

[2] R. Wei, Y. Luo, Z. Li, Synthesis of structured nanoparticles of styrene/butadiene block copolymers via RAFT seeded emulsion polymerization, Polymer 51(17) (2010) 3879-3886.

[3] Y. Chen, W. Luo, Y. Wang, C. Sun, M. Han, C. Zhang, Synthesis and self-assembly of amphiphilic gradient copolymer via RAFT emulsifier-free emulsion polymerization, Journal of Colloid and Interface Science 369(1) (2012) 46-51.

[4] K. Matyjaszewski, J. Spanswick, Controlled/living radical polymerization, Materials Today 8(3) (2005) 26-33.

[5] S.b. Fre'al-Saison, M. Save, C. Bui, B. Charleux, S. Magnet, Emulsifier-free controlled free-radical emulsion polymerization of styrene via RAFT using dibenzyltrithiocarbonate as a chain transfer agent and acrylic acid as an ionogenic comonomer: batch and spontaneous phase inversion processes, Macromolecules 39(25) (2006) 8632-8638.

[6] B. Hojjati, P.A. Charpentier, Synthesis of TiO_2-polymer nanocomposite in supercritical CO_2 via RAFT polymerization, Polymer 51(23) (2010) 5345-5351.

[7] J. Chiefari, Y.K. Chong, F. Ercole, J. Krstina, J. Jeffery, T.P.T. Le, R.T.A. Mayadunne, G.F. Meijs, C.L. Moad, G. Moad, E. Rizzardo, S.H. Thang, Living free-radical polymerization by reversible addition−fragmentation chain transfer: the RAFT process, Macromolecules 31(16) (1998) 5559-5562.

[8] D.J. Keddie, G. Moad, E. Rizzardo, S.H. Thang, RAFT agent design and synthesis, Macromolecules 45(13) (2012) 5321-5342.

[9] G. Moad, RAFT (Reversible addition-fragmentation chain transfer) crosslinking (co)polymerization of multi-olefinic monomers to form polymer networks, Polymer International 64(1) (2015) 15-24.

[10] M. Beija, J.-D. Marty, M. Destarac, RAFT/MADIX polymers for the preparation of polymer/inorganic nanohybrids, Progress in Polymer Science 36(7) (2011) 845-886.

[11] N. Yeole, D. Hundiwale, Effect of hydrophilic macro-RAFT agent in surfactant-free emulsion polymerization, Colloids and Surfaces A: Physicochemical and Engineering Aspects 392(1) (2011) 329-334.

[12] J. Ji, L. Yan, D. Xie, Surfactant-free synthesis of amphiphilic diblock copolymer in aqueous phase by a self-stability process, Journal of Polymer Science Part A: Polymer Chemistry 46(9) (2008) 3098-3107.

[13] C.J. Ferguson, R.J. Hughes, B.T.T. Pham, B.S. Hawkett, R.G. Gilbert, A.K. Serelis, C.H. Such, Effective ab initio emulsion polymerization under RAFT control, Macromolecules 35(25) (2002) 9243-9245.

[14] I. Chaduc, A.s. Crepet, O. Boyron, B. Charleux, F. D'Agosto, M. Lansalot, Effect of the pH on the RAFT polymerization of acrylic acid in water. Application to the synthesis of poly(acrylic acid)-stabilized polystyrene particles by RAFT emulsion polymerization, Macromolecules 46(15) (2013) 6013-6023.

[15] J. Rieger, F. Stoffelbach, C. Bui, D. Alaimo, C. Je'ro^me, B. Charleux, Amphiphilic poly(ethylene oxide) macromolecular RAFT agent as a stabilizer and control agent in ab initio batch emulsion polymerization, Macromolecules 41(12) (2008) 4065-4068.

[16] J. Rieger, G. Osterwinter, C. Bui, F. Stoffelbach, ois, B. Charleux, Surfactant-free controlled/living radical emulsion (co)polymerization of n-butyl acrylate and methyl methacrylate via RAFT using amphiphilic poly(ethylene oxide)-based trithiocarbonate chain transfer agents, Macromolecules 42(15) (2009) 5518-5525.

[17] Y. Mitsukami, M.S. Donovan, A.B. Lowe, C.L. McCormick, Water-soluble polymers. 81. Direct synthesis of hydrophilic styrenic-based homopolymers and block copolymers in aqueous solution via RAFT, Macromolecules 34(7) (2001) 2248-2256.

[18] A. Kongsinlark, G.L. Rempel, P. Prasassarakich, Synthesis of monodispersed polyisoprene-silica nanoparticles via differential microemulsion polymerization and mechanical properties of polyisoprene nanocomposite, Chemical Engineering Journal 193-194 (2012) 215-226.

[19] K. Shibuya, D. Nagao, H. Ishii, M. Konno, Advanced soap-free emulsion polymerization for highly pure, micron-sized, monodisperse polymer particles, Polymer 55(2) (2014) 535-539.

[20] N. Yeole, D. Hundiwale, T. Jana, Synthesis of core–shell polystyrene nanoparticles by surfactant free emulsion polymerization using macro-RAFT agent, Journal of Colloid and Interface Science 354(2) (2011) 506-510.

[21] J.O. Stoffer, T. Bone, Polymerization in water-in-oil microemulsion systems. I, Journal of Polymer Science: Polymer Chemistry Edition 18(8) (1980) 2641-2648.

[22] C. Larpent, Microemulsion polymerization, Colloidal Polymers, CRC Press2003.

[23] F. Candau, Microemulsion polymerization, in: J.M. Asua (Ed.), Polymeric Dispersions: Principles and Applications, Springer Netherlands, Dordrecht, 1997, pp. 127-140.

[24] L.M. Gan, C.H. Chew, I. Lye, T. Imae, Microemulsion polymerization of styrene, Polymer Bulletin 25(2) (1991) 193-198.

[25] C. Larpent, E. Bernard, J. Richard, S. Vaslin, Polymerization in microemulsions with polymerizable cosurfactants: a route to highly functionalized nanoparticles, Macromolecules 30(3) (1997) 354-362.

[26] G. He, Q. Pan, G.L. Rempel, Synthesis of poly(methyl methacrylate) nanosize particles by differential microemulsion polymerization, Macromolecular Rapid Communications 24(9) (2003) 585-588.

[27] C. Norakankorn, Q. Pan, G.L. Rempel, S. Kiatkamjornwong, Synthesis of poly(methyl methacrylate) nanoparticles initiated by 2,2′-azoisobutyronitrile via differential microemulsion polymerization, Macromolecular Rapid Communications 28(9) (2007) 1029-1033.

[28] L. Yuan, Y. Wang, M. Pan, G.L. Rempel, Q. Pan, Synthesis of poly(methyl methacrylate) nanoparticles via differential microemulsion polymerization, European Polymer Journal 49(1) (2013) 41-48.

[29] B.J. Jankiewicz, D. Jamiola, J. Choma, M. Jaroniec, Silica-metal core-shell nanostructures, Advances in Colloid and Interface Science 170 (2012) 28-47.

[30] R.P. Bagwe, L.R. Hilliard, W. Tan, Surface Modification of silica nanoparticles to reduce aggregation and nonspecific binding, Langmuir 22(9) (2006) 4357-4362.

[31] M. Conradi, Nanosilica-reinforced polymer composites, Material and Thechnology 47(3) (2013) 285-293.

[32] S.H. Ahn, S.H. Kim, S.G. Lee, Surface-modified silica nanoparticle–reinforced poly(ethylene 2,6-naphthalate), Journal of Applied Polymer Science 94(2) (2004) 812-818.

[33] X.-k. Ma, N.-H. Lee, H.-J. Oh, J.-W. Kim, C.-K. Rhee, K.-S. Park, S.-J. Kim, Surface modification and characterization of highly dispersed silica nanoparticles by a cationic surfactant, Colloids and Surfaces A: Physicochemical and Engineering Aspects 358(1) (2010) 172-176.

[34] J. Ramier, L. Chazeau, C. Gauthier, L. Guy, M.N. Bouchereau, Grafting of silica during the processing of silica-filled SBR: comparison between length and content of the silane, Journal of Polymer Science Part B: Polymer Physics 44(1) (2006) 143-152.

[35] H. Zou, S. Wu, J. Shen, Polymer/silica nanocomposites: preparation, characterization, properties, and applications, Chemical Reviews 108(9) (2008) 3893-3957.

[36] Q. Liu, J. Ding, D.E. Chambers, S. Debnath, S.L. Wunder, G.R. Baran, Filler-coupling agent-matrix interactions in silica/polymethylmethacrylate composites, Journal of Biomedical Materials Research 57(3) (2001) 384-393.

[37] T. Jesionowski, A. Krysztafkiewicz, Influence of silane coupling agents on surface properties of precipitated silicas, Applied Surface Science 172(1–2) (2001) 18-32.

[38] S. Sun, C. Li, L. Zhang, H.L. Du, J.S. Burnell-Gray, Effects of surface modification of fumed silica on interfacial structures and mechanical properties of poly(vinyl chloride) composites, European Polymer Journal 42(7) (2006) 1643-1652.

[39] J. Lin, J.A. Siddiqui, R.M. Ottenbrite, Surface modification of inorganic oxide particles with silane coupling agent and organic dyes, Polymers for Advanced Technologies 12(5) (2001) 285-292.

[40] Y. Haldorai, W.S. Lyoo, S.K. Noh, J.-J. Shim, Ionic liquid mediated synthesis of silica/polystyrene core–shell composite nanospheres by radical dispersion polymerization, Reactive and Functional Polymers 70(7) (2010) 393-399.

[41] J. Moraes, K. Ohno, T. Maschmeyer, S.b. Perrier, Synthesis of silica-polymer core-shell nanoparticles by reversible addition-fragmentation chain transfer polymerization, Chemical Communications 49(80) (2013) 9077-9088.

[42] M. Salami-Kalajahi, V. Haddadi-Asl, S. Rahimi-Razin, F. Behboodi-Sadabad, M. Najafi, H. Roghani-Mamaqani, A study on the properties of PMMA/silica nanocomposites prepared via RAFT polymerization, Journal of Polymer Research 19(2) (2012) 9793.

[43] A.C. Balazs, T. Emrick, T.P. Russell, Nanoparticle polymer composites: where two small worlds meet, Science 314(5802) (2006) 1107-1110.

[44] D.W. Schaefer, R.S. Justice, How nano are nanocomposites?, Macromolecules 40(24) (2007) 8501-8517.

[45] M.Z. Rong, M.Q. Zhang, Y.X. Zheng, H.M. Zeng, R. Walter, K. Friedrich, Structure–property relationships of irradiation grafted nano-inorganic particle filled polypropylene composites, Polymer 42(1) (2001) 167-183.

[46] C.L. Wu, M.Q. Zhang, M.Z. Rong, K. Friedrich, Silica nanoparticles filled polypropylene: effects of particle surface treatment, matrix ductility and particle species on mechanical performance of the composites, Composites Science and Technology 65(3–4) (2005) 635-645.

[47] E. Kontou, G. Anthoulis, The effect of silica nanoparticles on the thermomechanical properties of polystyrene, Journal of Applied Polymer Science 105(4) (2007) 1723-1731.

[48] E. Kontou, M. Niaounakis, Thermo-mechanical properties of LLDPE/SiO$_2$ nanocomposites, Polymer 47(4) (2006) 1267-1280.

[49] C.S. Reddy, C.K. Das, HLDPE/organic functionalized SiO$_2$ nanocomposites with improved thermal stability and mechanical properties, Composite Interfaces 11(8-9) (2005) 687-699.

[50] L. Huang, R. Zhan, Y. Lu, Mechanical properties and crystallization behavior of polypropylene/nano-SiO$_2$ composites, Journal of Reinforced Plastics and Composites 25(9) (2006) 1001-1012.

[51] F. Yang, G.L. Nelson, PMMA/silica nanocomposite studies: synthesis and properties, Journal of Applied Polymer Science 91(6) (2004) 3844-3850.

[52] C.-F. Ou, M.-C. Hsu, Preparation and characterization of cyclo olefin copolymer (COC)/silica nanoparticle composites by solution blending, Journal of Polymer Research 14(5) (2007) 373-378.

[53] M.Z. Rong, M.Q. Zhang, Y.X. Zheng, H.M. Zeng, R. Walter, K. Friedrich, Irradiation graft polymerization on nano-inorganic particles: an effective means to design polymer-based nanocomposites, Journal of Materials Science Letters 19(13) (2000) 1159-1161.

[54] M.Q. Zhang, M.Z. Rong, H.M. Zeng, S. Schmitt, B. Wetzel, K. Friedrich, Atomic force microscopy study on structure and properties of irradiation grafted silica particles in polypropylene-based nanocomposites, Journal of Applied Polymer Science 80(12) (2001) 2218-2227.

[55] J. Lee, C.K. Hong, S. Choe, S.E. Shim, Synthesis of polystyrene/silica composite particles by soap-free emulsion polymerization using positively charged colloidal silica, Journal of Colloid and Interface Science 310(1) (2007) 112-120.

[56] Y. Yang, Y. Dan, Preparation of PMMA/SiO$_2$ composite particles via emulsion polymerization, Colloid & Polymer Science 281(8) (2003) 794-799.

[57] Y. Li, B.C. Benicewicz, Functionalization of silica nanoparticles via the combination of surface-initiated RAFT polymerization and click reactions, Macromolecules 41(21) (2008) 7986-7992.

[58] C.-H. Liu, C.-Y. Pan, Grafting polystyrene onto silica nanoparticles via RAFT polymerization, Polymer 48(13) (2007) 3679-3685.

[59] A.J. Crosby, J.Y. Lee, Polymer nanocomposites: the "nano" effect on mechanical properties, Polymer Reviews 47(2) (2007) 217-229.

[60] D.N. Bikiaris, G.Z. Papageorgiou, E. Pavlidou, N. Vouroutzis, P. Palatzoglou, G.P. Karayannidis, Preparation by melt mixing and characterization of isotactic polypropylene/SiO$_2$ nanocomposites containing untreated and surface-treated nanoparticles, Journal of Applied Polymer Science 100(4) (2006) 2684-2696.

[61] R.Y. Hong, H.P. Fu, Y.J. Zhang, L. Liu, J. Wang, H.Z. Li, Y. Zheng, Surface-modified silica nanoparticles for reinforcement of PMMA, Journal of Applied Polymer Science 105(4) (2007) 2176-2184.

[62] A. Zhu, Z. Shi, A. Cai, F. Zhao, T. Liao, Synthesis of core–shell PMMA–SiO$_2$ nanoparticles with suspension–dispersion–polymerization in an aqueous system

and its effect on mechanical properties of PVC composites, Polymer Testing 27(5) (2008) 540-547.

[63] Z. Buhin, S.L. Blagojević, M. Leskovac, In situ emulsion polymerization and characterization of poly(butyl acrylate-co-methyl methacrylate)/silica nanosystems, Polymer Engineering & Science 53(11) (2013) 2292-2298.

[64] N. Rattanasom, T. Saowapark, C. Deeprasertkul, Reinforcement of natural rubber with silica/carbon black hybrid filler, Polymer Testing 26(3) (2007) 369-377.

[65] C. Gauthier, E. Reynaud, R. Vassoille, L. Ladouce-Stelandre, Analysis of the non-linear viscoelastic behaviour of silica filled styrene butadiene rubber, Polymer 45(8) (2004) 2761-2771.

[66] N. Suzuki, M. Ito, F. Yatsuyanagi, Effects of rubber/filler interactions on deformation behavior of silica filled SBR systems, Polymer 46(1) (2005) 193-201.

[67] Z. Peng, L.X. Kong, S.D. Li, Y. Chen, M.F. Huang, Self-assembled natural rubber/silica nanocomposites: its preparation and characterization, Composites Science and Technology 67(15-16) (2007) 3130-3139.

[68] X. Liu, S. Zhao, Measurement of the condensation temperature of nanosilica powder organically modified by a silane coupling agent and its effect evaluation, Journal of Applied Polymer Science 108(5) (2008) 3038-3045.

[69] S. Chuayjuljit, A. Boonmahitthisud, Natural rubber nanocomposites using polystyrene-encapsulated nanosilica prepared by differential microemulsion polymerization, Applied Surface Science 256(23) (2010) 7211-7216.

[70] S. Sinha Ray, M. Okamoto, Polymer/layered silicate nanocomposites: a review from preparation to processing, Progress in Polymer Science 28(11) (2003) 1539-1641.

[71] S.-D. Li, Z. Peng, L.X. Kong, J.-P. Zhong, Thermal degradation kinetics and morphology of natural rubber/silica nanocomposites, Journal of Nanoscience and Nanotechnology 6(2) (2006) 541-546.

[72] X.-y. Shang, Z.-k. Zhu, J. Yin, X.-d. Ma, Compatibility of soluble polyimide/silica hybrids induced by a coupling agent, Chemistry of Materials 14(1) (2002) 71-77.

[73] Q. Wang, Y. Luo, C. Feng, Z. Yi, Q. Qiu, L.X. Kong, Z. Peng, Reinforcement of natural rubber with core-shell structure silica-poly(methyl methacrylate) nanoparticles, Journal of Nanomaterials 2012 (2012) 1-9.

[74] Z.-l. Xu, L.-y. Yu, L.-f. Han, Polymer-nanoinorganic particles composite membranes: a brief overview, Frontiers of Chemical Engineering in China 3(3) (2009) 318-329.

[75] X. Feng, R.Y.M. Huang, Liquid separation by membrane pervaporation: a review, Industrial & Engineering Chemistry Research 36(4) (1997) 1048-1066.

[76] Y.-L. Liu, C.-Y. Hsu, Y.-H. Su, J.-Y. Lai, Chitosan−silica complex membranes from sulfonic acid functionalized silica nanoparticles for pervaporation dehydration of ethanol−water solutions, Biomacromolecules 6(1) (2005) 368-373.

[77] R. Guo, X. Ma, C. Hu, Z. Jiang, Novel PVA–silica nanocomposite membrane for pervaporative dehydration of ethylene glycol aqueous solution, Polymer 48(10) (2007) 2939-2945.

[78] G.L. Jadav, P.S. Singh, Synthesis of novel silica-polyamide nanocomposite membrane with enhanced properties, Journal of Membrane Science 328(1–2) (2009) 257-267.

[79] Q. Zhao, J. Qian, C. Zhu, Q. An, T. Xu, Q. Zheng, Y. Song, A novel method for fabricating polyelectrolyte complex/inorganic nanohybrid membranes with high isopropanol dehydration performance, Journal of Membrane Science 345(1–2) (2009) 233-241.

[80] D. Sun, B.-B. Li, Z.-L. Xu, Pervaporation of ethanol/water mixture by organophilic nano-silica filled PDMS composite membranes, Desalination 322 (2013) 159-166.

[81] D. Tumnantong, G.L. Rempel, P. Prasassarakich, Synthesis of polystyrene-silica nanoparticles via RAFT emulsifier-free emulsion polymerization, European Polymer Journal 80 (2016) 145-157.

[82] B. Chaichua, P. Prasassarakich, S. Poompradub, In situ silica reinforcement of natural rubber by sol–gel process via rubber solution, Journal of Sol-Gel Science and Technology 52(2) (2009) 219-227.

[83] P. Satraphan, A. Intasiri, V. Tangpasuthadol, S. Kiatkamjornwong, Effects of methyl methacrylate grafting and in situ silica particle formation on the morphology and mechanical properties of natural rubber composite films, Polymers for Advanced Technologies 20(5) (2009) 473-486.

[84] S. Poompradub, M. Thirakulrati, P. Prasassarakich, In situ generated silica in natural rubber latex via the sol–gel technique and properties of the silica rubber composites, Materials Chemistry and Physics 144(1–2) (2014) 122-131.

[85] M. Joubert, C. Delaite, E. Bourgeat-Lami, P. Dumas, Hairy PEO-silica nanoparticles through surface-initiated polymerization of ethylene oxide, Macromolecular Rapid Communications 26(8) (2005) 602-607.

[86] J.-C. Daigle, J.P. Claverie, A simple method for forming hybrid core-shell nanoparticles suspended in water, Journal of Nanomaterials 2008 (2008) 8.

[87] T. Tancharernrat, G.L. Rempel, P. Prasassarakich, Preparation of styrene butadiene copolymer-silica nanocomposites via differential microemulsion polymerization and NR/SBR-SiO2 membranes for pervaporation of water-ethanol mixtures, Chemical Engineering Journal 258 (2014) 290-300.

[88] M.T. Ramesan, R. Alex, N.V. Khanh, Studies on the cure and mechanical properties of blends of natural rubber with dichlorocarbene modified styrene–butadiene rubber and chloroprene rubber, Reactive and Functional Polymers 62(1) (2005) 41-50.

[89] S. Angnanon, P. Prasassarakich, N. Hinchiranan, Styrene/acrylonitrile graft natural rubber as compatibilizer in rubber blends, Polymer-Plastics Technology and Engineering 50(11) (2011) 1170-1178.

[90] T. Tancharernrat, G.L. Rempel, P. Prasassarakich, Synthesis of polybutadiene-silica nanoparticles via differential microemulsion polymerization and their hydrogenated nanoparticles by diimide reduction, Polymer Degradation and Stability 118 (2015) 69-81.

[91] L. Petersson, K. Oksman, Biopolymer based nanocomposites: comparing layered silicates and microcrystalline cellulose as nanoreinforcement, Composites Science and Technology 66(13) (2006) 2187-2196.

[92] H. Xia, C. Zhang, Q. Wang, Study on ultrasonic induced encapsulating emulsion polymerization in the presence of nanoparticles, Journal of Applied Polymer Science 80(8) (2001) 1130-1139.

[93] N. Hinchiranan, W. Lertweerasirikun, W. Poonsawad, G.L. Rempel, P. Prasassarakich, Hydrogenated natural rubber blends: aspect on thermal stability and oxidative behavior, Journal of Applied Polymer Science 113(3) (2009) 1566-1575.

[94] E.d.S. Silva, L.A. Ribeiro, M.C.B.C.d. Nascimento, E.N. Ito, Rheological and mechanical characterization of poly (methyl methacrylate)/silica (PMMA/SiO$_2$) composites, Materials Research 17 (2014) 926-932.

[95] L. Thiraphattaraphun, S. Kiatkamjornwong, P. Prasassarakich, S. Damronglerd, Natural rubber-g-methyl methacrylate/poly(methyl methacrylate) blends, Journal of Applied Polymer Science 81(2) (2001) 428-439.

[96] X. Liu, Y. Sun, X. Deng, Studies on the pervaporation membrane of permeation water from methanol/water mixture, Journal of Membrane Science 325(1) (2008) 192-198.

[97] Y. Ma, X. Cao, X. Feng, Y. Ma, H. Zou, Fabrication of super-hydrophobic film from PMMA with intrinsic water contact angle below 90°, Polymer 48(26) (2007) 7455-7460.

APPENDICES

APPENDIX A

Data of Mechanical Properties of NR/PS-R-SiO$_2$

Table A-1 Mechanical properties of NR filled with PS-R-SiO$_2$ nanocomposites.

NR/PS-R-SiO$_2$[a] (wt/wt)	100/0	90/10	85/15	80/20	75/25
SiO$_2$ content[b] (wt%)	-	1.0	1.5	2.0	2.5
	17.5	27.3	21.6	17.6	16.5
Tensile strength (MPa)	21.3	26.3	23.1	16.1	15.2
	18.8	26.6	20.3	16.8	15.7
Mean	19.2	26.7	22.2	16.9	15.8
SD	2.1	0.6	1.4	0.8	0.7
	1.29	1.70	2.31	2.91	2.99
300% Modulus (MPa)	1.42	1.76	2.42	3.10	2.80
	1.33	1.82	2.39	3.09	2.96
Mean	1.35	1.76	2.38	3.03	2.92
SD	0.07	0.05	0.06	0.12	0.11
	801	791	745	746	720
Elongation at break (%)	819	829	719	703	714
	839	800	752	699	698
Mean	819	806	739	716	710
SD	22	20	17	26	12

[a] PS-co-R4-Si was used as PS-R-SiO$_2$.
[b] Silica content based on total rubber.

APPENDIX B

Data of Mechanical Properties of NR/PIP-R-SiO₂

Table B-1 Mechanical properties of NR filled with PIP-R-SiO₂ nanocomposites.

NR/PIP-R-SiO₂ (wt/wt)	100/0	ACP initiator[a]		V50 initiator[b]		
		90/10	80/20	90/10	80/20	70/30
SiO₂ content[c] (wt%)	-	1.0	2.0	1.0	2.0	3.0
Tensile strength (MPa)	18.6	26.0	24.4	19.9	16.7	14.7
	17.1	24.8	23.6	17.0	15.3	13.5
	17.9	22.0	22.4	18.3	17.3	17.1
Mean	17.9	24.2	23.5	18.4	16.0	15.1
SD	0.7	2.1	1.0	1.6	1.2	2.8
300% Modulus (MPa)	1.11	1.18	1.23	1.07	1.19	1.36
	1.12	1.21	1.24	1.11	1.19	1.29
	1.09	1.17	1.25	1.08	1.20	1.45
Mean	1.11	1.19	1.24	1.09	1.19	1.37
SD	0.02	0.02	0.01	0.01	0.01	0.08
Elongation at break (%)	838	956	973	856	887	887
	902	941	986	880	921	991
	872	943	957	932	865	928
Mean	871	947	972	889	891	935
SD	32	08	15	39	34	77

[a] PIP-co-R3-ACP_Si was used as PIP-R-SiO₂.
[b] PIP-co-R4-V50_Si was used as PIP-R-SiO₂.
[c] Silica content based on total rubber.

APPENDIX C

Data of Mechanical Properties of NR/PMMA-SiO$_2$

Table C-1 Mechanical properties of NR filled with PMMA-SiO$_2$ nanocomposites.

NR/PMMA-SiO$_2$[a] (wt/wt)	100/0	90/10	80/20	70/30	60/40
SiO$_2$ content[b] (wt%)	-	1.0	2.0	3.0	4.0
	23.6	23.9	22.9	11.2	6.0
Tensile strength (MPa)	23.6	23.0	23.1	11.9	7.8
	21.9	25.1	23.1	10.1	8.0
Mean	23.0	24.0	23.0	11.1	7.3
SD	1.0	1.1	0.1	0.9	1.1
	1.06	1.29	2.02	2.65	4.93
300% Modulus (MPa)	1.03	1.35	2.00	2.86	4,87
	1.04	1.32	2.09	2.80	5.12
Mean	1.04	1.32	2.04	2.77	4.97
SD	0.02	0.03	0.05	0.11	0.13
	884	885	741	599	404
Elongation at break (%)	884	852	765	590	406
	913	894	753	590	347
Mean	894	877	753	593	386
SD	16	22	12	05	33

[a] PMMA-SiO$_2$ preparation condition: M/H$_2$O = 0.4, SiO$_2$ = 10 wt%, SDS = 5.34 wt%, APS = 0.61 wt% based on monomer.
[b] Silica content based on total rubber.

APPENDIX D

Data of Mechanical Properties of NR/Poly(ST-*co*-MMA)-SiO$_2$

Table D-1 Mechanical properties of NR filled with Poly(ST-*co*-MMA)-SiO$_2$ nanocomposites.

NR/poly(ST-*co*-MMA)-SiO$_2$[a] (wt/wt)	100/0	90/10	85/15	80/20	75/25
SiO$_2$ content[b] (wt%)	-	1.0	1.5	2.0	2.5
Tensile strength (MPa)	23.1	8.2	8.4	6.5	8.3
	17.8	8.9	7.9	6.7	7.9
	21.3	7.3	8.0	5.7	6.7
Mean	20.6	8.1	8.0	6.2	7.6
SD	5.5	0.7	0.3	0.5	0.8
300% Modulus (MPa)	1.16	1.34	1.67	1.47	1.83
	1.08	1.31	1.93	1.37	1.61
	1.17	1.25	1.55	1.56	1.55
Mean	1.13	1.30	1.71	1.46	1.66
SD	0.04	0.04	0.22	0.07	0.12
Elongation at break (%)	828	685	773	662	759
	834	722	825	691	682
	800	715	746	750	678
Mean	820	707	781	700	707
SD	24	27	39	53	47

[a] Poly(ST-*co*-MMA)-SiO$_2$ preparation condition: H$_2$O = 30 g, SiO$_2$ = 10 wt%, ST:MMA = 1:1, SDS = 3 wt%, APS = 1 wt% base on monomer.
[b] Silica content based on total rubber.

VITA

The author who is responsible for this dissertation is Miss Dusadee Tumnantong. She was born on December 16th, 1985 in Ratchaburi, Thailand. She received her B.Sc. and M.Sc. degree from the Department of Chemical Technology, Chulalongkorn University in 2008 and 2010, respectively. She continued studying for a Doctoral Degree in Chemical Technology, Chulalongkorn University. She has received the Royal Golden Jubilee Scholarship from Thailand Research Fund for her Ph.D. study. She also carried out some of her Ph.D. research for one year (2014-2015) at "Advanced Rubber Technology and Applied Catalysis Laboratory" in Chemical Engineering, University of Waterloo, ON, Canada.

Journal Publications:

1. Tumnantong, D., Rempel, G.L., and Prasassarakich, P. Synthesis of Polystyrene-Silica Nanoparticles via RAFT Emulsifier-Free Emulsion Polymerization. European Polymer Journal 80 (2016) 145-157.

2. Tumnantong, D., Rempel, G.L., and Prasassarakich, P. Preparation of Poly(methyl methacrylate)-Silica Nanoparticles via Differential Microemulsion Polymerization and Physical Properties of NR/PMMA-SiO2 Hybrid Membranes. Polymer Engineering and Science (2017), DOI: 10.1002/pen.24611.

3. Tumnantong, D., Rempel, G.L., and Prasassarakich, P. RAFT Emulsifier-Free Emulsion Polymerization of Polyisoprene-Silica Nanoparticles Using Water-Soluble Initiators. To be submitted to Colloid and Polymer Science (2017).

Conference Presentations:

1. Tumnantong, D., Rempel, G.L., and Prasassarakich, P. (2014) "Synthesis of Polystyrene-Silica Nanoparticles via RAFT Emulsifier-Free Emulsion Polymerization". The 4th Polymer Conference of Thailand (4th PCT), March 20 – 21, 2014 at Pathumwan Princess Hotel, Bangkok, Thailand. (Poster presentation).

2. Tumnantong, D., Rempel, G.L., and Prasassarakich, P. (2014) "Synthesis of Polystyrene-Silica Nanoparticles via RAFT Emulsifier-Free Emulsion Polymerization". The Royal Golden Jubilee Ph.D. Congress XV (RGJ-Ph.D. Congress XV), May 28 – 30, 2014 at Jomtien Palm Beach Hotel, Chonburi, Thailand. (Oral presentation).

3. Tumnantong, D., Rempel, G.L., and Prasassarakich, P. (2014) "Synthesis of Polystyrene-Silica Nanoparticles via RAFT Emulsifier-Free Emulsion Polymerization". The 2014 IUPAC World Polymer Congress, July 6 – 11, 2014 at Chiang Mai International Convention and Exhibition Centre, Chiang Mai, Thailand. (Poster presentation).